The Nonlinear Schrödinger Equation and Applications in Bose-Einstein Condensation and Plasma Physics

Weizhu Bao

Department of Mathematics
Center for Computational Science and Engineering
National University of Singapore
117543 Singapore
E-mail: bao@math.nus.edu.sg,
URL: http://www.math.nus.edu.sg/~bao/

Contents

1. Introduction

The Schrödinger equation was proposed to model a system when the quantum effect was considered. For a system with N particles, the Schrödinger equation is defined in $3N+1$ dimensions. With such high dimensions, even use today's supercomputer, it is impossible to solve the Schrödinger equation for dynamics of N particles with $N > 10$. After assumed Hatree or Hatree-Fork ansatz, the $3N+1$ dimensions linear Schrödinger equation was approximated by a $3+1$ dimensions nonlinear Schrödinger equation (NLSE) or Schrödinger-Poisson (S-P) system. Although nonlinearity in NLSE brought some new difficulties, but the dimensions were reduced significantly compared with the original problem. This opened a light to study dynamics of N particles when N is large. Later, it was found that NLSE had applications in different subjects, e.g. quantum mechanics, solid state physics, condensed matter physics, quantum chemistry, nonlinear optics, wave propagation, optical communication, protein folding and bending, semiconductor industry, laser propagation, nano technology and industry, biology etc. Currently, the study of NLSE including analysis, numerics and applications becomes a very important subject in applied and computational mathematics. This study has very important impact to the progress of other science and technology subjects.

A typical application of NLSE is for wave motion and interaction in plasma physics where the Zakharov system (ZS) was derived by Zakharov [121] in 1972 for governing the coupled dynamics of the electric-field amplitude and the low-frequency density fluctuations of ions. Then it has become commonly accepted that ZS is a general model to govern interaction of dispersive wave and nondispersive (acoustic) wave. It has important applications in plasma physics (interaction between Langmuir and ion acoustic waves [121, 101]), in the theory of molecular chains (interaction of the intramolecular vibrations forming Davydov solitons with the acoustic disturbances in the chain [39]), in hydrodynamics (interaction between short-wave and long-wave gravitational disturbances in the atmosphere [110, 40]), and so on. In three spatial dimensions, ZS was also derived to model the collapse of caverns [121]. Later, the standard ZS was extended to generalized Zakharov system (GZS) [72, 73], vector Zakharov system (VZS) [113] and vector Zakharov system for multi-component plasma (VZSM) [72, 73].

In this chapter, we first review derivation of NLSE from wave propagation and Bose-Einstein condensation (BEC). Then we present variational formulation of NLSE including conservation laws, Lagrangian structure, Hamiltonian structure and variance identity. Plane and soliton wave solutions, existence/blowup results of NLSE are then presented. Ground, excited and central vortex states of NLSE with an external potential are studied. We also study formally semiclassical limits of NLSE by WKB expansion and Wigner transform when the (scaled) Planck constant $\varepsilon \to 0$. In addition, numerical methods for computing ground states and dynamics of NLSE are presented and numerical results are also reported. Then we review derivation of VZS from the two-fluid model [113] for ion-electron dynamics in plasma physics and generalize VZS to VZSM, reduce VZSM to generalized vector Zakharov system (GVZS), GVZS to GZS or vector nonlinear Schrödinger (VNLS) equations, and GZS to NLSE, as well as generalize GZS and GVZS with a linear damping term to arrest blowup. Conservation laws of the systems and well-posedness of GZS are presented, and plane wave, soliton wave and periodic wave solutions of GZS are reviewed. Furthermore, we present a time-splitting spectral (TSSP) method to discretize GZS and compare it with the standard Crank-Nicolson finite difference (CNFD) method.

Throughout this notes, we use f^*, Re(f) and Im(f) denote the conjugate, real part and imaginary part of a complex function f respectively. We also adopt the standard Sobolev norms.

2. Derivation of NLSE from wave propagation

In this section, we review briefly derivation of NLSE from wave propagation, i.e. parabolic or paraxial approximation for forward propagation time harmonic waves, to analyze high frequency asymptotics.

The wave equation

$$\frac{1}{c^2}\,\frac{\partial^2 u(\mathbf{x},t)}{\partial t^2} - \triangle u(\mathbf{x},t) = 0, \qquad \mathbf{x} \in \mathbb{R}^3, \tag{2.1}$$

where $\mathbf{x} = (x, y, z)$ is the Cartesian coordinate, t is time and $c = c(\mathbf{x}, |u|)$ is the propagation speed, has time harmonic solutions of the form $e^{i\omega t}u(\mathbf{x})$ with the complex wave function u satisfying the Helmholtz or reduced wave equation

$$\triangle u(\mathbf{x}) + \frac{\omega^2}{c^2}\,u = 0, \qquad \mathbf{x} \in \mathbb{R}^3. \tag{2.2}$$

Let c_0 be a uniform reference speed, $k_0 = \omega/c_0$ be the wave number and $n(\mathbf{x}, |u|) = c_0/c(\mathbf{x}, |u|)$ be the index of refraction. The reduced wave equation has then the form

$$\triangle u(\mathbf{x}) + k_0^2 n^2(\mathbf{x}, |u|)u = 0. \tag{2.3}$$

When wave propagates in a uniform medium, $n(\mathbf{x}, |u|) = 1$; in a linear medium, $n(\mathbf{x}, |u|) = n(\mathbf{x})$; and in a Kerr medium, $n(\mathbf{x}, |u|) = \sqrt{1 + 4n_2|u|^2/n_0}$ with n_0 linear index of refraction and n_2 Kerr coefficient.

When waves are approximately plane and move in one direction primarily, say the z direction, e.g. propagation of laser beams, we look for solutions of the form

$$u(x, y, z) = e^{ik_0 z}\psi(\mathbf{x}, z) \tag{2.4}$$

where $\mathbf{x} = (x, y)$ denotes the transverse variables. We insert (2.4) into the reduced wave equation (2.3) and get

$$2ik_0\psi_z + \triangle_\perp\psi + k_0^2\mu(\mathbf{x}, z, |\psi|)\psi + \psi_{zz} = 0, \tag{2.5}$$

where $\triangle_\perp$ is the Laplacian in the transverse variables and $\mu(\mathbf{x}, z, |\psi|) = n^2(\mathbf{x}, z, |\psi|) - 1$ is the fluctuation in the refractive index. Note that the direction of propagation z ploys the role of time and $-k_0^2\mu(\mathbf{x}, z, |\psi|)$ is the (time dependent) potential.

Introduce nondimensional variables:

$$\tilde{x} = \frac{x}{r_0}, \qquad \tilde{y} = \frac{y}{r_0}, \qquad \tilde{t} = \frac{z}{k_0 r_0^2}, \qquad \tilde{\psi}(\tilde{x}, \tilde{y}, \tilde{t}) = \frac{\psi(x, y, z)}{\psi_s}, \tag{2.6}$$

where r_0 is the dimensionless length unit, e.g. width of the input laser beam, and ψ_s is dimensionless unit for ψ to be determined. Plugging (2.6) into (2.5), multiplying by $r_0^2/2$, and then removing all $\tilde{}$, we get the following dimensionless equation:

$$i\psi_t = -\frac{1}{2}\triangle_\perp \psi + f(\mathbf{x}, t, |\psi|)\psi - \frac{\delta}{2}\psi_{tt}, \tag{2.7}$$

where $\delta = 1/r_0^2 k_0^2$ and the real-valued function f depends on μ. Due to the input beam width $r_0 \gg \lambda = 2\pi/k_0$, we get

$$\delta/2 = \lambda^2/8\pi^2 r_0^2 \ll 1.$$

Thus we drop the nonparaxial term ψ_{tt} in (2.7) and obtain the NLSE:

$$i\psi_t = -\frac{1}{2}\triangle_\perp \psi + f(\mathbf{x}, t, |\psi|)\psi, \tag{2.8}$$

Of course (2.7) is only an approximation to the full reduced wave equation and it is valid when the variations in the index of refraction are smooth and the bulk of the wave energy is away from boundaries. This important and very useful approximation for wave propagation is well suited for numerical approximation since we now have an initial value problem for ψ, assuming that $\psi(\mathbf{x}, 0)$ is known, rather than a boundary value problem for u.

When $n(\mathbf{x}, z, |u|) = 1$ in (2.3), then $\mu(\mathbf{x}, z, |\psi|) = 0$ in (2.5) and $f(\mathbf{x}, t, |\psi|) = 0$ in (2.7), thus (2.7) collapses to the free Schrödinger equation:

$$i\psi_t = -\frac{1}{2} \triangle_\perp \psi. \tag{2.9}$$

When $n(\mathbf{x}, z, |u|) = n(\mathbf{x}, z)$ in (2.3), then $\mu(\mathbf{x}, z, |\psi|) = \mu(\mathbf{x}, z)$ in (2.5) and $f(\mathbf{x}, t, |\psi|) = V(\mathbf{x}, t)$ in (2.7), thus (2.7) collapses to a linear Schrödinger equation with potential $V(\mathbf{x}, t)$:

$$i\psi_t = -\frac{1}{2} \triangle_\perp \psi + V(\mathbf{x}, t)\psi. \tag{2.10}$$

When $n(\mathbf{x}, z, |u|) = \sqrt{1 + 4n_2|u|^2/n_0}$, i.e. laser beam in Kerr medium, then $\mu(\mathbf{x}, z, |\psi|) = 2n_2 r_0^2 k_0^2 |\psi|^2/n_0$ in (2.5) and $f(\mathbf{x}, t, |\psi|) = -|\psi|^2$ in (2.7) by choosing $\psi_s = \sqrt{n_0}/r_0 k_0 \sqrt{2n_2}$, thus (2.7) collapses to NLSE with a cubic focusing nonlinearity:

$$i\psi_t = -\frac{1}{2} \triangle_\perp \psi - |\psi|^2\psi. \tag{2.11}$$

The wave energy or power of the beam is conserved:

$$N(\psi) = \int_{\mathbb{R}^2} |\psi(\mathbf{x}, t)|^2 \, d\mathbf{x} \equiv \int_{\mathbb{R}^2} |\psi(\mathbf{x}, 0)|^2 \, d\mathbf{x}, \qquad t \geq 0. \tag{2.12}$$

Remark 2.1: When we consider high frequency asymptotics which concerns approximate solutions of (2.10) that are good approximations to oscillatory solutions. For such solutions the propagation distance is long compared to the wavelength, the propagation time is large compared to the period and the potential $V(\mathbf{x})$ varies slowly. To make this precise, we introduce slow time and space variables $t \to t/\varepsilon$, $\mathbf{x} \to \mathbf{x}/\varepsilon$ with $0 < \varepsilon \ll 1$ the (scaled) Planck constant and the scaled wave function $\psi^\varepsilon(\mathbf{x}, t) = \psi(\mathbf{x}/\varepsilon, t/\varepsilon)$ which satisfies the NLSE in the semiclassical regime

$$i\varepsilon\psi_t^\varepsilon = -\frac{\varepsilon^2}{2} \triangle_\perp \psi^\varepsilon + V^\varepsilon(\mathbf{x}, t)\psi^\varepsilon, \qquad \mathbf{x} \in \mathbb{R}^2, \ t > 0, \tag{2.13}$$

where $V^\varepsilon(\mathbf{x}, t) = V(\mathbf{x}/\varepsilon, t/\varepsilon)$.

3. Derivation of NLSE from BEC

Since its realization in dilute bosonic atomic gases [3, 26], BEC of alkali atoms and hydrogen has been produced and studied extensively in the laboratory [71], and has spurred great excitement in the atomic physics community and renewed the interest in studying the collective dynamics of macroscopic ensembles of atoms occupying the same one-particle quantum state [99, 34, 68]. The condensate typically consists of a few thousands to millions of atoms which are confined by a trap potential. In fact, beside the effects of the internal interactions between the atoms, the macroscopic behavior of BEC matter is highly sensitive to the shape of this external trapping potential. Theoretical predictions of the properties of a BEC like the density profile [19], collective excitations [43] and the formation of vortices [105] can now be compared with experimental data [3]. Needless to say that this dramatic progress on the experimental front has stimulated a wave of activity on both the theoretical and the numerical front.

At temperatures T much smaller than the critical temperature T_c [84], a BEC is well described by the macroscopic wave function $\psi = \psi(\mathbf{x}, t)$ whose evolution is governed by a self-consistent, mean field NLSE known as the Gross-Pitaevskii equation (GPE) [69, 103]

$$\begin{aligned} i\hbar\frac{\partial\psi(\mathbf{x},t)}{\partial t} &= \frac{\delta H(\psi)}{\delta\psi^*} \\ &= -\frac{\hbar^2}{2m}\nabla^2\psi(\mathbf{x},t) + V(\mathbf{x})\psi(\mathbf{x},t) + NU_0|\psi(\mathbf{x},t)|^2\psi(\mathbf{x},t), \end{aligned} \tag{3.1}$$

where $\mathbf{x} = (x, y, z)$, m is the atomic mass, $\hbar$ is the Planck constant, N is the number of atoms in the condensate, $V(\mathbf{x})$ is an external trapping potential. When a harmonic trap potential is considered, $V(\mathbf{x}) = \frac{m}{2}\left(\omega_x^2 x^2 + \omega_y^2 y^2 + \omega_z^2 z^2\right)$ with ω_x, ω_y and ω_z being the trap frequencies in x, y and z-direction, respectively. The Hamiltonian (or energy) of the system $H(\psi)$ per particle is defined as

$$\begin{aligned} H(\psi) = &\int_{\mathbb{R}^3} \psi^*(\mathbf{x},t)\left[-\frac{\hbar^2}{2m}\nabla^2 + V(\mathbf{x})\right]\psi(\mathbf{x},t)d\mathbf{x} \\ &+\frac{1}{2}\int_{\mathbb{R}^3\times\mathbb{R}^3} \psi^*(\mathbf{x},t)\ \psi^*(\mathbf{x}',t)\Phi(\mathbf{x}-\mathbf{x}')\psi(\mathbf{x}',t)\psi(\mathbf{x},t)d\mathbf{x}d\mathbf{x}', \end{aligned} \tag{3.2}$$

where the interaction potential is taken as the Fermi form

$$\Phi(\mathbf{x}) = (N-1)U_0\delta(\mathbf{x}). \tag{3.3}$$

$U_0 = 4\pi\hbar^2 a_s/m$ describes the interaction between atoms in the condensate with the s-wave scattering length a_s (positive for repulsive interaction and negative for attractive interaction). It is convenient to normalize the wave function by requiring

$$\int_{\mathbb{R}^3} |\psi(\mathbf{x},t)|^2\, d\mathbf{x} = 1. \tag{3.4}$$

3.1. *Dimensionless GPE*

In order to scale the Eq. (3.1) under the normalization (3.4), we introduce

$$\tilde{t} = \omega_m t, \ \tilde{\mathbf{x}} = \frac{\mathbf{x}}{a_0}, \ \tilde{\psi}(\tilde{\mathbf{x}}, \tilde{t}) = a_0^{3/2}\psi(\mathbf{x}, t), \ \text{with } a_0 = \sqrt{\hbar/m\omega_m}, \qquad (3.5)$$

where $\omega_m = \min\{\omega_x, \omega_y, \omega_z\}$, a_0 is the length of the harmonic oscillator ground state. In fact, we choose $1/\omega_m$ and a_0 as the dimensionless time and length units, respectively. Plugging (3.5) into (3.1), multiplying by $1/m\omega_m^2 a_0^{1/2}$, and then removing all $\tilde{}$, we get the following dimensionless GPE under the normalization (3.4) in three dimension

$$i\,\frac{\partial\psi(\mathbf{x}, t)}{\partial t} = -\frac{1}{2}\nabla^2\psi(\mathbf{x}, t) + V(\mathbf{x})\psi(\mathbf{x}, t) + \beta\,|\psi(\mathbf{x}, t)|^2\psi(\mathbf{x}, t), \qquad (3.6)$$

where $\beta = \frac{U_0 N}{a_0^3\hbar\omega_m} = \frac{4\pi a_s N}{a_0}$ and

$$V(\mathbf{x}) = \frac{1}{2}\left(\gamma_x^2 x^2 + \gamma_y^2 y^2 + \gamma_z^2 z^2\right), \text{ with } \gamma_\alpha = \frac{\omega_\alpha}{\omega_m} \ (\alpha = x, y, z).$$

There are two extreme regimes of the interaction parameter β: (1) $\beta = o(1)$, the Eq. (3.6) describes a weakly interacting condensation; (2) $\beta \gg 1$, it corresponds to a strongly interacting condensation or to the semiclassical regime.

There are two typical extreme regimes between the trap frequencies: (1) $\gamma_x = 1$, $\gamma_y \approx 1$ and $\gamma_z \gg 1$, it is a disk-shaped condensation; (2) $\gamma_x = 1$, $\gamma_y \gg 1$ and $\gamma_z \gg 1$, it is a cigar-shaped condensation. In these two cases, the three-dimensional (3D) GPE (3.6) can be approximately reduced to a 2D and 1D equation respectively [85, 8, 5] as explained below.

3.2. *Reduction to lower dimension*

Case I (disk-shaped condensation):

$$\omega_x \approx \omega_y, \quad \omega_z \gg \omega_x, \qquad \Longleftrightarrow \qquad \gamma_x = 1, \ \gamma_y \approx 1, \quad \gamma_z \gg 1.$$

Here, the 3D GPE (3.6) can be reduced to a 2D GPE with $\mathbf{x} = (x, y)$ by assuming that the time evolution does not cause excitations along the z-axis, since the excitations along the z-axis have large energy (of order $\hbar\omega_z$) compared to that along the x and y-axis with energies of order $\hbar\omega_x$. Thus, we may assume that the condensation wave function along the z-axis is always well described by the harmonic oscillator ground state wave function, and set

$$\psi = \psi_2(x, y, t)\phi_{\text{ho}}(z) \qquad \text{with} \quad \phi_{\text{ho}}(z) = (\gamma_z/\pi)^{1/4}\, e^{-\gamma_z z^2/2}. \qquad (3.7)$$

Plugging (3.7) into (3.6), multiplying by $\phi_{\rm ho}^*(z)$, integrating with respect to z over $(-\infty, \infty)$, we get

$$i\,\frac{\partial\psi_2(\mathbf{x},t)}{\partial t} = -\frac{1}{2}\nabla^2\psi_2 + \frac{1}{2}\left(\gamma_x^2x^2+\gamma_y^2y^2+C\right)\psi_2 + \beta_2|\psi_2|^2\psi_2, \tag{3.8}$$

where

$$\beta_2 = \beta\int_{-\infty}^{\infty}\phi_{\rm ho}^4(z)\,dz = \beta\sqrt{\frac{\gamma_z}{2\pi}},\ C = \int_{-\infty}^{\infty}\left(\gamma_z^2z^2|\phi_{\rm ho}(z)|^2 + \left|\frac{d\phi_{\rm ho}}{dz}\right|^2\right)\,dz.$$

Since this GPE is time-transverse invariant, we can replace $\psi_2 \to \psi\ e^{-i\frac{Ct}{2}}$ so that the constant C in the trap potential disappears, and we obtain the 2D effective GPE:

$$i\,\frac{\partial\psi(\mathbf{x},t)}{\partial t} = -\frac{1}{2}\nabla^2\psi + \frac{1}{2}\left(\gamma_x^2x^2+\gamma_y^2y^2\right)\psi + \beta_2|\psi|^2\psi. \tag{3.9}$$

Note that the observables, e.g. the position density $|\psi|^2$, are not affected by dropping the constant C in (3.8).

Case II (cigar-shaped condensation):

$$\omega_y \gg \omega_x, \quad \omega_z \gg \omega_x \qquad \Longleftrightarrow \qquad \gamma_x = 1, \quad \gamma_y \gg 1,\ \gamma_z \gg 1.$$

Here, the 3D GPE (3.6) can be reduced to a 1D GPE with $\mathbf{x} = x$. Similarly as in the 2D case, we can derive the following 1D GPE [85, 8, 5]:

$$i\,\frac{\partial\psi(x,t)}{\partial t} = -\frac{1}{2}\psi_{xx}(x,t) + \frac{\gamma_x^2x^2}{2}\psi(x,t) + \beta_1|\psi(x,t)|^2\psi(x,t), \tag{3.10}$$

where $\beta_1 = \beta\sqrt{\gamma_y\gamma_z}/2\pi$.

The 3D GPE (3.6), 2D GPE (3.9) and 1D GPE (3.10) can be written in a unified form:

$$i\,\frac{\partial\psi(\mathbf{x},t)}{\partial t} = -\frac{1}{2}\nabla^2\psi + V_d(\mathbf{x})\psi + \beta_d\,|\psi|^2\psi, \quad \mathbf{x}\in\mathbb{R}^d, \tag{3.11}$$

$$\psi(\mathbf{x},0) = \psi_0(\mathbf{x}), \qquad \mathbf{x}\in\mathbb{R}^d, \tag{3.12}$$

with

$$\beta_d = \beta\begin{cases}\sqrt{\gamma_y\gamma_z}/2\pi,\\ \sqrt{\gamma_z/2\pi},\\ 1,\end{cases} \qquad V_d(\mathbf{x}) = \begin{cases}\gamma_x^2x^2/2, & d=1,\\ \left(\gamma_x^2x^2+\gamma_y^2y^2\right)/2, & d=2,\\ \left(\gamma_x^2x^2+\gamma_y^2y^2+\gamma_z^2z^2\right)/2, & d=3,\end{cases} \tag{3.13}$$

where $\gamma_x > 0$, $\gamma_y > 0$ and $\gamma_z > 0$ are constants. The normalization condition for (3.11) is

$$N(\psi) = \|\psi(\cdot,t)\|^2 = \int_{\mathbb{R}^d}|\psi(\mathbf{x},t)|^2\,d\mathbf{x} \equiv \int_{\mathbb{R}^d}|\psi_0(\mathbf{x})|^2\,d\mathbf{x} = 1. \tag{3.14}$$

Remark 3.1: When $\beta_d \gg 1$, i.e. in a strongly repulsive interacting condensation or in semiclassical regime, another scaling of the GPE (3.11) is also very useful. In fact, after a rescaling in (3.11) under the normalization (3.14): $\mathbf{x} \to \varepsilon^{-1/2}\mathbf{x}$ and $\psi \to \varepsilon^{d/4}\psi$ with $\varepsilon = \beta_d^{-2/(d+2)}$, then the GPE (3.11) can be rewritten as

$$i\varepsilon \, \frac{\partial \psi(\mathbf{x},t)}{\partial t} = -\frac{\varepsilon^2}{2}\nabla^2\psi + V_d(\mathbf{x})\psi + |\psi|^2\psi, \quad \mathbf{x} \in \mathbb{R}^d. \tag{3.15}$$

4. The NLSE and variational formulation

Consider the following NLSE:

$$i\psi_t = -\frac{1}{2} \triangle \psi + V(\mathbf{x})\psi + \beta|\psi|^{2\sigma}\psi, \qquad \mathbf{x} \in \mathbb{R}^d, \quad t \geq 0, \tag{4.1}$$

$$\psi(\mathbf{x},0) = \psi_0(\mathbf{x}), \qquad \mathbf{x} \in \mathbb{R}^d, \tag{4.2}$$

where $\sigma > 0$ is a positive constant ($\sigma = 1$ corresponds to a cubic nonlinearity and $\sigma = 2$ corresponds to a quintic nonlinearity), $V(\mathbf{x})$ is a real-valued potential whose shape is determined by the type of system under investigation, β positive/negative corresponds to defocusing/focusing NLSE.

4.1. *Conservation laws*

Two important invariants of (4.1) are the *normalization of the wave function*

$$N(\psi(\cdot,t)) = \int_{\mathbb{R}^d} |\psi(\mathbf{x},t)|^2 \, d\mathbf{x} \equiv N = N(\psi_0), \qquad t \geq 0 \tag{4.3}$$

and the *energy*

$$\begin{aligned} E(\psi(\cdot,t)) &= \int_{\mathbb{R}^d} \left[\frac{1}{2}|\nabla\psi(\mathbf{x},t)|^2 + V(\mathbf{x})|\psi(\mathbf{x},t)|^2 + \frac{\beta}{\sigma+1}|\psi(\mathbf{x},t)|^{2\sigma+2}\right] d\mathbf{x} \\ &= E(\psi_0), \qquad t \geq 0. \end{aligned} \tag{4.4}$$

When $V(\mathbf{x}) \equiv 0$, another important invariant of (4.1) is the *momentum*

$$\mathbf{P}(\psi(\cdot,t)) = \frac{i}{2}\int_{\mathbb{R}^d} (\psi\nabla\psi^* - \psi^*\nabla\psi) \, d\mathbf{x} \equiv \mathbf{P}(\psi_0), \quad t \geq 0. \tag{4.5}$$

Define the *mass center*

$$\bar{\mathbf{x}}(t) = \frac{1}{N}\int_{\mathbb{R}^d} \mathbf{x}|\psi(\mathbf{x},t)|^2 \, d\mathbf{x}. \tag{4.6}$$

Note that the *mass center* obeys

$$N\frac{d\bar{\mathbf{x}}}{dt} = \int \mathbf{x}\partial_t|\psi|^2\, d\mathbf{x} = -\frac{i}{2}\int \mathbf{x}\nabla\cdot[\psi\nabla\psi^* - \psi^* \triangle \psi]\ d\mathbf{x}$$
$$= \frac{i}{2}\int [\psi\nabla\psi^* - \psi^* \triangle \psi]\, d\mathbf{x} = \mathbf{P}(\psi_0) \tag{4.7}$$

and thus moves at a constant speed.

To get more conservation laws, one can use the Noether theorem [113].

4.2. *Lagrangian structure*

Define the Lagrangian density $\mathcal{L}$ associated to (4.1) in terms of the real and imaginary parts u and v of ψ, or equivalently in terms of ψ and ψ^* viewed as independent variables in the form

$$\mathcal{L} = \frac{i}{2}(\psi^*\psi_t - \psi\psi_t^*) - \frac{1}{2}\nabla\psi\cdot\nabla\psi^* - V(\mathbf{x})\psi\psi^* - \frac{\beta}{\sigma+1}\psi^{\sigma+1}(\psi^*)^{\sigma+1}. \tag{4.8}$$

Consider the action

$$\mathcal{S}\{\psi,\psi^*\} = \int_{t_0}^{t_1}\int_{\mathbb{R}^d}\mathcal{L}\ d\mathbf{x}dt \tag{4.9}$$

as a functional on all admissible regular function satisfying the prescribed conditions $\psi(\mathbf{x},t_0) = \psi_0(\mathbf{x})$ and $\psi(\mathbf{x},t_1) = \psi_1(\mathbf{x})$. Its variation

$$\delta\mathcal{S} = \mathcal{S}\{\psi+\delta\psi, \psi^*+\delta\psi^*\} - S\{\psi,\psi^*\} \tag{4.10}$$

for infinitesimal $\delta\psi$ and $\delta\psi^*$ reads

$$\delta\mathcal{S} = \int_{t_0}^{t_1}\int_{\mathbb{R}^d}\left[\frac{\partial\mathcal{L}}{\partial\psi}\delta\psi + \frac{\partial\mathcal{L}}{\partial\nabla\psi}\cdot\nabla\delta\psi + \frac{\partial\mathcal{L}}{\partial\psi_t}\delta\psi_t\right]d\mathbf{x}dt + \text{c.c.}$$
$$= \int_{t_0}^{t_1}\int_{\mathbb{R}^d}\left[\frac{\partial\mathcal{L}}{\partial\psi} - \nabla\cdot\left(\frac{\partial\mathcal{L}}{\partial\nabla\psi}\right) - \partial_t\left(\frac{\partial\mathcal{L}}{\partial\psi_t}\right)\right]\delta\psi\ d\mathbf{x}dt$$
$$+ \left[\frac{\partial\mathcal{L}}{\partial\psi_t}\delta\psi\right]_{t_0}^{t_1} + \text{c.c.} \tag{4.11}$$

A necessary and sufficient condition for a function $\psi(\mathbf{x},t)$ to lead to an extremum for the action $\mathcal{S}$ among the functions with prescribed values $\psi(\cdot,t_0)$ and $\psi(\cdot,t_1)$, thus reduces to the Euler-Lagrange equations

$$\frac{\partial\mathcal{L}}{\partial\psi} = \nabla\cdot\left(\frac{\partial\mathcal{L}}{\partial\nabla\psi}\right) + \partial_t\left(\frac{\partial\mathcal{L}}{\partial\psi_t}\right), \tag{4.12}$$

which, when the Lagrangian (4.8) is used, reduces to the NLSE (4.1). This system is easily rewritten in terms of the real fields $u = (\psi + \psi^*)/2$ and $v = (\psi - \psi^*)/2i$ as

$$\frac{\partial \mathcal{L}}{\partial u} = \nabla \cdot \left(\frac{\partial \mathcal{L}}{\partial \nabla u} \right) + \partial_t \left(\frac{\partial \mathcal{L}}{\partial u_t} \right), \tag{4.13}$$

$$\frac{\partial \mathcal{L}}{\partial v} = \nabla \cdot \left(\frac{\partial \mathcal{L}}{\partial \nabla v} \right) + \partial_t \left(\frac{\partial \mathcal{L}}{\partial v_t} \right). \tag{4.14}$$

4.3. *Hamiltonian structure*

As usual, a Hamiltonian structure is easily derived from the existence of a Lagrangian. Writing $\psi = u + iv$ in order to deal with real fields, the Hamiltonian density $\mathcal{H} = \frac{i}{2}(\psi^* \partial_t \psi - \psi \partial_t \psi^*) - \mathcal{L}$ becomes

$$\mathcal{H} = v \partial_t u - u \partial_t v - \mathcal{L}. \tag{4.15}$$

Introducing the canonical variables

$$q_1 \equiv u, \qquad p_1 \equiv \frac{\partial \mathcal{L}}{\partial(\partial_t q_1)}, \tag{4.16}$$

$$q_2 \equiv v, \qquad p_2 \equiv \frac{\partial \mathcal{L}}{\partial(\partial_t q_2)}, \tag{4.17}$$

it takes the form

$$\mathcal{H} = \sum_j p_j \partial_t q_j - \mathcal{L}. \tag{4.18}$$

Define

$$\rho_j \equiv \frac{\partial \mathcal{L}}{\partial(\nabla q_j)}, \tag{4.19}$$

and rewrite the Euler-Lagrange equations as

$$\frac{\partial \mathcal{L}}{\partial q} = \nabla \cdot \rho_j + \partial_t p_j. \tag{4.20}$$

Using that

$$\partial_t \mathcal{L} = \sum_j \frac{\partial \mathcal{L}}{\partial q_j} \partial_t q_j + \frac{\partial \mathcal{L}}{\partial \nabla q_j} \partial_t \nabla q_j + \frac{\partial \mathcal{L}}{\partial(\partial_t q_j)} \partial_{tt} q_j, \tag{4.21}$$

and the Euler-Lagrange equations, we get

$$\partial_t \mathcal{H} = -\nabla \cdot \sum_j \rho_j \partial_t q_j, \tag{4.22}$$

which ensures that the conservation fo the Hamiltonian or energy $H = \int_{\mathbb{R}^d} \mathcal{H}\, d\mathbf{x}$.

Similarly, from the variation of the Lagrangian density

$$\delta\mathcal{L} = \sum_j \frac{\delta\mathcal{L}}{\delta q_j}\delta q_j + \frac{\delta\mathcal{L}}{\delta\nabla q_j}\nabla\delta q_j + \frac{\delta\mathcal{L}}{\delta(\partial_t q_j)}\partial_t\delta q_j, \tag{4.23}$$

the Euler-Lagrange equations, and the definition of p_j we obtain the variation of the Hamiltonian H, in the form

$$\delta H = \sum_j \int (\partial_t q_j \delta p_j - \partial_t p_j \delta q_j) d\mathbf{x}, \tag{4.24}$$

which leads to the Hamilton equaitons

$$\frac{\partial q_j}{\partial t} = \frac{\delta H}{\delta p_j}, \qquad \frac{\partial p_j}{\partial t} = -\frac{\delta H}{\delta q_j}, \tag{4.25}$$

or in complex form,

$$i\partial_t\psi = \frac{\delta H}{\delta\psi^*}. \tag{4.26}$$

4.4. *Variance identity*

Define the 'variance' (or 'momentum of inertia' in a context where N is referred to as the mass of the wave packet) as

$$\delta_{V} = \int_{\mathbb{R}^d} |\mathbf{x}|^2|\psi|^2\, d\mathbf{x} = \sum_{j=1}^{d}\delta_j,\ \ \delta_j = \int_{\mathbb{R}^d} x_j^2|\psi|^2\, d\mathbf{x},\ \ j = 1, \cdots, d \tag{4.27}$$

and the square width of the wave packet

$$\delta_{\mathbf{x}} = \frac{1}{N}\int_{\mathbb{R}^d} |\mathbf{x}-\bar{\mathbf{x}}|^2|\psi|^2\, d\mathbf{x} = \frac{1}{N}\int_{\mathbb{R}^d} (|\mathbf{x}|^2 - |\bar{\mathbf{x}}|^2)|\psi|^2\, d\mathbf{x} = \frac{\delta_{V}}{N} - |\bar{\mathbf{x}}|^2. \tag{4.28}$$

Here we use $\mathbf{x} = (x_1, \cdots, x_d) \in \mathbb{R}^d$.

When $V(\mathbf{x}) \equiv 0$ in (4.1), due to the conservation of the wave energy N and of the linear momentum $\mathbf{P}$, we have

$$\frac{d^2\delta_{\mathbf{x}}}{dt^2} = \frac{1}{N}\frac{d^2\delta_{V}}{dt^2} - 2\,\frac{|\mathbf{P}|^2}{N^2}. \tag{4.29}$$

Lemma 4.1: *Suppose $\psi(\mathbf{x},t)$ be the solution of the problem (4.1), (4.2), then we have*

$$\frac{d^2\delta_j(t)}{dt^2} = \int_{\mathbb{R}^d}\left[2|\partial_{x_j}\psi|^2 + \frac{2\sigma\beta}{\sigma+1}|\psi|^{2\sigma+2} - 2x_j|\psi|^2\partial_{x_j}(V(\mathbf{x}))\right]d\mathbf{x}, \quad (4.30)$$

$$\delta_j(0) = \delta_j^{(0)} = \int_{\mathbb{R}^d} x_j^2|\psi_0(\mathbf{x})|^2\, d\mathbf{x}, \qquad j = 1,\cdots,d, \quad (4.31)$$

$$\delta_j'(0) = \delta_j^{(1)} = 2\ \mathrm{Im}\left[\int_{\mathbb{R}^d} x_j\psi_0^*\,\partial_{x_j}\psi_0 d\mathbf{x}\right]. \quad (4.32)$$

Proof: Differentiate (4.27) with respect to t, notice (4.1), integrate by parts, we have

$$\begin{aligned}\frac{d\delta_j(t)}{dt} &= \frac{d}{dt}\int_{\mathbb{R}^d} x_j^2|\psi(\mathbf{x},t)|^2\, d\mathbf{x} = \int_{\mathbb{R}^d} x_j^2\left(\psi\,\partial_t\psi^* + \psi^*\,\partial_t\psi\right)\, d\mathbf{x}\\ &= \frac{i}{2}\int_{\mathbb{R}^d} x_j^2\left(\psi^*\triangle\psi - \psi\triangle\psi^*\right)d\mathbf{x}\\ &= i\int_{\mathbb{R}^d} x_j\left(\psi\,\partial_{x_j}\psi^* - \psi^*\,\partial_{x_j}\psi\right)d\mathbf{x}. \qquad (4.33)\end{aligned}$$

Similarly, differentiate (4.33) with respect to t, notice (4.1), integrate by parts, we have

$$\begin{aligned}\frac{d^2\delta_j(t)}{dt^2} &= i\int_{\mathbb{R}^d} x_j\left[\partial_t\psi\,\partial_{x_j}\psi^* + \psi\,\partial_{x_j t}\psi^* - \partial_t\psi^*\,\partial_{x_j}\psi - \psi^*\,\partial_{x_j t}\psi\right]d\mathbf{x}\\ &= \int_{\mathbb{R}^d}\left[2ix_j\left(\partial_t\psi\,\partial_{x_j}\psi^* - \partial_t\psi^*\,\partial_{x_j}\psi\right) + i\left(\psi^*\,\partial_t\psi - \psi\,\partial_t\psi^*\right)\right]d\mathbf{x}\\ &= \int_{\mathbb{R}^d}\Big[-x_j\left(\partial_{x_j}\psi^*\ \triangle\psi + \partial_{x_j}\psi\ \triangle\psi^*\right) - \frac{1}{2}\left(\psi^*\ \triangle\psi + \psi\ \triangle\psi^*\right)\\ &\quad +2x_jV(\mathbf{x})\left(\psi\,\partial_{x_j}\psi^* + \psi^*\,\partial_{x_j}\psi\right) + 2V(\mathbf{x})|\psi|^2 + 2\beta|\psi|^{2\sigma+2}\\ &\quad +2\beta x_j|\psi|^{2\sigma}\left(\psi\,\partial_{x_j}\psi^* + \psi^*\,\partial_{x_j}\psi\right)\Big]d\mathbf{x}\\ &= \int_{\mathbb{R}^d}\Big[2|\partial_{x_j}\psi|^2 - |\nabla\psi|^2 - |\psi|^2\partial_{x_j}\left(2x_jV(\mathbf{x})\right) + |\nabla\psi|^2\\ &\quad -\frac{2\beta}{\sigma+1}|\psi|^{2\sigma+2} + 2V(\mathbf{x})|\psi|^2 + 2\beta|\psi|^{2\sigma+2}\Big]d\mathbf{x}\\ &= \int_{\mathbb{R}^d}\left[2|\partial_{x_j}\psi|^2 + \frac{2\sigma\beta}{\sigma+1}|\psi|^{2\sigma+2} - 2x_j|\psi|^2\,\partial_{x_j}(V(\mathbf{x}))\right]d\mathbf{x}. \qquad (4.34)\end{aligned}$$

Thus we obtain the desired equality (4.30). Setting $t = 0$ in (4.27) and (4.33), we get (4.31) and (4.32) respectively. □

Lemma 4.2: *When $V(\mathbf{x}) \equiv 0$ in the NLSE (4.1), we have*

$$\frac{d^2\delta_{_V}}{dt^2} = 4E(\psi_0) + \frac{2\beta(d\sigma-2)}{\sigma+1}\int_{\mathbb{R}^d} |\psi^{2\sigma+2}\, d\mathbf{x}. \tag{4.35}$$

Proof: Sum (4.30) from $j = 1$ to d, we get

$$\begin{aligned}\frac{d^2\delta_{_V}(t)}{dt^2} &= \sum_{j=1}^{d}\frac{d^2\delta_j(t)}{dt^2} = \sum_{j=1}^{d}\int_{\mathbb{R}^d}\left(2|\partial_{x_j}\psi|^2 + \frac{2\sigma\beta}{\sigma+1}|\psi|^{2\sigma+2}\right)d\mathbf{x}\\ &= \int_{\mathbb{R}^d}\left[2|\nabla\psi|^2 + \frac{2d\sigma\beta}{\sigma+1}|\psi|^{2\sigma+2}\right]d\mathbf{x}\\ &= 4E + \frac{2\beta(\sigma d-2)}{\sigma+1}\int_{\mathbb{R}^d}|\psi|^{2\sigma+2}d\mathbf{x}.\end{aligned} \tag{4.36}$$

Here we use conservation of energy of the NLSE. □

From this lemma, when $V(\mathbf{x}) \equiv 0$ and at critical dimension, i.e. $d\sigma - 2 = 0$, (4.35) reduces to

$$\frac{d^2\delta_{_V}}{dt^2} = 4E, \tag{4.37}$$

leading to

$$\delta_{_V}(t) = 2Et^2 + \delta_{_V}'(0)t + \delta_{_V}(0). \tag{4.38}$$

When the external potential $V(\mathbf{x})$ is chosen as harmonic oscillator (3.13) and $\sigma = 1$ in (4.1), we have

Lemma 4.3: *(i) In 1D without interaction, i.e. $d = 1$ and $\beta = 0$ in (4.1), we have*

$$\delta_x(t) = \frac{E(\psi_0)}{\gamma_x^2} + \left(\delta_x^{(0)} - \frac{E(\psi_0)}{\gamma_x^2}\right)\cos(2\gamma_x t) + \frac{\delta_x^{(1)}}{2\gamma_x}\sin(2\gamma_x t), \qquad t \geq 0. \tag{4.39}$$

(ii) In 2D with radial symmetry, i.e. $d = 2$ and $\gamma_x = \gamma_y := \gamma_r$ in (4.1), for any initial data $\psi_0(x, y)$ in (4.2), we have

$$\delta_r(t) = \frac{E(\psi_0)}{\gamma_r^2} + \left(\delta_r^{(0)} - \frac{E(\psi_0)}{\gamma_r^2}\right)\cos(2\gamma_r t) + \frac{\delta_r^{(1)}}{2\gamma_r}\sin(2\gamma_r t), \qquad t \geq 0, \tag{4.40}$$

where

$$\begin{aligned}&\delta_r(t) = \delta_x(t) + \delta_y(t),\\ &\delta_r^{(0)} := \delta_r(0) = \delta_x(0) + \delta_y(0),\\ &\delta_r^{(1)} := \delta_r'(0) = \delta_x'(0) + \delta_y'(0).\end{aligned}$$

Furthermore, when $d = 2$ and $\gamma_x = \gamma_y$ in (4.1) and the initial data $\psi_0(\mathbf{x})$ in (4.2) satisfying

$$\psi_0(x,y) = f(r)e^{im\theta} \qquad \textit{with} \quad m \in \mathbb{Z} \quad \textit{and } f(0)=0 \textit{ when } m \neq 0, \tag{4.41}$$

we have for $t \geq 0$

$$\begin{aligned}\delta_x(t) = \delta_y(t) &= \frac{1}{2}\delta_r(t) \\ &= \frac{E(\psi_0)}{2\gamma_x^2} + \left(\delta_x^{(0)} - \frac{E(\psi_0)}{2\gamma_x^2}\right)\cos(2\gamma_x t) + \frac{\delta_x^{(1)}}{2\gamma_x}\sin(2\gamma_x t). \end{aligned}\tag{4.42}$$

(iiii) For all other cases, we have for $t \geq 0$

$$\delta_j(t) = \frac{E(\psi_0)}{\gamma_{x_j}^2} + \left(\delta_j^{(0)} - \frac{E(\psi_0)}{\gamma_{x_j}^2}\right)\cos(2\gamma_{x_j} t) + \frac{\delta_j^{(1)}}{2\gamma_{x_j}}\sin(2\gamma_{x_j} t) + g_j(t), \tag{4.43}$$

where $g_j(t)$ is a solution of the following problem

$$\frac{d^2 g_j(t)}{dt^2} + 4\gamma_{x_j}^2 g_j(t) = f_j(t), \qquad g_j(0) = \frac{dg_j(0)}{dt} = 0, \tag{4.44}$$

with

$$f_j(t) = \int_{\mathbb{R}^d}\left[2|\partial_{x_j}\psi|^2 - 2|\nabla\psi|^2 - \beta|\psi|^4 + (2\gamma_{x_j}^2 x_j^2 - 4V(\mathbf{x}))|\psi|^2\right]d\mathbf{x}$$

satisfying

$$|f_\alpha(t)| < 4E_\beta(\psi_0), \qquad t \geq 0.$$

Proof: (i) From (4.30) with $d = 1$ and $\beta_1 = 0$, we have

$$\frac{d^2\delta_x(t)}{dt^2} = 4E(\psi_0) - 4\gamma_x^2\delta_x(t), \qquad t > 0, \tag{4.45}$$

$$\delta_x(0) = \delta_x^{(0)}, \qquad \delta_x'(0) = \delta_x^{(1)}. \tag{4.46}$$

Thus (4.39) is the unique solution of this ordinary differential equation (ODE).

(ii). From (4.30) with $d = 2$, we have

$$\frac{d^2\delta_x(t)}{dt^2} = -2\gamma_x^2\delta_x(t) + \int_{\mathbb{R}^d}\left(2|\partial_x\psi|^2 + \beta|\psi|^4\right)d\mathbf{x}, \tag{4.47}$$

$$\frac{d^2\delta_y(t)}{dt^2} = -2\gamma_y^2\delta_y(t) + \int_{\mathbb{R}^d}\left(2|\partial_y\psi|^2 + \beta|\psi|^4\right)d\mathbf{x}. \tag{4.48}$$

Sum (4.47) and (4.48), notice (4.4) and $\gamma_x = \gamma_y$, we have the ODE for $\delta_r(t)$:

$$\frac{d^2\delta_r(t)}{dt^2} = 4E(\psi_0) - 4\gamma_x^2\delta_r(t), \qquad t > 0, \tag{4.49}$$

$$\delta_r(0) = 2\delta_x^{(0)}, \qquad \delta_r'(0) = 2\delta_x^{(1)}. \tag{4.50}$$

Thus (4.40) is the unique solution of the second order ODE (4.49) with the initial data (4.50). Furthermore, when the initial data $\psi_0(\mathbf{x})$ in (4.2) satisfies (4.41), due to the radial symmetry, the solution $\psi(\mathbf{x}, t)$ of (4.1)-(4.2) satisfies

$$\psi(x, y, t) = g(r, t)e^{im\theta} \qquad \text{with} \quad g(r, 0) = f(r). \tag{4.51}$$

This implies

$$\begin{aligned}
\delta_x(t) &= \int_{\mathbb{R}^2} x^2\, |\psi(x, y, t)|^2\, d\mathbf{x} = \int_0^\infty \int_0^{2\pi} r^2 \cos^2\theta\, |g(r, t)|^2 r\, d\theta dr \\
&= \pi \int_0^\infty r^2 |g(r, t)|^2 r\, dr = \int_0^\infty \int_0^{2\pi} r^2 \sin^2\theta\, |g(r, t)|^2 r\, d\theta dr \\
&= \int_{\mathbb{R}^2} y^2 |\psi(x, y, t)|^2\, d\mathbf{x} = \delta_y(t), \qquad t \geq 0.
\end{aligned} \tag{4.52}$$

Thus the equality (4.42) is a combination of (4.52) and (4.40).

(iii). From (4.30), notice the energy conservation (4.4) of the GPE (4.1), we have

$$\frac{d^2\delta_j(t)}{dt^2} = 4E(\psi_0) - 4\gamma_{x_j}^2\delta_j(t) + f_j(t), \qquad t \geq 0. \tag{4.53}$$

Thus (4.43) is the unique solution of this ODE (4.53). □

5. Plane and solitary wave solutions of NLSE

For simplicity, we assume $V(\mathbf{x}) \equiv 0$, $d = 1$ and $\sigma = 1$ in this section. In this case, the NLSE (4.1) collapses to

$$i\psi_t = -\frac{1}{2}\psi_{xx} + \beta|\psi|^2\psi. \tag{5.1}$$

To find the plane wave solution of (5.1), we take the ansatz

$$\psi = Ae^{i(kx-\omega t)}, \tag{5.2}$$

where A, ω and k are amplitude, angular frequency and wavenumber respectively. Plugging (5.2) into (5.1), we get the dispersive relation

$$\omega = \frac{1}{2}k^2 + \beta|A|^2 \tag{5.3}$$

This implies that the dispersive relation depends on wavenumber and amplitude. Define the group velocity

$$c_g \equiv \frac{d\omega}{dk} = k. \tag{5.4}$$

So the NLSE has the plane wave solution (5.2) provided the dispersive relation is satisfied. In fact, (5.3) can be viewed as zeroth-order approximation of the NLSE (5.1), and (5.2) can be viewed as zeroth-order solution of the NLSE (5.1).

To find the solitary wave solution, we take the ansatz

$$\psi = \phi(\xi) e^{i(kx-\omega t)}, \qquad \xi = x - c_g t, \tag{5.5}$$

where ϕ is a real-valued function. Plugging (5.5) into (5.1), we get

$$\frac{1}{2}\frac{d^2\phi}{d\xi^2} + (\omega - k^2/2)\phi - \beta\phi^3 + i(k - c_g)\frac{d\phi}{d\xi} = 0. \tag{5.6}$$

This implies

$$-\frac{d^2\phi}{d\xi^2} + \gamma\phi + 2\beta\phi^3 = 0, \qquad \gamma = k^2 - 2\omega > 0; \qquad c_g = k. \tag{5.7}$$

When $\beta < 0$, we have a solution for (5.7)

$$\phi(\xi) = \pm\sqrt{\frac{\gamma}{-\beta(2-k^2)}}\,\mathrm{dn}\left(\sqrt{\frac{\gamma}{2-k^2}}(\xi - \xi_0), k\right), \tag{5.8}$$

where dn is the Jacobian elliptic function. Letting $k \to 1$, we have

$$\phi(\xi) = \pm\sqrt{\frac{\gamma}{-\beta}}\,\mathrm{sech}\sqrt{\gamma}(\xi - \xi_0). \tag{5.9}$$

Thus we get a solitary wave solution for the NLSE (5.1) with $\beta < 0$:

$$\psi(x,t) = \sqrt{\frac{\gamma}{-\beta}}\,\mathrm{sech}\sqrt{\gamma}(x - t - x_0)e^{i[x-(1-\gamma)t/2]}, \tag{5.10}$$

where $\gamma > 0$ is a constant.

For $\beta > 0$, one can get a traveling wave in a similar manner.

6. Existence/blowup results of NLSE

For simplicity, in this section, we assume $V(\mathbf{x}) \equiv 0$ in (4.1).

6.1. *Integral form*

When $\beta = 0$ in (4.1), the free Schrödinger equation is solved as

$$\psi(\mathbf{x}, t) = U(t)\psi_0(\mathbf{x}), \qquad \mathbf{x} \in \mathbb{R}^d, \quad t \geq 0, \tag{6.1}$$

where free Schrödinger operator $U(t) = e^{it\triangle/2}$ given by

$$U(t)\psi_0(\mathbf{x}) = \left(\frac{1}{4\pi i t}\right)^{d/2} \int_{\mathbb{R}^d} e^{i\frac{|\mathbf{x}-\mathbf{x}'|^2}{4t}} \psi_0(\mathbf{x}')\, d\mathbf{x}' \tag{6.2}$$

defines a unitary transformation group in L^2.

Theorem 6.1: *(Decay estimates) For conjugate p and p' ($\frac{1}{p} + \frac{1}{p'} = 1$), with $2 \leq p \leq \infty$, and $t \neq 0$, the transformation $U(t)$ maps continuously $L^{p'}(\mathbb{R}^d)$ into $L^p(\mathbb{R}^d)$ and*

$$\|U(t)\psi_0\|_{L^p} \leq (4\pi|t|)^{-d(\frac{1}{2}-\frac{1}{p})} \|\psi_0\|_{L^{p'}}. \tag{6.3}$$

Proof (scratch): Use the conservation of L^2-norm $\|\psi(t)\|_{L^2} = \|\psi_0\|_{L^2}$, the estimate $|\psi(\mathbf{x}, t)| \leq (4\pi|t|)^{-d/2}\|\psi_0\|_{L^1}$ and the Riesz-Thorin interpolation theorem. □

When $\beta \neq 0$ in (4.1), the problem is conveniently rewritten in the integral form

$$\psi(t) = U(t)\psi_0 - i\beta \int_0^t U(t-t')|\psi(t')|^{2\sigma}\psi(t')\, dt'. \tag{6.4}$$

6.2. *Existence results*

Based on a fixed point theorem to (6.4), the following existence results for NLSE is proved [113]:

Theorem 6.2: *(Solution in H^1) For $0 \leq \sigma < \frac{2}{d-2}$ (no condition on σ when $d = 1$ or 2) and an initial condition $\psi_0 \in H^1(\mathbb{R}^d)$, there exists, locally in time, a unique maximal solution ψ in $C((-T^*, T^*), H^1(\mathbb{R}^d))$, where maximal means that if $T^* < \infty$, then $\|\psi\|_{H^1} \to \infty$ as t approaches T^*. In addition, ψ satisfies the normalization and energy (or Hamiltonian) conservation laws*

$$N(\psi) \equiv \int_{\mathbb{R}^d} |\psi|^2\, d\mathbf{x} = N(\psi_0), \tag{6.5}$$

$$E(\psi) \equiv \int_{\mathbb{R}^d} \left[\frac{1}{2}|\nabla\psi|^2 + \frac{\beta}{\sigma+1}|\psi|^{2\sigma+2}\right] d\mathbf{x} = E(\psi_0), \tag{6.6}$$

and depends continuously on the initial condition ψ in H^1.

If in addition, the initial condition ψ_0 belongs to the space $\sum = \{f, f \in H^1(\mathbb{R}^d), |\mathbf{x}f(\mathbf{x})| \in L^2(\mathbb{R}^d)\}$ of the functions in H^1 with finite variance, the above maximal solution belongs to $C((-T^*, T^*), \sum)$. The variance $\delta_{_V}(t) = \int_{\mathbb{R}^d} |\mathbf{x}|^2|\psi|^2\, d\mathbf{x}$ belongs to $C^2(-T^*, T^*)$ and satisfies the identity

$$\frac{d^2\delta_{_V}}{dt^2} = 4E(\psi_0) + \frac{2\beta(d\sigma - 2)}{\sigma + 1}\int_{\mathbb{R}^d} |\psi|^{2\sigma+2}\, d\mathbf{x}. \tag{6.7}$$

Theorem 6.3: *(Solution in L^2) For $0 \le \sigma < \frac{2}{d}$ and an initial condition $\psi_0 \in L^2(\mathbb{R}^d)$, there exist a unique solution ψ in $C((-T^*, T^*), L^2(\mathbb{R}^d)) \cap L^q((-T^*, T^*), L^{2\sigma+2}(\mathbb{R}^d))$ with $q = \frac{4(\sigma+1)}{d\sigma}$, satisfying the L^2-norm conservation law (6.5).*

Theorem 6.4: *(Global existence in H^1) Assume $0 \le \sigma < 2/(d-2)$ if $\beta < 0$ (attractive nonlinearity), or $0 \le \sigma < 2/d$ if $\beta > 0$ (repulsive nonlinearity). For any $\psi \in H^1(\mathbb{R}^d)$, there exists a unique solution ψ in $C(\mathbb{R}, H^1(\mathbb{R}^d))$. It satisfies the conservation laws (6.5) and (6.6) and depends continuously on initial conditions in $H^1(\mathbb{R}^d)$.*

Theorem 6.5: *(Global existence in L^2) For $0 \le \sigma < 2/d$ and $\psi_0 \in L^2(\mathbb{R}^d)$, there exists a unique solution ψ in $C(\mathbb{R}, L^2(\mathbb{R}^d)) \cap L^q_{\text{loc}}(\mathbb{R}, L^{2\sigma+2}(\mathbb{R}^d))$ with $q = 4(\sigma+1)/d\sigma$ that satisfies the L^2-norm conservation (6.5) and depends continuously on initial conditions in L^2.*

6.3. *Finite time blowup results*

Classical blowup results are based on the "variance identity", also known as the "viral theorem", and "uncertainty principle". Define the variance $\delta_{_V}(t) = \int_{\mathbb{R}^d} |\mathbf{x}|^2|\psi|^2\, d\mathbf{x}$, we have the identity

$$\frac{d^2}{dt^2}\delta_{_V}(t) = 4E + \frac{2\beta(d\sigma - 2)}{\sigma + 1}\int_{\mathbb{R}^d} |\psi|^{2\sigma+2}\, d\mathbf{x}. \tag{6.8}$$

Theorem 6.6: *Suppose that $\beta < 0$ and $d\sigma \ge 2$. Consider an initial condition $\psi_0 \in H^1$ with $\delta_{_V}(0)$ finite that satisfies one of the conditions below:*
(i) $E(\psi_0) < 0$,
(ii) $E(\psi_0) = 0$ and $\delta'_{_V}(0) = 2\, \mathrm{Re} \int_{\mathbb{R}^d} \psi_0^*(\mathbf{x} \cdot \nabla\psi_0) d\mathbf{x} < 0$,
(iii) $E(\psi_0) > 0$ and $\left|\delta'_{_V}(0)\right| \ge 2\sqrt{2E(\psi_0)\delta_{_V}(0)} = 2\sqrt{2E(\psi_0)}\|\mathbf{x}\psi_0\|_{L^2}$.
Then, there exists a time $t_* < \infty$ such that

$$\lim_{t\to t_*} \|\nabla\psi\|_{L^2} = \infty \qquad \text{and} \qquad \lim_{t\to t_*} \|\psi\|_{L^\infty} = \infty. \tag{6.9}$$

Proof: If $\beta < 0$ and $d\sigma \geq 2$,

$$\frac{d^2}{dt^2}\delta_V(t) \leq 4E, \tag{6.10}$$

and by time integration,

$$\delta_V(t) \leq 2Et^2 + \delta_V'(0)t + \delta_V(0). \tag{6.11}$$

Under any of the hypotheses (i)-(iii) of the above theorem, there exists a time t_0 such that the right-hand side of (6.11) vanishes, and thus also $t_1 \leq t_0$ such that

$$\lim_{t\to t_1} \delta_V(t) = 0. \tag{6.12}$$

Furthermore, from the equality

$$\int_{\mathbb{R}^d} |f|^2 \, d\mathbf{x} = \frac{1}{d}\int_{\mathbb{R}^d} (\nabla\cdot\mathbf{x})|f|^2 \, d\mathbf{x} = -\frac{1}{d}\int_{\mathbb{R}^d} \mathbf{x}\cdot\nabla(|f|^2)\, d\mathbf{x}, \tag{6.13}$$

one gets the "uncertainty principle"

$$\|f\|_{L^2}^2 \leq \frac{2}{d}\|\nabla f\|_{L^2}\ \|\mathbf{x}f\|_{L^2}. \tag{6.14}$$

When this inequality is applied to a solution ψ, one gets from (6.14) and from the conservation of $\|\psi\|_{L^2}^2$, that there exists a time $t_* \leq t_1$ such that $\lim_{t\to t_*}\|\nabla\psi\|_{L^2} = \infty$. The conservation of E then ensures that $\lim_{t\to t_*}\|\psi\|_{L^{2\sigma+2}}^{2\sigma+2} = \infty$, and since $\|\psi\|_{L^2}^2$ is conserved, this implies that $\lim_{t\to t_*}\|\psi\|_{L^\infty} = \infty$. $\square$

7. WKB expansion and quantum hydrodynamics

In this section, we consider the NLSE in semiclassical regime

$$i\varepsilon\psi_t^\varepsilon = -\frac{\varepsilon^2}{2}\triangle\psi^\varepsilon + V(\mathbf{x})\psi^\varepsilon + f(|\psi^\varepsilon|^2)\psi^\varepsilon, \qquad \mathbf{x}\in\mathbb{R}^d, \quad t\geq 0, \tag{7.1}$$

$$\psi^\varepsilon(\mathbf{x},0) = \psi_0^\varepsilon(\mathbf{x}), \qquad \mathbf{x}\in\mathbb{R}^d, \tag{7.2}$$

where $0 < \varepsilon \ll 1$ is the (scaled) Planck constant, $f(\rho)$ is a given real-valued function; and find its semiclassical limit by using WKB expansion.

Suppose that the initial datum ψ_0^ε in (7.2) is rapidly oscillating on the scale ε, given in WKB form:

$$\psi_0^\varepsilon(\mathbf{x}) = A_0(\mathbf{x})\exp\left(\frac{i}{\varepsilon}S_0(\mathbf{x})\right), \qquad \mathbf{x}\in\mathbb{R}^d, \tag{7.3}$$

where the amplitude A_0 and the phase S_0 are smooth real-valued functions. Plugging the radial-representation of the wave-function

$$\psi^\varepsilon(\mathbf{x},t) = A^\varepsilon(\mathbf{x},t)\exp\left(\frac{i}{\varepsilon}S^\varepsilon(\mathbf{x},t)\right) = \sqrt{\rho^\varepsilon(\mathbf{x},t)}\exp\left(\frac{i}{\varepsilon}S^\varepsilon(\mathbf{x},t)\right) \quad (7.4)$$

into (7.1), one obtains the following quantum hydrodynamic (QHD) form of the NLSE for $\rho^\varepsilon = |A^\varepsilon|^2$, $\mathbf{J}^\varepsilon = \rho^\varepsilon \nabla S^\varepsilon$ [58, 41, 79]

$$\rho_t^\varepsilon + \text{div}\, \mathbf{J}^\varepsilon = 0, \quad (7.5)$$

$$\mathbf{J}_t^\varepsilon + \text{div}\left(\frac{\mathbf{J}^\varepsilon \otimes \mathbf{J}^\varepsilon}{\rho^\varepsilon}\right) + \nabla P(\rho^\varepsilon) + \rho^\varepsilon \nabla V = \frac{\varepsilon^2}{4}\text{div}(\rho^\varepsilon \nabla^2 \log \rho^\varepsilon); \quad (7.6)$$

with initial data

$$\rho^\varepsilon(\mathbf{x},0) = \rho_0^\varepsilon(\mathbf{x}) = |A_0(\mathbf{x})|^2,\ \mathbf{J}^\varepsilon(\mathbf{x},0) = \rho_0^\varepsilon(\mathbf{x})\,\nabla S_0(\mathbf{x}) = |A_0(\mathbf{x})|^2\,\nabla S_0(\mathbf{x}), \quad (7.7)$$

(see Grenier [66], Jüngel [79, 80], for mathematical analyses of this system). Here the hydrodynamic pressure $P(\rho)$ is related to the nonlinear potential $f(\rho)$ by

$$P(\rho) = \rho f(\rho) - \int_0^\rho f(s)\,ds, \quad (7.8)$$

i.e. f' is the enthalpy. Letting $\varepsilon \to 0+$, one obtains formally the following Euler system

$$\rho_t + \text{div}\, \mathbf{J} = 0, \quad (7.9)$$

$$\mathbf{J}_t + \text{div}\left(\frac{\mathbf{J}\otimes\mathbf{J}}{\rho}\right) + \nabla P(\rho) + \rho\nabla V = 0. \quad (7.10)$$

which can be viewed formally as the dispersive (semiclassical) limit of the NLSE (7.1). In the case $f' > 0$ we expect (7.9), (7.10) to be the 'rigorous' semiclassical limit of (7.1) as long as caustics do not occur, i.e. in the pre-breaking regime. After caustics the dispersive behavior of the NLSE takes over and (7.9), (7.10) is not correct any more.

8. Wigner transform and semiclassical limit

In this section, we consider the linear Schrödinger equation in semiclassical regime

$$i\varepsilon\psi_t^\varepsilon = -\frac{\varepsilon^2}{2}\triangle\psi^\varepsilon + V(\mathbf{x})\psi^\varepsilon, \qquad \mathbf{x}\in\mathbb{R}^d, \quad t\geq 0, \quad (8.1)$$

$$\psi^\varepsilon(\mathbf{x},0) = \psi_0^\varepsilon(\mathbf{x}), \qquad \mathbf{x}\in\mathbb{R}^d, \quad (8.2)$$

and find its semiclassical limit by using Wigner transformation.

Let $f, g \in L^2(\mathbb{R}^d)$. Then the Wigner-transform of (f, g) on the scale $\varepsilon > 0$ is defined as the phase-space function:

$$w^\varepsilon(f,g)(\mathbf{x},\xi) = \frac{1}{(2\pi)^d}\int_{\mathbb{R}^d} f^*\left(\mathbf{x}+\frac{\varepsilon}{2}\mathbf{y}\right)\ g\left(\mathbf{x}-\frac{\varepsilon}{2}\mathbf{y}\right) e^{i\mathbf{y}\cdot\xi}\ d\mathbf{y} \tag{8.3}$$

(cf. [58], [91] for a detailed analysis of the Wigner-transform). It is well-known that the estimate

$$\|w^\varepsilon(f,g)\|_{\mathcal{E}^*} \le \|f\|_{L^2(\mathbb{R}^d)}\ \|g\|_{L^2(\mathbb{R}^d)} \tag{8.4}$$

holds, where $\mathcal{E}$ is the Banach space

$$\mathcal{E} := \{\phi \in C_0(\mathbb{R}^d_{\mathbf{x}} \times \mathbb{R}^d_\xi)\ :\ (\mathcal{F}_{\xi\to\mathbf{v}}\phi)(\mathbf{x},\mathbf{v}) \in L^1(\mathbb{R}^d_{\mathbf{v}}; C_0(\mathbb{R}^d_{\mathbf{x}}))\},$$
$$\|\phi\|_{\mathcal{E}} := \int_{\mathbb{R}^d_{\mathbf{v}}} \sup_{\mathbf{x}\in\mathbb{R}^d_{\mathbf{x}}} |(\mathcal{F}_{\xi\to\mathbf{v}}\phi)(\mathbf{x},\mathbf{v})|\ d\mathbf{v},$$

(cf. [91]). $\mathcal{E}^*$ denotes the dual space of $\mathcal{E}$ and $(\mathcal{F}_{\xi\to\mathbf{v}}\sigma)(\mathbf{v}) := \int_{\mathbb{R}^d_\xi} \sigma(\xi)\ e^{-i\mathbf{v}\cdot\xi}\ d\xi$ the Fourier transform.

Now let $\psi^\varepsilon(t)$ be the solution of the linear Schrödinger equation (8.1), (8.2) and denote

$$w^\varepsilon(t) := w^\varepsilon(\psi^\varepsilon(t), \psi^\varepsilon(t)). \tag{8.5}$$

Then w^ε satisfies the Wigner equation

$$w^\varepsilon_t + \xi\cdot\nabla_{\mathbf{x}} w^\varepsilon + \Theta^\varepsilon[V]w^\varepsilon = 0, \qquad (\mathbf{x},\xi) \in \mathbb{R}^d_{\mathbf{x}} \times \mathbb{R}^d_\xi, \quad t \in \mathbb{R}, \tag{8.6}$$
$$w^\varepsilon(t=0) = w^\varepsilon(\psi^\varepsilon_0, \psi^\varepsilon_0), \tag{8.7}$$

where $\Theta^\varepsilon[V]$ is the pseudo-differential operator:

$$\Theta^\varepsilon[V]w^\varepsilon(\mathbf{x},\xi,t) := \frac{i}{(2\pi)^d}\int_{\mathbb{R}^d_\alpha} \frac{V(\mathbf{x}+\frac{\varepsilon}{2}\alpha) - V(\mathbf{x}-\frac{\varepsilon}{2}\alpha)}{\varepsilon}\ \hat{w}^\varepsilon(\mathbf{x},\alpha,t) e^{i\alpha\cdot\xi} d\alpha, \tag{8.8}$$

here $\hat{w}^\varepsilon$ stands for the Fourier-transform

$$\mathcal{F}_{\xi\to\alpha}\ w^\varepsilon(\mathbf{x},\cdot,t) := \int_{\mathbb{R}^d_\xi} w^\varepsilon(\mathbf{x},\xi,t) e^{-i\alpha\cdot\xi}\ d\xi.$$

The main advantage of the formulation (8.6), (8.7) is that the semiclassical limit $\varepsilon \to 0$ can easily be carried out. Taking ε to 0 gives the Vlasov-equation (or Liouville equation):

$$w^0_t + \xi\cdot\nabla_{\mathbf{x}} w^0 - \nabla_{\mathbf{x}} V(\mathbf{x})\cdot\nabla_\xi w^0 = 0,\ (\mathbf{x},\xi) \in \mathbb{R}^d_{\mathbf{x}} \times \mathbb{R}^d_\xi,\ t \in \mathbb{R}, \tag{8.9}$$
$$w^0(t=0) = w_0 := \lim_{\varepsilon\to 0} w^\varepsilon(\psi^\varepsilon_0, \psi^\varepsilon_0), \tag{8.10}$$

(cf. [58], [91]), where

$$w^0 := \lim_{\varepsilon\to 0} w^\varepsilon.$$

Here, the limits hold in an appropriate weak sense (i.e. in $\mathcal{E}^* - \omega^*$) and have to be understood for subsequences $(\varepsilon_{n_k}) \to 0$ of sequence ε_n. We recall that w_0, $w^0(t)$ are positive bounded measures on the phase-space $\mathbb{R}^d_{\mathbf{x}} \times \mathbb{R}^d_\xi$.

When the initial Wigner distribution has the high frequency form

$$w_0 = |A_0(\mathbf{x})|^2 \delta(\xi - \nabla S_0(\mathbf{x})), \tag{8.11}$$

then it is easy to see that the solution of (8.9) is given that

$$w^0(\mathbf{x}, \xi, t) = |A(\mathbf{x}, t)|^2 \delta(\xi - \nabla S(\mathbf{x}, t)), \tag{8.12}$$

where $A(\mathbf{x}, t)$ is the solution of the transport equation

$$(|A|^2)_t + \nabla \cdot (|A|^2 \nabla S) = 0, \qquad |A(\mathbf{x}, 0)|^2 = |A_0(\mathbf{x})|^2 \tag{8.13}$$

and $S(\mathbf{x}, t)$ is the solution of the Eiconal equation

$$S_t + \frac{1}{2}|\nabla S|^2 + V(\mathbf{x}) = 0, \qquad S(\mathbf{x}, 0) = S_0(\mathbf{x}). \tag{8.14}$$

Define the moments

$$\rho(\mathbf{x}, t) = \int_{\mathbb{R}^d_\xi} w^0(\mathbf{x}, \xi, t)\, d\xi, \tag{8.15}$$

$$\mathbf{J}(\mathbf{x}, t) = \int_{\mathbb{R}^d_\xi} \xi w^0(\mathbf{x}, \xi, t)\, d\xi. \tag{8.16}$$

Then ρ and $\mathbf{J}$ satisfy the pressureless Euler equation:

$$\rho_t + \mathrm{div}\, \mathbf{J} = 0, \tag{8.17}$$

$$\mathbf{J}_t + \mathrm{div}\, \left(\frac{\mathbf{J} \otimes \mathbf{J}}{\rho}\right) + \rho \nabla V = 0; \tag{8.18}$$

with initial data

$$\rho(\mathbf{x}, 0) = \rho_0(\mathbf{x}) = |A_0(\mathbf{x})|^2,\ \mathbf{J}(\mathbf{x}, 0) = \rho_0(\mathbf{x})\, \nabla S_0(\mathbf{x}) = |A_0(\mathbf{x})|^2\, \nabla S_0(\mathbf{x}). \tag{8.19}$$

9. Ground, excited and central vortex states of GPE

For simplicity, in this section, we take $\sigma = 1$ and the potential $V(\mathbf{x})$ as a harmonic oscillator (4.1), i.e. NLSE is considered in terms of BEC setup.

9.1. *Stationary states*

To find a stationary solution of (4.1), we write

$$\psi(\mathbf{x},t) = e^{-i\mu t}\phi(\mathbf{x}), \tag{9.1}$$

where μ is the chemical potential and ϕ is a function independent of time. Inserting (9.1) into (4.1) gives the following equation for $\phi(\mathbf{x})$

$$\mu\, \phi(\mathbf{x}) = -\frac{1}{2} \triangle\, \phi(\mathbf{x}) + V(\mathbf{x})\, \phi(\mathbf{x}) + \beta|\phi(\mathbf{x})|^2\phi(\mathbf{x}), \qquad \mathbf{x}\in\mathbb{R}^d, \tag{9.2}$$

under the normalization condition

$$\|\phi\|^2 = \int_{\mathbb{R}^d} |\phi(\mathbf{x})|^2\, d\mathbf{x} = 1. \tag{9.3}$$

This is a nonlinear eigenvalue problem under a constraint and any eigenvalue μ can be computed from its corresponding eigenfunction ϕ by

$$\begin{aligned}\mu = \mu(\phi) &= \int_{\mathbb{R}^d} \left[\frac{1}{2}\left|\nabla\phi(\mathbf{x})\right|^2 + V(\mathbf{x})\left|\phi(\mathbf{x})\right|^2 + \beta\left|\phi(\mathbf{x})\right|^4\right] d\mathbf{x} \\ &= E(\phi) + \int_{\mathbb{R}^d} \frac{\beta}{2}\left|\phi(\mathbf{x})\right|^4\, d\mathbf{x}. \end{aligned}\tag{9.4}$$

In fact, the eigenfunctions of (9.2) under the constraint (9.3) are equivalent to the critical points of the energy functional over the unit sphere $S = \{\phi \mid \|\phi\| = 1, E(\phi) < \infty\}$. Furthermore, as noted in [6], they are equivalent to the steady state solutions of the following continuous normalized gradient flow (CNGF):

$$\partial_t\phi = \frac{1}{2}\triangle\,\phi - V(\mathbf{x})\phi - \beta\,|\phi|^2\phi + \frac{\mu(\phi)}{\|\phi(\cdot,t)\|^2}\,\phi,\ \ \mathbf{x}\in\mathbb{R}^d,\ \ t\geq 0, \tag{9.5}$$

$$\phi(\mathbf{x},0) = \phi_0(\mathbf{x}), \quad \mathbf{x}\in\mathbb{R}^d \qquad \text{with} \qquad \|\phi_0\| = 1. \tag{9.6}$$

9.2. *Ground state*

The BEC ground state wave function $\phi_g(\mathbf{x})$ is found by minimizing the energy functional $E(\phi)$ over the unit sphere $S = \{\phi \mid \|\phi\| = 1, E(\phi) < \infty\}$:

(V) Find $(\mu_\beta^g, \phi_\beta^g \in S)$ such that

$$E_\beta^g = E(\phi_\beta^g) = \min_{\phi\in S}\ E(\phi), \qquad \mu_\beta^g = \mu(\phi_\beta^g) = E(\phi_\beta^g) + \int_{\mathbb{R}^d} \frac{\beta}{2}|\phi_\beta^g|^2\, d\mathbf{x}. \tag{9.7}$$

In the case of a defocusing condensate, i.e. $\beta \geq 0$, the energy functional $E(\phi)$ is positive, coercive and weakly lower semicontinuous on S, thus the existence of a minimum follows from the standard theory. For understanding the uniqueness question note that $E(\alpha\phi_\beta^g) = E(\phi_\beta^g)$ for all $\alpha \in \mathbb{C}$ with $|\alpha| = 1$. Thus an additional constraint has to be introduced to show uniqueness. For non-rotating BECs, the minimization problem (9.7) has a unique real valued nonnegative ground state solution $\phi_\beta^g(\mathbf{x}) > 0$ for $\mathbf{x} \in \mathbb{R}^d$ [87].

When $\beta = 0$, the ground state solution is given explicitly [5]

$$\mu_0^g = \frac{1}{2}\begin{cases} \gamma_x, & d = 1, \\ \gamma_x + \gamma_y, & d = 2, \\ \gamma_x + \gamma_y + \gamma_z, & d = 3, \end{cases} \tag{9.8}$$

$$\phi_0^g(\mathbf{x}) = \frac{1}{\pi^{d/4}}\begin{cases} \gamma_x^{1/4} e^{-\gamma_x x^2/2}, & d = 1, \\ (\gamma_x\gamma_y)^{1/4} e^{-(\gamma_x x^2 + \gamma_y y^2)/2}, & d = 2, \\ (\gamma_x\gamma_y\gamma_z)^{1/4} e^{-(\gamma_x x^2 + \gamma_y y^2 + \gamma_z z^2)/2}, & d = 3. \end{cases} \tag{9.9}$$

In fact, this solution can be viewed as an approximation of the ground state for weakly interacting condensate, i.e. $|\beta_d| \ll 1$. For a condensate with strong repulsive interaction, i.e. $\beta \gg 1$ and $\gamma_\alpha = O(1)$ $(\alpha = x, y, z)$, the ground state can be approximated by the Thomas-Fermi approximation in this regime [5]:

$$\phi_\beta^{\mathrm{TF}}(\mathbf{x}) = \begin{cases} \sqrt{(\mu_\beta^{\mathrm{TF}} - V(\mathbf{x}))/\beta}, & V(\mathbf{x}) < \mu_\beta^{\mathrm{TF}}, \\ 0, & \text{otherwise}, \end{cases} \tag{9.10}$$

$$\mu_\beta^{\mathrm{TF}} = \frac{1}{2}\begin{cases} (3\beta\gamma_x/2)^{2/3}, & d = 1, \\ (4\beta\gamma_x\gamma_y/\pi)^{1/2}, & d = 2, \\ (15\beta\gamma_x\gamma_y\gamma_z/4\pi)^{2/5}, & d = 3. \end{cases} \tag{9.11}$$

Due to ϕ_β^{TF} is not differentiable at $V(\mathbf{x}) = \mu_\beta^{\mathrm{TF}}$, as noticed in [5, 8], $E(\phi_\beta^{\mathrm{TF}}) = \infty$ and $\mu(\phi_\beta^{\mathrm{TF}}) = \infty$. This shows that we **can't** use (4.4) to define the energy of the Thomas-Fermi approximation (9.10). How to define the energy of the Thomas-Fermi approximation is not clear in the literatures. Using (9.4), (9.11) and (9.10), here we present a way to define the energy of the Thomas-Fermi approximation (9.10):

$$\begin{aligned} E_\beta^{\mathrm{TF}} &= \mu_\beta^{\mathrm{TF}} - \int_{\mathbb{R}^d} \frac{\beta}{2}|\phi_\beta^{\mathrm{TF}}(\mathbf{x})|^4\, d\mathbf{x} = \int_{\mathbb{R}^d} \left[V(\mathbf{x})|\phi_\beta^{\mathrm{TF}}(\mathbf{x})|^2 + \frac{\beta}{2}|\phi_\beta^{\mathrm{TF}}(\mathbf{x})|^4\right] d\mathbf{x} \\ &= \frac{d+2}{d+4}\, \mu_\beta^{\mathrm{TF}}, \qquad d = 1, 2, 3. \end{aligned} \tag{9.12}$$

From the numerical results in [6, 5], when $\gamma_x = O(1)$, $\gamma_y = O(1)$ and $\gamma_z = O(1)$, we can get

$$E_\beta^g - E_\beta^{\mathrm{TF}} = E(\phi_\beta^g) - E_\beta^{\mathrm{TF}} \to 0, \qquad \text{as} \quad \beta_d \to \infty.$$

Any eigenfunction $\phi(\mathbf{x})$ of (9.2) under constraint (9.3) whose energy $E(\phi) > E(\phi_\beta^g)$ is usually called as excited states in physical literatures.

9.3. *Central vortex states*

To find central vortex states in 2D with radial symmetry, i.e. $d = 2$ and $\gamma_x = \gamma_y = 1$ in (4.1), we write

$$\psi(\mathbf{x}, t) = e^{-i\mu_m t}\phi_m(x, y) = e^{-i\mu_m t}\phi_m(r)e^{im\theta}, \tag{9.13}$$

where (r, θ) is the polar coordinate, $m \neq 0$ is an integer and called as index or winding number, μ_m is the chemical potential, and $\phi_m(r)$ is a real function independent of time. Inserting (9.13) into (4.1) gives the following equation for $\phi_m(r)$ with $0 < r < \infty$

$$\mu_m\ \phi_m(r) = \left[-\frac{1}{2r}\frac{d}{dr}\left(r\frac{d}{dr}\right) + \frac{1}{2}\left(r^2 + \frac{m^2}{r^2}\right) + \beta_2|\phi_m|^2\right]\phi_m, \tag{9.14}$$

$$\phi_m(0) = 0, \qquad \lim_{r\to\infty}\phi_m(r) = 0. \tag{9.15}$$

under the normalization condition

$$2\pi\int_0^\infty |\phi_m(r)|^2\ r\ dr = 1. \tag{9.16}$$

In order to find the central vortex state $\phi_\beta^m(x, y) = \phi_\beta^m(r)e^{im\theta}$ with index m, we find a real nonnegative function $\phi_\beta^m(r)$ which minimizes the energy functional

$$\begin{aligned} E^m(\phi(r)) &= E(\phi(r)e^{im\theta}) \\ &= \pi\int_0^\infty \left[|\phi'(r)|^2 + \left(r^2 + \frac{m^2}{r^2}\right)|\phi(r)|^2 + \beta_2|\phi(r)|^4\right] rdr, \end{aligned} \tag{9.17}$$

over the set $S_0 = \{\phi \mid 2\pi\int_0^\infty |\phi(r)|^2 r\ dr = 1,\ \phi(0) = 0,\ E^m(\phi) < \infty\}$. The existence and uniqueness of nonnegative minimizer for this minimization problem can be obtained similarly as for the ground state [87]. Note that the set $S_m = \{\phi(r)e^{im\theta} \mid \phi \in S_0\} \subset S$ is a subset of the unit sphere, so $\phi_\beta^m(r)e^{im\theta}$ is a minimizer of the energy functional E_β over the set $S_m \subset S$. When $\beta_2 = 0$ in (4.1), $\phi_0^m(r) = \frac{1}{\sqrt{\pi|m|!}}r^{|m|}e^{-r^2/2}$ [6].

Similarly, in order to find central vortex line states in 3D with cylindrical symmetry, i.e. $d = 3$ and $\gamma_x = \gamma_y = 1$ in (4.1), we write

$$\psi(\mathbf{x}, t) = e^{-i\mu_m t}\phi_m(x, y, z) = e^{-i\mu_m t}\phi_m(r, z)e^{im\theta}, \tag{9.18}$$

where $m \neq 0$ is an integer and called as index, μ_m is the chemical potential, and $\phi_m(r,z)$ is a real function independent of time. Inserting (9.18) into (4.1) with $d=3$ gives the following equation for $\phi_m(r,z)$

$$\mu_m\ \phi_m = \left[-\frac{1}{2r}\frac{\partial}{\partial r}\left(r\frac{\partial}{\partial r}\right) - \frac{\partial^2}{2\ \partial z^2} + \frac{1}{2}\left(r^2 + \frac{m^2}{r^2} + \gamma_z^2 z^2\right) + \beta_3|\phi_m|^2\right]\phi_m, \quad (9.19)$$

$$\phi_m(0,z) = 0, \qquad \lim_{r\to\infty}\phi_m(r,z) = 0, \qquad -\infty < z < \infty, \quad (9.20)$$

$$\lim_{|z|\to\infty}\phi_m(r,z) = 0, \qquad 0 \le r < \infty, \quad (9.21)$$

under the normalization condition

$$2\pi\int_0^\infty\int_{-\infty}^\infty |\phi_m(r,z)|^2\ r\ drdz = 1. \quad (9.22)$$

In order to find the central vortex line state $\phi_\beta^m(x,y,z) = \phi_\beta^m(r,z)e^{im\theta}$ with index m, we find a real nonnegative function $\phi_\beta^m(r,z)$ which minimizes the energy functional

$$E^m(\phi(r,z)) = E(\phi(r,z)e^{im\theta}) \quad (9.23)$$
$$= \pi\int_0^\infty\int_{-\infty}^\infty\left[|\partial_r\phi|^2 + |\partial_z\phi|^2 + \left(r^2 + \gamma_z^2 z^2 + \frac{m^2}{r^2}\right)|\phi|^2 + \beta_3|\phi|^4\right] r\ drdz,$$

over the set $S_0 = \{\phi \mid 2\pi\int_0^\infty\int_{-\infty}^\infty |\phi(r,z)|^2 r\ drdz = 1,\ \phi(0,z) = 0,\ -\infty < z < \infty,\ E_\beta^m(\phi) < \infty\}$. The existence and uniqueness of nonnegative minimizer for this minimization problem can be obtained similarly as for the ground state [87]. Note that the set $S_m = \{\phi(r,z)e^{im\theta} \mid \phi \in S_0\} \subset S$ is a subset of the unit sphere, so $\phi_\beta^m(r,z)e^{im\theta}$ is a minimizer of the energy functional E_β over the set S_m. When $\beta_3 = 0$ in (3.11), $\phi_0^m(r,z) = \frac{\gamma_z^{1/4}}{\pi^{3/4}\sqrt{|m|!}} r^{|m|} e^{-(r^2+\gamma_z z^2)/2}$ [6].

9.4. *Variation of stationary states over the unit sphere*

For the stationary states of (9.2), we have the following lemma:

Lemma 9.1: *Suppose $\beta = 0$ and $V(\mathbf{x}) \ge 0$ for $\mathbf{x} \in \mathbb{R}^d$, we have*

(i) The ground state ϕ_g is a global minimizer of $E(\phi)$ over S.

(ii) Any excited state ϕ_j is a saddle point of $E(\phi)$ over S.

Proof: Let ϕ_e be an eigenfunction of the eigenvalue problem (9.2) and (9.3). The corresponding eigenvalue is μ_e. For any function ϕ such that $E(\phi) < \infty$

and $\|\phi_e+\phi\|=1$, notice (9.3), we have that

$$\|\phi\|^2 = \|\phi+\phi_e-\phi_e\|^2 = \|\phi+\phi_e\|^2 - \|\phi_e\|^2 - \int_{\mathbb{R}^d} (\phi^*\phi_e + \phi\phi_e^*)\ d\mathbf{x}$$
$$= -\int_{\mathbb{R}^d} (\phi^*\phi_e + \phi\phi_e^*)\ d\mathbf{x}. \tag{9.24}$$

From (4.4) with $\psi=\phi_e+\phi$ and $\beta=0$, notice (9.3) and (9.24), integration by parts, we get

$$\begin{aligned}
E(\phi_e+\phi) &= \int_{\mathbb{R}^d} \left[\frac{1}{2}|\nabla\phi_e+\nabla\phi|^2 + V(\mathbf{x})|\phi_e+\phi|^2\right]\ d\mathbf{x}\\
&= \int_{\mathbb{R}^d} \left[\frac{1}{2}|\nabla\phi_e|^2 + V(\mathbf{x})|\phi_e|^2\right] + \int_{\mathbb{R}^d} \left[\frac{1}{2}|\nabla\phi|^2 + V(\mathbf{x})|\phi|^2\right]\ d\mathbf{x}\\
&\quad + \int_{\mathbb{R}^d} \left[\left(-\frac{1}{2}\triangle\phi_e + V(\mathbf{x})\phi_e\right)^*\phi + \left(-\frac{1}{2}\triangle\phi_e + V(\mathbf{x})\phi_e\right)\phi^*\right]\ d\mathbf{x}\\
&= E(\phi_e) + E(\phi) + \int_{\mathbb{R}^d} (\mu_e\phi_e^* + \mu_e\phi_e\phi^*)\ d\mathbf{x}\\
&= E(\phi_e) + E(\phi) - \mu_e\|\phi\|^2\\
&= E(\phi_e) + [E(\phi/\|\phi\|) - \mu_e]\,\|\phi\|^2.
\end{aligned} \tag{9.25}$$

(i) Taking $\phi_e=\phi_g$ and $\mu_e=\mu_g$ in (9.25) and noticing $E(\phi/\|\phi\|)\ge E(\phi_g)=\mu_g$ for any $\phi\ne 0$, we get immediately that ϕ_g is a global minimizer of $E(\phi)$ over S.

(ii). Taking $\phi_e=\phi_j$ and $\mu_e=\mu_j$ in (9.25), since $E(\phi_g)<E(\phi_j)$ and it is easy to find an eigenfunction ϕ of (9.2) such that $E(\phi)>E(\phi_j)$, we get immediately that ϕ_j is a saddle point of the functional $E(\phi)$ over S. □

9.5. *Conservation of angular momentum expectation*

Another important quantity for studying dynamics of BEC in 2&3d, especially for measuring the appearance of vortex, is the angular momentum expectation value defined as

$$\langle L_z\rangle(t) := \int_{\mathbb{R}^d} \psi^*(\mathbf{x},t)L_z\psi(\mathbf{x},t)\ d\mathbf{x}, \qquad t\ge 0, \qquad d=2,3, \tag{9.26}$$

where $L_z = i\,(y\partial_x - x\partial_y)$ is the z-component angular momentum.

Lemma 9.2: *Suppose $\psi(\mathbf{x},t)$ is the solution of the problem (4.1), (4.2) with $d=2$ or 3, then we have*

$$\frac{d\langle L_z\rangle(t)}{dt} = \left(\gamma_x^2-\gamma_y^2\right)\delta_{xy}(t), \quad \delta_{xy}(t) = \int_{\mathbb{R}^d} xy|\psi(\mathbf{x},t)|^2\ d\mathbf{x}, \quad t\ge 0. \tag{9.27}$$

This implies that, at least in the following two cases, the angular momentum expectation is conserved:

i) For any given initial data $\psi_0(\mathbf{x})$ in (4.2), if the trap is radial symmetric in 2d, and resp., cylindrical symmetric in 3d, i.e. $\gamma_x = \gamma_y$;

ii) For any given $\gamma_x > 0$ and $\gamma_y > 0$ in (3.13), if the initial data $\psi_0(\mathbf{x})$ in (4.2) is either odd or even in the first variable x or second variable y.

Proof: Differentiate (9.26) with respect to t, notice (4.1), integrate by parts, we have

$$\begin{aligned}
\frac{d\langle L_z\rangle(t)}{dt} &= \int_{\mathbb{R}^d} \left[(i\psi_t^*)\ (y\partial_x - x\partial_y)\psi + \psi^*\ (y\partial_x - x\partial_y)(i\psi_t)\right]\ d\mathbf{x} \\
&= \int_{\mathbb{R}^d} \left[\left(\frac{1}{2}\nabla^2\psi^* - V(\mathbf{x})\psi^* - \beta|\psi|^2\psi^*\right)(y\partial_x - x\partial_y)\psi\right. \\
&\qquad \left. +\psi^*\ (y\partial_x - x\partial_y)\left(-\frac{1}{2}\nabla^2\psi + V(\mathbf{x})\psi + \beta|\psi|^2\psi\right)\right]\ d\mathbf{x} \\
&= \int_{\mathbb{R}^d} \frac{1}{2}\left[\nabla^2\psi^*\ (y\partial_x - x\partial_y)\psi - \psi^*\ (y\partial_x - x\partial_y)\nabla^2\psi\right]\ d\mathbf{x} \\
&\quad + \int_{\mathbb{R}^d} \left[\psi^*\ (y\partial_x - x\partial_y)\left(V(\mathbf{x})\psi + \beta|\psi|^2\psi\right)\right. \\
&\qquad \left. - \left(V(\mathbf{x})\psi^* + \beta|\psi|^2\psi^*\right)\ (y\partial_x - x\partial_y)\psi\ \right]\ d\mathbf{x} \\
&= \int_{\mathbb{R}^d} |\psi|^2(y\partial_x - x\partial_y)\left(V(\mathbf{x}) + \beta|\psi|^2\right)\ d\mathbf{x} \\
&= \int_{\mathbb{R}^d} |\psi|^2(y\partial_x - x\partial_y)V_d(\mathbf{x})\ d\mathbf{x} = \int_{\mathbb{R}^d} |\psi|^2(\gamma_x^2 - \gamma_y^2)xy\ d\mathbf{x} \\
&= (\gamma_x^2 - \gamma_y^2)\int_{\mathbb{R}^d} xy|\psi|^2\ d\mathbf{x}, \qquad t \geq 0. \qquad (9.28)
\end{aligned}$$

For case i), since $\gamma_x = \gamma_y$, we get the conservation of $\langle L_z\rangle$ immediately from the first order ODE:

$$\frac{d\langle L_z\rangle(t)}{dt} = 0, \qquad t \geq 0. \qquad (9.29)$$

For case ii), we know the solution $\psi(\mathbf{x}, t)$ is either odd or even in the first variable x or second variable y due to the assumption of the initial data and symmetry of $V(\mathbf{x})$. Thus $|\psi(\mathbf{x}, t)|$ is even in either x or y, which immediately implies that $\langle L_z\rangle$ satisfies the first order ODE (9.29). $\square$

10. Numerical methods for computing ground states of GPE

In this section, we present the continuous normalized gradient flow (CNGF), prove its energy diminishing and propose its semi-discretization for computing ground states in BEC. For simplicity, we take $\sigma = 1$ in (4.1).

10.1. *Gradient flow with discrete normalization (GFDN)*

Various algorithms for computing the minimizer of the energy functional $E(\phi)$ under the constraint (9.3) have been studied in the literature. For instance, second order in time discretization scheme that preserves the normalization and energy diminishing properties were presented in [2, 6]. Perhaps one of the more popular technique for dealing with the normalization constraint (9.3) is through the following construction: choose a time sequence $0 = t_0 < t_1 < t_2 < \cdots < t_n < \cdots$ with $\triangle t_n = t_{n+1} - t_n > 0$ and $k = \max_{n\geq 0} \triangle t_n$. To adapt an algorithm for the solution of the usual gradient flow to the minimization problem under a constraint, it is natural to consider the following splitting (or projection) scheme which was widely used in physical literatures [6] for computing the ground state solution of BEC:

$$\phi_t = -\frac{1}{2}\frac{\delta E(\phi)}{\delta \phi} = \frac{1}{2}\triangle \phi - V(\mathbf{x})\phi - \beta\,|\phi|^2\phi,$$
$$\mathbf{x}\in\Omega,\ t_n < t < t_{n+1},\ n\geq 0, \tag{10.1}$$

$$\phi(x, t_{n+1}) \stackrel{\triangle}{=} \phi(\mathbf{x}, t_{n+1}^+) = \frac{\phi(\mathbf{x}, t_{n+1}^-)}{\|\phi(\cdot, t_{n+1}^-)\|}, \qquad \mathbf{x}\in\Omega, \quad n\geq 0, \tag{10.2}$$

$$\phi(\mathbf{x}, t) = 0, \quad \mathbf{x}\in\Gamma = \partial\Omega, \qquad \phi(\mathbf{x}, 0) = \phi_0(\mathbf{x}), \quad \mathbf{x}\in\Omega; \tag{10.3}$$

where $\phi(\mathbf{x}, t_n^{\pm}) = \lim_{t\to t_n^{\pm}} \phi(\mathbf{x}, t)$, $\|\phi_0\| = 1$ and $\Omega\subset\mathbb{R}^d$. In fact, the gradient flow (10.1) can be viewed as applying the steepest decent method to the energy functional $E(\phi)$ without constraint and (10.2) then projects the solution back to the unit sphere in order to satisfying the constraint (9.3). From the numerical point of view, the gradient flow (10.1) can be solved via traditional techniques and the normalization of the gradient flow is simply achieved by a projection at the end of each time step.

10.2. *Energy diminishing of GFDN*

Let

$$\tilde{\phi}(\cdot, t) = \frac{\phi(\cdot, t)}{\|\phi(\cdot, t)\|}, \qquad t_n \leq t \leq t_{n+1}, \qquad n\geq 0. \tag{10.4}$$

For the gradient flow (10.1), it is easy to establish the following basic facts:

Lemma 10.1: *Suppose $V(\mathbf{x}) \ge 0$ for all $\mathbf{x} \in \Omega$, $\beta \ge 0$ and $\|\phi_0\| = 1$, then*
(i). $\|\phi(\cdot,t)\| \le \|\phi(\cdot,t_n)\| = 1$ for $t_n \le t \le t_{n+1}$, $n \ge 0$.
(ii). For any $\beta \ge 0$,

$$E(\phi(\cdot,t)) \le E(\phi(\cdot,t')), \qquad t_n \le t' < t \le t_{n+1}, \qquad n \ge 0. \tag{10.5}$$

(iii). For $\beta = 0$,

$$E(\tilde{\phi}(\cdot,t)) \le E(\tilde{\phi}(\cdot,t_n)), \qquad t_n \le t \le t_{n+1}, \qquad n \ge 0. \tag{10.6}$$

Proof: (i) and (ii) follows the standard techniques used for gradient flow. As for (iii), from (4.4) with $\psi = \tilde{\phi}$ and $\beta = 0$, (10.1), (10.3) and (10.4), integration by parts and Schwartz inequality, we obtain

$$\begin{aligned}
&\frac{d}{dt}E(\tilde{\phi}) = \frac{d}{dt}\int_\Omega \left[\frac{|\nabla\phi|^2}{2\|\phi\|^2} + \frac{V(\mathbf{x})\phi^2}{\|\phi\|^2}\right]\, d\mathbf{x} \\
&= 2\int_\Omega \left[\frac{\nabla\phi\cdot\nabla\phi_t}{2\|\phi\|^2} + \frac{V(\mathbf{x})\phi\ \phi_t}{\|\phi\|^2}\right] d\mathbf{x} - \left(\frac{d}{dt}\|\phi\|^2\right)\int_\Omega \left[\frac{|\nabla\phi|^2}{2\|\phi\|^4} + \frac{V(\mathbf{x})\phi^2}{\|\phi\|^4}\right] d\mathbf{x} \\
&= 2\int_\Omega \frac{\left[-\frac{1}{2}\triangle\phi + V(\mathbf{x})\phi\right]\phi_t}{\|\phi\|^2}\, d\mathbf{x} - \left(\frac{d}{dt}\|\phi\|^2\right)\int_\Omega \frac{\frac{1}{2}|\nabla\phi|^2 + V(\mathbf{x})\phi^2}{\|\phi\|^4}\, d\mathbf{x} \\
&= -2\frac{\|\phi_t\|^2}{\|\phi\|^2} + \frac{1}{2\|\phi\|^4}\left(\frac{d}{dt}\|\phi\|^2\right)^2 = \frac{2}{\|\phi\|^4}\left[\left(\int_\Omega \phi\ \phi_t\, d\mathbf{x}\right)^2 - \|\phi\|^2\|\phi_t\|^2\right] \\
&\le 0\,, \qquad t_n \le t \le t_{n+1}.
\end{aligned} \tag{10.7}$$

This implies (10.6). □

Remark 10.2: The property (10.5) is often referred as the energy diminishing property of the gradient flow. It is interesting to note that (10.6) implies that the energy diminishing property is preserved even with the normalization of the solution of the gradient flow for $\beta = 0$, that is, for linear evolution equations.

Remark 10.3: When $\beta > 0$, the solution of (10.1)-(10.3) may not preserve the normalized energy diminishing property

$$E(\tilde{\phi}(\cdot,t)) \le E(\tilde{\phi}(\cdot,t')), \qquad 0 \le t' < t \le t_1$$

for any $t_1 > 0$ [6].

From Lemma 10.1, we get immediately

Theorem 10.4: *Suppose $V(\mathbf{x}) \geq 0$ for all $\mathbf{x} \in \Omega$ and $\|\phi_0\| = 1$. For $\beta = 0$, GFDN (10.1)-(10.3) is energy diminishing for any time step k and initial data ϕ_0, i.e.*

$$E(\phi(\cdot, t_{n+1})) \leq E(\phi(\cdot, t_n)) \leq \cdots \leq E(\phi(\cdot, 0)) = E(\phi_0), \quad n = 0, 1, 2, \cdots. \tag{10.8}$$

10.3. *Continuous normalized gradient flow (CNGF)*

In fact, the normalized step (10.2) is equivalent to solve the following ODE *exactly*

$$\phi_t(\mathbf{x}, t) = \mu_\phi(t, k)\phi(\mathbf{x}, t), \qquad \mathbf{x} \in \Omega, \quad t_n < t < t_{n+1}, \quad n \geq 0, \tag{10.9}$$

$$\phi(\mathbf{x}, t_n^+) = \phi(\mathbf{x}, t_{n+1}^-), \qquad \mathbf{x} \in \Omega; \tag{10.10}$$

where

$$\mu_\phi(t, k) \equiv \mu_\phi(t_{n+1}, \triangle t_n) = -\frac{1}{2\ \triangle t_n} \ln \|\phi(\cdot, t_{n+1}^-)\|^2, \qquad t_n \leq t \leq t_{n+1}. \tag{10.11}$$

Thus the GFDN (10.1)-(10.3) can be viewed as a first-order splitting method for the gradient flow with discontinuous coefficients:

$$\phi_t = \frac{1}{2} \triangle \phi - V(\mathbf{x})\phi - \beta\, |\phi|^2\phi + \mu_\phi(t, k)\phi, \quad \mathbf{x} \in \Omega,\ t \geq 0, \tag{10.12}$$

$$\phi(\mathbf{x}, t) = 0, \qquad \mathbf{x} \in \Gamma, \qquad \phi(\mathbf{x}, 0) = \phi_0(\mathbf{x}), \qquad \mathbf{x} \in \Omega. \tag{10.13}$$

Let $k \to 0$, we see that

$$\begin{aligned} \mu_\phi(t) &:= \lim_{k \to 0^+} \mu_\phi(t, k) \\ &= \frac{1}{\|\phi(\cdot, t)\|^2} \int_\Omega \left[\frac{1}{2}|\nabla\phi(\mathbf{x}, t)|^2 + V(\mathbf{x})\phi^2(\mathbf{x}, t) + \beta\phi^4(\mathbf{x}, t)\right] d\mathbf{x}. \end{aligned} \tag{10.14}$$

This suggests us to consider the following continuous normalized gradient flow:

$$\phi_t = \frac{1}{2} \triangle \phi - V(\mathbf{x})\phi - \beta\, |\phi|^2\phi + \mu_\phi(t)\phi, \qquad \mathbf{x} \in \Omega, \quad t \geq 0, \tag{10.15}$$

$$\phi(\mathbf{x}, t) = 0, \qquad \mathbf{x} \in \Gamma, \qquad \phi(\mathbf{x}, 0) = \phi_0(\mathbf{x}), \qquad \mathbf{x} \in \Omega. \tag{10.16}$$

In fact, the right hand side of (10.15) is the same as (9.2) if we view $\mu_\phi(t)$ as a Lagrange multiplier for the constraint (9.3). Furthermore for the above CNGF, as observed in [6], the solution of (10.15) also satisfies the following theorem:

Theorem 10.5: *Suppose $V(\mathbf{x}) \geq 0$ for all $\mathbf{x} \in \Omega$, $\beta \geq 0$ and $\|\phi_0\| = 1$. Then the CNGF (10.15)-(10.16) is normalization conservation and energy diminishing, i.e.*

$$\|\phi(\cdot,t)\|^2 = \int_\Omega \phi^2(\mathbf{x},t)\, d\mathbf{x} = \|\phi_0\|^2 = 1, \qquad t \geq 0, \tag{10.17}$$

$$\frac{d}{dt}E(\phi) = -2\,\|\phi_t(\cdot,t)\|^2 \leq 0\ , \qquad t \geq 0, \tag{10.18}$$

which in turn implies

$$E(\phi(\cdot,t_1)) \geq E(\phi(\cdot,t_2)), \qquad 0 \leq t_1 \leq t_2 < \infty.$$

Remark 10.6: We see from the above theorem that the energy diminishing property is preserved in the continuous dynamic system (10.15).

Using argument similar to that in [88, 106], we may also get as $t \to \infty$, ϕ approaches to a steady state solution which is a critical point of the energy. In non-rotating BEC, it has a unique real valued nonnegative ground state solution $\phi_g(\mathbf{x}) \geq 0$ for all $\mathbf{x} \in \Omega$ [87]. We choose the initial data $\phi_0(\mathbf{x}) \geq 0$ for $\mathbf{x} \in \Omega$, e.g. the ground state solution of linear Schrödinger equation with a harmonic oscillator potential [5, 8]. Under this kind of initial data, the ground state solution ϕ_g and its corresponding chemical potential μ_g can be obtained from the steady state solution of the CNGF (10.15)-(10.16), i.e.

$$\phi_g(\mathbf{x}) = \lim_{t\to\infty} \phi(\mathbf{x},t), \quad \mathbf{x} \in \Omega,\ \mu_g = \mu_\beta(\phi_g) = E(\phi_g) + \frac{\beta}{2}\int_\Omega |\phi_g(\mathbf{x})|^4\, d\mathbf{x}. \tag{10.19}$$

10.4. *Semi-implicit time discretization*

To further discretize the equation (10.1), we here consider the following semi-implicit time discretization scheme:

$$\frac{\tilde\phi^{n+1} - \phi^n}{k} = \frac{1}{2} \triangle \tilde\phi^{n+1} - V(\mathbf{x})\tilde\phi^{n+1} - \beta\, |\phi^n|^2 \tilde\phi^{n+1}\ , \quad \mathbf{x} \in \Omega, \tag{10.20}$$

$$\tilde\phi^{n+1}(\mathbf{x}) = 0, \quad \mathbf{x} \in \Gamma, \quad \phi^{n+1}(\mathbf{x}) = \tilde\phi^{n+1}(\mathbf{x})/\|\tilde\phi^{n+1}\|\ , \quad \mathbf{x} \in \Omega \tag{10.21}$$

Notice that since the equation (10.20) becomes linear, the solution at the new time step becomes relatively simple. In other words, in each discrete time interval, we may view (10.20) as a discretization of a linear gradient flow with a modified potential $\tilde V_n(\mathbf{x}) = V(\mathbf{x}) + \beta|\phi^n(\mathbf{x})|^2$.

We now first present the following lemma:

Lemma 10.7: *Suppose $\beta \geq 0$ and $V(\mathbf{x}) \geq 0$ for all $\mathbf{x} \in \Omega$ and $\|\phi^n\| = 1$. Then,*

$$\int_\Omega |\tilde{\phi}^{n+1}|^2 \, d\mathbf{x} \leq \int_\Omega \phi^n \, \tilde{\phi}^{n+1} \, d\mathbf{x}, \qquad \int_\Omega |\tilde{\phi}^{n+1}|^4 \, d\mathbf{x} \leq \int_\Omega |\phi^n|^2 \, |\tilde{\phi}^{n+1}|^2 \, d\mathbf{x}. \tag{10.22}$$

Proof: Multiplying both sides of (10.20) by $\tilde{\phi}^{n+1}$, integrating over Ω, and applying integration by parts, we obtain

$$\int_\Omega \left(|\tilde{\phi}^{n+1}|^2 - \phi^n \tilde{\phi}^{n+1}\right) d\mathbf{x} = -k \int_\Omega \left[\frac{1}{2}|\nabla \tilde{\phi}^{n+1}|^2 + \tilde{V}_n(\mathbf{x})|\tilde{\phi}^{n+1}|^2\right] d\mathbf{x} \leq 0 \ ,$$

which leads to the first inequality in (10.22). Similarly,

$$\begin{aligned}
&\int_\Omega |\tilde{\phi}^{n+1}|^2 |\phi^n|^2 d\mathbf{x} = \int_\Omega |\tilde{\phi}^{n+1}|^2 \left|\tilde{\phi}^{n+1} - \frac{k}{2} \triangle \tilde{\phi}^{n+1} + k\tilde{V}_n(\mathbf{x})\tilde{\phi}^{n+1}\right|^2 d\mathbf{x} \\
&= \int_\Omega |\tilde{\phi}^{n+1}|^2 \left[|\tilde{\phi}^{n+1}|^2 - 2\, \frac{k}{2}\tilde{\phi}^{n+1} \triangle \tilde{\phi}^{n+1} + 2k\tilde{V}_n(\mathbf{x})|\tilde{\phi}^{n+1}|^2\right] d\mathbf{x} \\
&\qquad + \int_\Omega |\tilde{\phi}^{n+1}|^2 \left|\frac{k}{2} \triangle \tilde{\phi}^{n+1} - k\tilde{V}_n(\mathbf{x})\tilde{\phi}^{n+1}\right|^2 d\mathbf{x} \\
&= \int_\Omega |\tilde{\phi}^{n+1}|^2 \left[|\tilde{\phi}^{n+1}|^2 + 3k|\nabla \tilde{\phi}^{n+1}|^2 + 2k\tilde{V}_n(\mathbf{x})|\tilde{\phi}^{n+1}|^2\right] d\mathbf{x} \\
&\qquad + \int_\Omega |\tilde{\phi}^{n+1}|^2 \left|\frac{k}{2} \triangle \tilde{\phi}^{n+1} - k\tilde{V}_n(\mathbf{x})\tilde{\phi}^{n+1}\right|^2 d\mathbf{x} \\
&\geq \int_\Omega |\tilde{\phi}^{n+1}|^4 d\mathbf{x} \ .
\end{aligned} \tag{10.23}$$

This implies the second inequality in (10.22). □

Given a linear self-adjoint operator A in a Hilbert space H with inner product $(\cdot, \cdot)$, and assume that A is positive definite in the sense that for some positive constant c, $(u, Au) \geq c(u, u)$ for any $u \in H$. We now present a simple lemma:

Lemma 10.8: *For any $k > 0$, and $(I + kA)u = v$, we have*

$$\frac{(u, Au)}{(u, u)} \leq \frac{(v, Av)}{(v, v)} \ . \tag{10.24}$$

Proof: Since A is self-adjoint and positive definite, by Hölder inequality, we have for any $p, q \geq 1$ with $p + q = pq$, that

$$(u, Au) \leq (u, u)^{1/p} \, (u, A^q u)^{1/q} \ ,$$

which leads to

$$(u, Au) \le (u,u)^{1/2} \left(u, A^2u\right)^{1/2} \ , \qquad (u, Au) \left(u, A^2u\right) \le (u,u) \left(u, A^3u\right) \ .$$

Direct calculation then gives

$$\begin{aligned}
&(u, Au)\ ((I+kA)u, (I+kA)u) \\
&= (u, Au)\ (u,u) + 2k\,(u,Au)^2 + k^2\,(u,Au)\left(u, A^2u\right) \\
&\le (u, Au)\ (u,u) + 2k\,(u,u)\ \left(u, A^2u\right) + k^2\,(u,u)\ \left(u, A^3u\right) \\
&= (u,u)\,((I+kA)u, A(I+kA)u)\,. \qquad (10.25)
\end{aligned}$$

□

Let us define a modified energy $\tilde{E}_{\phi^n}$ as

$$\begin{aligned}
\tilde{E}_{\phi^n}(u) &= \int_\Omega \left[\frac{1}{2}|\nabla u|^2 + \tilde{V}_n(\mathbf{x})|u|^2\right]\, d\mathbf{x} \\
&= \int_\Omega \left[\frac{1}{2}|\nabla u|^2 + V(\mathbf{x})|u|^2 + \beta|\phi^n|^2|u|^2\right]\, d\mathbf{x}\,,
\end{aligned}$$

we then get from the above lemma that

Lemma 10.9: *Suppose $V(\mathbf{x}) \ge 0$ for all $\mathbf{x} \in \Omega$, $\beta \ge 0$ and $\|\phi^n\| = 1$. Then,*

$$\begin{aligned}
\tilde{E}_{\phi^n}(\tilde{\phi}^{n+1}) &\le \frac{\tilde{E}_{\phi^n}(\tilde{\phi}^{n+1})}{\|\tilde{\phi}^{n+1}\|} = \tilde{E}_{\phi^n}\left(\frac{\tilde{\phi}^{n+1}}{\|\tilde{\phi}^{n+1}\|}\right) \\
&= \tilde{E}_{\phi^n}(\phi^{n+1}) \le \tilde{E}_{\phi^n}(\phi_n)\ . \qquad (10.26)
\end{aligned}$$

Using the inequality (10.22), we in turn get:

Lemma 10.10: *Suppose $V(\mathbf{x}) \ge 0$ for all $\mathbf{x} \in \Omega$ and $\beta \ge 0$, then,*

$$\tilde{E}(\tilde{\phi}^{n+1}) \le \tilde{E}(\phi^n),$$

where

$$\tilde{E}(u) = \int_\Omega \left[\frac{1}{2}|\nabla u|^2 + V(\mathbf{x})|u|^2 + \beta|u|^4\right]\, d\mathbf{x}\,.$$

Remark 10.11: As we noted earlier, for $\beta = 0$, the energy diminishing property is preserved in the GFDN (10.1)-(10.3) and semi-implicit time discretization (10.20)-(10.21). For $\beta > 0$, the energy diminishing property in general does **not** hold uniformly for all ϕ_0 and all step size $k > 0$, a justification on the energy diminishing is presently only possible for a modified energy within two adjacent steps.

10.5. *Discretized normalized gradient flow (DNGF)*

Consider a discretization for the GFDN (10.20)-(10.21) (or a fully discretization of (10.15)-(10.16))

$$\frac{\tilde{U}^{n+1}-U^n}{k} = -A\tilde{U}^{n+1}, \qquad U^{n+1} = \frac{\tilde{U}^{n+1}}{\|\tilde{U}^{n+1}\|}, \qquad n=0,1,2,\cdots; \tag{10.27}$$

where $U^n = (u_1^n, u_2^n, \cdots, u_{M-1}^n)^T$, $k > 0$ is time step and A is an $(M-1)\times(M-1)$ symmetric positive definite matrix. We adopt the inner product, norm and energy of vectors $U = (u_1, u_2, \cdots, u_{M-1})^T$ and $V = (v_1, v_2, \cdots, v_{M-1})^T$ as

$$(U,V) = U^T V = \sum_{j=1}^{M-1} u_j\, v_j, \quad \|U\|^2 = U^T U = (U,U), \tag{10.28}$$

$$E(U) = U^T A U = (U, AU), \tag{10.29}$$

respectively. Using the finite dimensional version of the lemmas given in the previous subsection, we have

Theorem 10.12: *Suppose $\|U^0\| = 1$ and A is symmetric positive definite. Then the DNGF (10.27) is energy diminishing, i.e.*

$$E\left(U^{n+1}\right) \le E\left(U^n\right) \le \cdots \le E\left(U^0\right), \qquad n=0,1,2,\cdots. \tag{10.30}$$

Furthermore if $I+kA$ is an M-matrix, then $(I+kA)^{-1}$ is a nonnegative matrix (i.e. with nonnegative entries). Thus the flow is monotone, i.e. if U^0 is a non-negative vector, then U^n is also a non-negative vector for all $n \ge 0$.

Remark 10.13: If a discretization for the GFDN (10.20)-(10.21) reads

$$\frac{\tilde{U}^{n+1}-U^n}{k} = -BU^n, \qquad U^{n+1} = \frac{\tilde{U}^{n+1}}{\|\tilde{U}^{n+1}\|}, \qquad n=0,1,2,\cdots. \tag{10.31}$$

For symmetric, positive definite B with $\rho(kB) < 1$ ($\rho(B)$ being the spectral radius of B), (10.30) is satisfied by choosing

$$A = \frac{1}{k}\left((I-kB)^{-1} - I\right) = (I-kB)^{-1}B.$$

Remark 10.14: If a discretization for the GFDN (10.20)-(10.21) reads

$$\tilde{U}^{n+1} = BU^n, \qquad U^{n+1} = \frac{\tilde{U}^{n+1}}{\|\tilde{U}^{n+1}\|}, \qquad n=0,1,2,\cdots. \tag{10.32}$$

For symmetric, positive definite B with $\rho(B) < 1$, (10.30) is satisfied by choosing

$$A = \frac{1}{k}\left(B^{-1} - I\right).$$

Remark 10.15: If a discretization for the GFDN (10.20)-(10.21) reads

$$\frac{\tilde{U}^{n+1} - U^n}{k} = -B\tilde{U}^{n+1} - CU^n, \quad U^{n+1} = \frac{\tilde{U}^{n+1}}{\|\tilde{U}^{n+1}\|}, \quad n = 0, 1, 2, \cdots. \tag{10.33}$$

Suppose B and C are symmetric, positive definite and $\rho(kC) < 1$. Then (10.30) is satisfied by choosing

$$A = (I - kC)^{-1}(B + C).$$

10.6. *Numerical methods*

In this section, we will present two numerical methods to discretize the GFDN (10.1)-(10.3) (or a full discretization of the CNGF (10.15)-(10.16)). For simplicity of notation we introduce the methods for the case of one spatial dimension ($d = 1$) with homogeneous periodic boundary conditions. Generalizations to higher dimension are straightforward for tensor product grids and the results remain valid without modifications. For $d = 1$, we have

$$\phi_t = \frac{1}{2}\phi_{xx} - V(x)\phi - \beta\,|\phi|^2\phi, \qquad x \in \Omega = (a, b),\ t_n < t < t_{n+1},\ n \geq 0, \tag{10.34}$$

$$\phi(x, t_{n+1}) \stackrel{\triangle}{=} \phi(x, t_{n+1}^+) = \frac{\phi(x, t_{n+1}^-)}{\|\phi(\cdot, t_{n+1}^-)\|}, \quad a \leq x \leq b,\ n \geq 0, \tag{10.35}$$

$$\phi(x, 0) = \phi_0(x),\ a \leq x \leq b, \quad \phi(a, t) = \phi(b, t) = 0,\ t \geq 0; \tag{10.36}$$

with

$$\|\phi_0\|^2 = \int_a^b \phi_0^2(x)\,dx = 1.$$

We choose the spatial mesh size $h = \triangle x > 0$ with $h = (b - a)/M$ and M an even positive integer, the time step is given by $k = \triangle t > 0$ and define grid points and time steps by

$$x_j := a + j\,h, \qquad t_n := n\,k, \qquad j = 0, 1, \cdots, M, \qquad n = 0, 1, 2, \cdots$$

Let ϕ_j^n be the numerical approximation of $\phi(x_j, t_n)$ and ϕ^n the solution vector at time $t = t_n = nk$ with components ϕ_j^n.

Backward Euler finite difference (BEFD) We use backward Euler for time discretization and second-order centered finite difference for spatial derivatives. The detail scheme is:

$$\begin{aligned}
&\frac{\phi_j^* - \phi_j^n}{k} = \frac{1}{2h^2}\left[\phi_{j+1}^* - 2\phi_j^* + \phi_{j-1}^*\right] - V(x_j)\phi_j^* - \beta\left(\phi_j^n\right)^2\phi_j^*,\\
&\qquad\qquad j = 1, \cdots, M-1,\\
&\phi_0^* = \phi_M^* = 0, \qquad \phi_j^0 = \phi_0(x_j), \qquad j = 0, 1, \cdots, M,\\
&\phi_j^{n+1} = \frac{\phi_j^*}{\|\phi^*\|}, \qquad j = 0, \cdots, M, \qquad n = 0, 1, \cdots;
\end{aligned} \tag{10.37}$$

where the norm is defined as $\|\phi^*\|^2 = h\sum_{j=1}^{M-1}\left(\phi_j^*\right)^2$.

Time-splitting sine-spectral method (TSSP) From time $t = t_n$ to time $t = t_{n+1}$, the equation (10.34) is solved in two steps. First, one solves

$$\phi_t = \frac{1}{2}\phi_{xx}, \tag{10.38}$$

for one time step of length k, then followed by solving

$$\phi_t(x,t) = -V(x)\phi(x,t) - \beta|\phi|^2\phi(x,t), \qquad t_n \le t \le t_{n+1}, \tag{10.39}$$

again for the same time step. Equation (10.38) is discretized in space by the sine-spectral method and integrated in time *exactly*. For $t \in [t_n, t_{n+1}]$, multiplying the ODE (10.39) by $\phi(x,t)$, one obtains with $\rho(x,t) = \phi^2(x,t)$

$$\rho_t(x,t) = -2V(x)\rho(x,t) - 2\beta\rho^2(x,t), \qquad t_n \le t \le t_{n+1}. \tag{10.40}$$

The solution of the ODE (10.40) can be expressed as

$$\rho(x,t) = \begin{cases} \dfrac{V(x)\rho(x,t_n)}{\left(V(x) + \beta\rho(x,t_n)\right)e^{2V(x)(t-t_n)} - \beta\rho(x,t_n)} & V(x) \ne 0,\\[2ex] \dfrac{\rho(x,t_n)}{1 + 2\beta\rho(x,t_n)(t-t_n)}, & V(x) = 0. \end{cases} \tag{10.41}$$

Combining the splitting step via the standard second-order Strang splitting for solving the GFDN (10.34)-(10.36), in detail, the steps for obtaining ϕ_j^{n+1}

from ϕ_j^n are given by

$$
\begin{aligned}
\phi_j^* &= \begin{cases} \sqrt{\dfrac{V(x_j)e^{-kV(x_j)}}{V(x_j)+\beta(1-e^{-kV(x_j)})|\phi_j^n|^2}}\ \phi_j^n & V(x_j)\neq 0, \\[2ex] \dfrac{1}{\sqrt{1+\beta k|\phi_j^n|^2}}\ \phi_j^n, & V(x_j)=0, \end{cases} \\
\phi_j^{**} &= \sum_{l=1}^{M-1} e^{-k\mu_l^2/2}\ \widehat{\phi}_l^*\ \sin(\mu_l(x_j-a)), \qquad j=1,2,\cdots,M-1, \\
\phi_j^{***} &= \begin{cases} \sqrt{\dfrac{V(x_j)e^{-kV(x_j)}}{V(x_j)+\beta(1-e^{-kV(x_j)})|\phi_j^{**}|^2}}\ \phi_j^{**} & V(x_j)\neq 0, \\[2ex] \dfrac{1}{\sqrt{1+\beta k|\phi_j^{**}|^2}}\ \phi_j^{**}, & V(x_j)=0, \end{cases} \\
\phi_j^{n+1} &= \frac{\phi_j^{***}}{\|\phi^{***}\|}, \qquad j=0,\cdots,M, \qquad n=0,1,\cdots; \qquad (10.42)
\end{aligned}
$$

where $\widehat{U}_l$ are the sine-transform coefficients of a real vector $U = (u_0, u_1, \cdots, u_M)^T$ with $u_0 = u_M = 0$ which are defined as

$$
\mu_l = \frac{\pi l}{b-a}, \quad \widehat{U}_l = \frac{2}{M}\sum_{j=1}^{M-1} u_j\ \sin(\mu_l(x_j-a)), \quad l=1,2,\cdots,M-1 \qquad (10.43)
$$

and

$$
\phi_j^0 = \phi(x_j,0) = \phi_0(x_j), \qquad j=0,1,2,\cdots,M.
$$

Note that the only time discretization error of TSSP is the splitting error, which is second order in k.

For comparison purposes we review a few other numerical methods which are currently used for solving the GFDN (10.34)-(10.36). One is the

Crank-Nicolson finite difference (CNFD) scheme:

$$\begin{aligned}
\frac{\phi_j^* - \phi_j^n}{k} &= \frac{1}{4h^2}\left[\phi_{j+1}^* - 2\phi_j^* + \phi_{j-1}^* + \phi_{j+1}^n - 2\phi_j^n + \phi_{j-1}^n\right] \\
&\quad - \frac{V(x_j)}{2}\left[\phi_j^* + \phi_j^n\right] - \frac{\beta\left|\phi_j^n\right|^2}{2}\left[\phi_j^* + \phi_j^n\right], \qquad j = 1, \cdots, M-1, \\
\phi_0^* &= \phi_M^* = 0, \qquad \phi_j^0 = \phi_0(x_j), \qquad j = 0, 1, \cdots, M, \\
\phi_j^{n+1} &= \frac{\phi_j^*}{\|\phi^*\|}, \qquad j = 0, \cdots, M, \qquad n = 0, 1, \cdots. \qquad (10.44)
\end{aligned}$$

Another one is the forward Euler finite difference (FEFD) method:

$$\begin{aligned}
\frac{\phi_j^* - \phi_j^n}{k} &= \frac{1}{2h^2}\left[\phi_{j+1}^n - 2\phi_j^n + \phi_{j-1}^n\right] - V(x_j)\phi_j^n - \beta\left|\phi_j^n\right|^2\phi_j^n, \\
&\qquad j = 1, \cdots, M-1, \\
\phi_0^* &= \phi_M^* = 0, \qquad \phi_j^0 = \phi_0(x_j), \quad j = 0, 1, \cdots, M, \\
\phi_j^{n+1} &= \frac{\phi_j^*}{\|\phi^*\|}, \qquad j = 0, \cdots, M, \qquad n = 0, 1, \cdots; \qquad (10.45)
\end{aligned}$$

10.7. *Energy diminishing of DNGF*

First we analyze the energy diminishing of the different numerical methods for linear case, i.e. $\beta = 0$ in (10.34). Introducing

$$\begin{aligned}
&\Phi^n = \left(\phi_1^n,\ \phi_2^n,\ \cdots,\ \phi_{M-1}^n\right)^T, \\
&D = (d_{jl})_{(M-1)\times(M-1)}, \text{ with } d_{jl} = \frac{1}{2h^2}\begin{cases} 2, & j = l, \\ -1, & |j-l| = -1, \\ 0, & \text{otherwise}, \end{cases} \\
&E = \operatorname{diag}\left(V(x_1),\ V(x_2),\ \cdots,\ V(x_{M-1})\right), \\
&F(\Phi) = \operatorname{diag}\left(\phi_1^2,\ \phi_2^2,\ \cdots,\ \phi_{M-1}^2\right), \quad \text{with } \Phi = \left(\phi_1,\ \phi_2,\ \cdots,\ \phi_{M-1}\right)^T, \\
&G = (g_{jl})_{(M-1)\times(M-1)}, \quad \text{with } g_{jl} = \frac{2}{M}\sum_{m=1}^{M-1}\sin\frac{\pi m j}{M}\ \sin\frac{\pi m l}{M}\ e^{-k\mu_m^2/2}, \\
&H = \operatorname{diag}\left(e^{-kV(x_1)/2},\ e^{-kV(x_2)/2},\ \cdots,\ e^{-kV(x_{M-1})/2}\right).
\end{aligned}$$

Then the BEFD discretization (10.37) (called as BEFD normalized flow) with $\beta = 0$ can be expressed as

$$\frac{\Phi^* - \Phi^n}{k} = -(D+E)\Phi^*, \quad \Phi^{n+1} = \frac{\Phi^*}{\|\Phi^*\|}, \qquad n = 0, 1, \cdots. \qquad (10.46)$$

The TSSP discretization (10.42) (called as TSSP normalized flow) with $\beta = 0$ can be expressed as

$$\Phi^{***} = H\Phi^{**} = HG\Phi^{*} = HGH\Phi^{n}, \qquad \Phi^{n+1} = \frac{\Phi^{*}}{\|\Phi^{*}\|}, \qquad n = 0, 1, \cdots. \tag{10.47}$$

The CNFD discretization (10.44) (called as CNFD normalized flow) with $\beta = 0$ can be expressed as

$$\frac{\Phi^{*} - \Phi^{n}}{k} = -\frac{1}{2}(D+E)\Phi^{*} - \frac{1}{2}(D+E)\Phi^{n}, \quad \Phi^{n+1} = \frac{\Phi^{*}}{\|\Phi^{*}\|}, \qquad n = 0, 1, \cdots. \tag{10.48}$$

The FEFD discretization (10.45) (called as FEFD normalized flow) with $\beta = 0$ can be expressed as

$$\frac{\Phi^{*} - \Phi^{n}}{k} = -(D+E)\Phi^{n}, \quad \Phi^{n+1} = \frac{\Phi^{*}}{\|\Phi^{*}\|}, \qquad n = 0, 1, \cdots. \tag{10.49}$$

It is easy to see that D and G are symmetric positive definite matrices. Furthermore D is also an M-matrix and $\rho(D) = \left(1 + \cos\frac{\pi}{M}\right)/h^2 < 2/h^2$ and $\rho(G) = e^{-k\mu_1^2/2} < 1$. Applying the theorem 10.12 and remarks 10.13, 10.14 and 10.15, we have

Theorem 10.16: *Suppose $V \geq 0$ in Ω and $\beta = 0$. We have that*

(i). The BEFD normalized flow (10.37) is energy diminishing and monotone for any $k > 0$.

(ii). The TSSP normalized flow (10.42) is energy diminishing for any $k > 0$.

(iii). The CNFD normalized flow (10.44) is energy diminishing and monotone provided that

$$k \leq \frac{2}{2/h^2 + \max_j V(x_j)} = \frac{2h^2}{2 + h^2\ \max_j V(x_j)}. \tag{10.50}$$

(iv). The FEFD normalized flow (10.45) is energy diminishing and monotone provided that

$$k \leq \frac{1}{2/h^2 + \max_j V(x_j)} = \frac{h^2}{2 + h^2\ \max_j V(x_j)}. \tag{10.51}$$

For nonlinear case, i.e. $\beta > 0$, we only analyze the *energy* between two steps of BEFD flow (10.37). In this case, consider

$$\frac{\tilde{\Phi}^{n+1} - \Phi^{n}}{k} = -\left(D + E + \beta F(\Phi^{n})\right)\tilde{\Phi}^{n+1}, \qquad \Phi^{n+1} = \frac{\tilde{\Phi}^{n+1}}{\|\tilde{\Phi}^{n+1}\|}. \tag{10.52}$$

Lemma 10.17: *Suppose $V \geq 0$, $\beta > 0$ and $\|\Phi^n\| = 1$. Then for the flow (10.52), we have*

$$\tilde{E}\left(\tilde{\Phi}^{n+1}\right) \leq \tilde{E}\left(\Phi^n\right), \qquad \tilde{E}_{\Phi^n}\left(\Phi^{n+1}\right) \leq \tilde{E}_{\Phi^n}\left(\Phi^n\right) \tag{10.53}$$

where

$$\tilde{E}\left(\Phi\right) = (\Phi, (D + E + \beta F(\Phi))\Phi) = \Phi^T(D+E)\Phi + \beta \sum_{j=1}^{M-1} \phi_j^4, \tag{10.54}$$

$$\begin{aligned} \tilde{E}_{\Phi^n}\left(\Phi\right) &= (\Phi, (D + E + \beta F(\Phi^n))\Phi) \\ &= \Phi^T(D+E)\Phi + \beta \sum_{j=1}^{M-1} \phi_j^2 \, \left(\phi_j^n\right)^2 \; . \end{aligned} \tag{10.55}$$

Proof: Combining (10.52), (10.27) and Theorem 10.12, we have

$$\begin{aligned} \left(\tilde{\Phi}^{n+1},\ (D+E+\beta F(\Phi^n))\tilde{\Phi}^{n+1}\right) &\leq \frac{\left(\tilde{\Phi}^{n+1},\ (D+E+\beta F(\Phi^n))\tilde{\Phi}^{n+1}\right)}{\left(\tilde{\Phi}^{n+1}, \tilde{\Phi}^{n+1}\right)} \\ &\leq \frac{(\Phi^n,\ (D+E+\beta F(\Phi^n))\Phi^n)}{(\Phi^n, \Phi^n)} = \tilde{E}\left(\Phi^n\right). \end{aligned} \tag{10.56}$$

Similar to the proof of (10.22), we have

$$\sum_{j=1}^{M-1} \left(\phi_j^n\right)^2 \left(\tilde{\phi}_j^{n+1}\right)^2 \geq \sum_{j=1}^{M-1} \left(\tilde{\phi}_j^{n+1}\right)^4. \tag{10.57}$$

The required result (10.53) is a combination of (10.57), and (10.56). □

10.8. *Numerical results*

Here we report the ground state solutions in BEC with different potentials by the method BEFD. Due to the ground state solution $\phi_g(\mathbf{x}) \geq 0$ for $\mathbf{x} \in \Omega$ in non-rotating BEC [87], in our computations, the initial condition (10.3) is always chosen such that $\phi_0(\mathbf{x}) \geq 0$ and decays to zero sufficiently fast as $|\mathbf{x}| \to \infty$. We choose an appropriately large interval, rectangle and box in 1d, 2d and 3d, respectively, to avoid that the homogeneous periodic boundary condition (10.36) introduce a significant (aliasing) error relative to the whole space problem. To quantify the ground state solution $\phi_g(\mathbf{x})$, we define the radius mean square

$$\alpha_{\rm rms} = \|\alpha\phi_g\|_{L^2(\Omega)} = \sqrt{\int_\Omega \alpha^2 \phi_g^2(\mathbf{x})\, d\mathbf{x}}, \qquad \alpha = x, y, \text{ or } z. \tag{10.58}$$

Example 1 Ground state solution of 1d BEC with harmonic oscillator potential

$$V(x) = \frac{x^2}{2}, \qquad \phi_0(x) = \frac{1}{(\pi)^{1/4}} e^{-x^2/2}, \quad x \in \mathbb{R}.$$

The CNGF (10.15)-(10.16) with $d = 1$ is solved on $\Omega = [-16, 16]$ with mesh size $h = 1/8$ and time step $k = 0.1$ by using BEFD. The steady state solution is reached when $\max\left|\Phi^{n+1} - \Phi^n\right| < \varepsilon = 10^{-6}$. Fig. 1 shows the ground state solution $\phi_g(x)$ and energy evolution for different β. Tab. 1 displays the values of $\phi_g(0)$, radius mean square $x_{\rm rms}$, energy $E(\phi_g)$ and chemical potential μ_g.

β	$\phi_g(0)$	$x_{\rm rms}$	$E(\phi_g)$	$\mu_g = \mu_\beta(\phi_g)$
0	0.7511	0.7071	0.5000	0.5000
3.1371	0.6463	0.8949	1.0441	1.5272
12.5484	0.5301	1.2435	2.2330	3.5986
31.371	0.4562	1.6378	3.9810	6.5587
62.742	0.4067	2.0423	6.2570	10.384
156.855	0.3487	2.7630	11.464	19.083
313.71	0.3107	3.4764	18.171	30.279
627.42	0.2768	4.3757	28.825	48.063
1254.8	0.2467	5.5073	45.743	76.312

Tab. 1: Maximum value of the wave function $\phi_g(0)$, root mean square size $x_{\rm rms}$, energy $E(\phi_g)$ and ground state chemical potential μ_g verus the interaction coefficient β in 1d.

The results in Fig. 1. and Tab. 1. agree very well with the ground state solutions of BEC obtained by directly minimizing the energy functional [5].

Example 2 Ground state solution of BEC in 2d. Two cases are considered:

I. With a harmonic oscillator potential [5, 8, 44], i.e.

$$V(x, y) = \frac{1}{2}\left(\gamma_x^2 x^2 + \gamma_y^2 y^2\right).$$

II. With a harmonic oscillator potential and a potential of a stirrer corresponding a far-blue detuned Gaussian laser beam [27] *which is used to generate vortices in BEC* [27], i.e.

$$V(x, y) = \frac{1}{2}\left(\gamma_x^2 x^2 + \gamma_y^2 y^2\right) + w_0 e^{-\delta((x-r_0)^2+y^2)}.$$

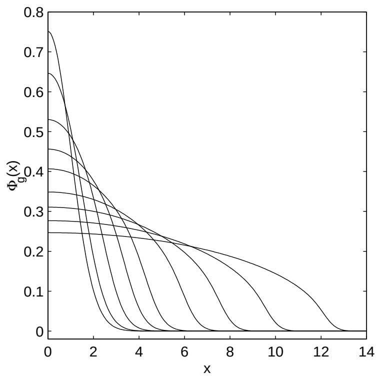

a)

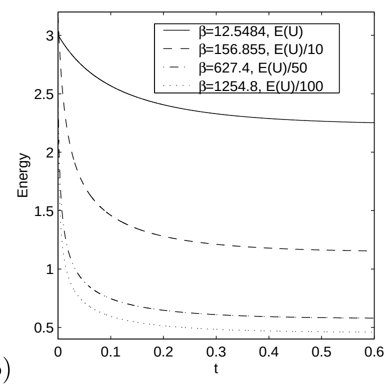

b)

Fig. 1: Ground state solution ϕ_g in Example 1. (a). For $\beta = 0,\ 3.1371,\ 12.5484,\ 31.371, 62.742, 156.855, 313.71, 627.42, 1254.8$ (with decreasing peak). (b). Energy evolution for different β.

The initial condition is chosen as

$$\phi_0(x,y) = \frac{(\gamma_x\gamma_y)^{1/4}}{\pi^{1/2}} e^{-(\gamma_x x^2+\gamma_y y^2)/2}.$$

For the case I, we choose $\gamma_x = 1$, $\gamma_y = 4$, $w_0 = \delta = r_0 = 0$, $\beta = 200$ and solve the problem by BEFD on $\Omega = [-8,8]\times[-4,4]$ with mesh size $h_x = 1/8$, $h_y = 1/16$ and time step $k = 0.1$. We get the following results from the ground state solution ϕ_g:

$$x_{\rm rms} = 2.2734, \quad y_{\rm rms} = 0.6074, \quad \phi_g^2(0) = 0.0808,$$
$$E(\phi_g) = 11.1563, \quad \mu_g = 16.3377.$$

For case II, we choose $\gamma_x = 1$, $\gamma_y = 1$, $w_0 = 4$, $\delta = r_0 = 1$, $\beta = 200$ and solve the problem by TSSP on $\Omega = [-8,8]^2$ with mesh size $h = 1/8$ and time step $k = 0.001$. We get the following results from the ground state solution ϕ_g:

$$x_{\rm rms} = 1.6951, \quad y_{\rm rms} = 1.7144, \quad \phi_g^2(0) = 0.034,$$
$$E(\phi_g) = 5.8507, \quad \mu_g = 8.3269.$$

In addition, Fig. 2 shows surface plots of the ground state solution ϕ_g.

Example 3 Ground state solution of BEC in 3d. Two cases are considered:

I. With a harmonic oscillator potential [5, 8, 44], i.e.

$$V(x,y,z) = \frac{1}{2}\left(\gamma_x^2x^2 + \gamma_y^2y^2 + \gamma_z^2z^2\right).$$

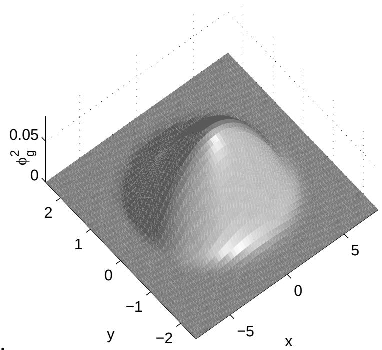

(a).

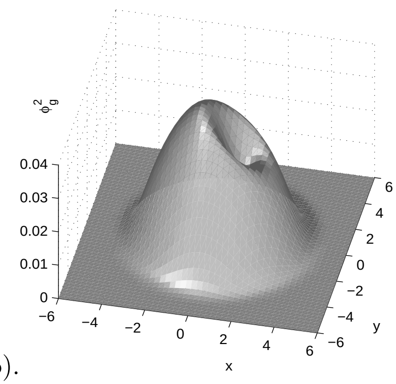

(b).

Fig. 2: Ground state solutions ϕ_g^2 in Example 2, case I (a), and case II (b).

II. With a harmonic oscillator potential and a potential of a stirrer corresponding a far-blue detuned Gaussian laser beam [27] *which is used to generate vortex in BEC* [27], i.e.

$$V(x,y,z) = \frac{1}{2}\left(\gamma_x^2 x^2 + \gamma_y^2 y^2 + \gamma_z^2 z^2\right) + w_0 e^{-\delta((x-r_0)^2+y^2)}.$$

The initial condition is chosen as

$$\phi_0(x,y,z) = \frac{(\gamma_x\gamma_y\gamma_z)^{1/4}}{\pi^{3/4}} e^{-(\gamma_x x^2+\gamma_y y^2+\gamma_z z^2)/2}.$$

For case I, we choose $\gamma_x = 1$, $\gamma_y = 2$, $\gamma_z = 4$, $w_0 = \delta = r_0 = 0$, $\beta = 200$ and solve the problem by TSSP on $\Omega = [-8,8]\times[-6,6]\times[-4,4]$ with mesh size $h_x = \frac{1}{8}$, $h_y = \frac{3}{32}$, $h_z = \frac{1}{16}$ and time step $k = 0.001$. The ground state solution ϕ_g gives:

$$x_{\rm rms} = 1.67, \quad y_{\rm rms} = 0.87, \quad z_{\rm rms} = 0.49,$$
$$\phi_g^2(0) = 0.052, \quad E(\phi_g) = 8.33, \quad \mu_g = 11.03.$$

For case II, we choose $\gamma_x = 1$, $\gamma_y = 1$, $\gamma_z = 2$, $w_0 = 4$, $\delta = r_0 = 1$, $\beta = 200$ and solve the problem by TSSP on $\Omega = [-8,8]^3$ with mesh size $h = \frac{1}{8}$ and time step $k = 0.001$. The ground state solution ϕ_g gives:

$$x_{\rm rms} = 1.37, \quad y_{\rm rms} = 1.43, \quad z_{\rm rms} = 0.70,$$
$$\phi_g^2(0) = 0.025, \quad E(\phi_g) = 5.27, \quad \mu_g = 6.71.$$

Furthermore, Fig. 3 shows surface plots of the ground state solution $\phi_g^2(x,0,z)$. BEFD gives similar results with $k = 0.1$.

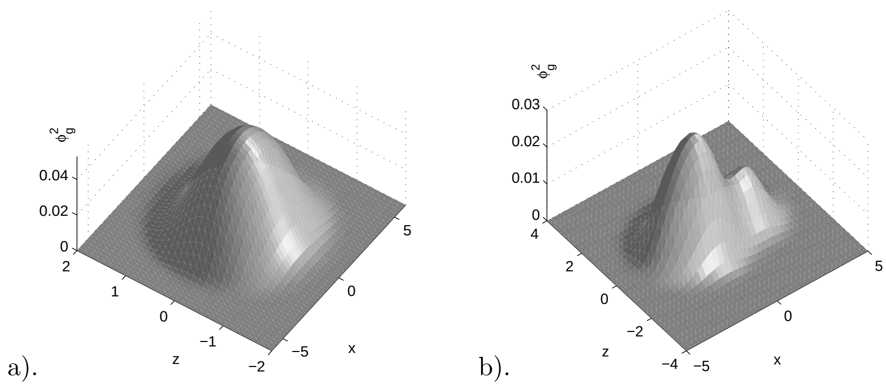

Fig. 3: Ground state solutions $\phi_g^2(x,0,z)$ in Example 3. (a). For case I. (b). For case II.

Example 4 2d central vortex states in BEC, i.e.

$$V(x,y) = V(r) = \frac{1}{2}\left(\frac{m^2}{r^2} + r^2\right),\ \phi_0(x,y) = \phi_0(r) = \frac{1}{\sqrt{\pi m!}}\, r^m\ e^{-r^2/2},\ 0 \le r.$$

The CNGF (10.15)-(10.16) is solved in polar coordinate with $\Omega = [0,8]$ with mesh size $h = \frac{1}{64}$ and time step $k = 0.1$ by using BEFD. Fig. 4a shows the ground state solution $\phi_g(r)$ with $\beta = 200$ for different index of the central vortex m. Tab. 2 displays the values of $\phi_g(0)$, radius mean square $r_{\rm rms}$, energy $E(\phi_g)$ and chemical potential μ_g.

Index m	$\phi_g(0)$	$r_{\rm rms}$	$E(\phi_g)$	$\mu_g = \mu_\beta(\phi_g)$
1	0.0000	2.4086	5.8014	8.2967
2	0.0000	2.5258	6.3797	8.7413
3	0.0000	2.6605	7.0782	9.3160
4	0.0000	2.8015	7.8485	9.9772
5	0.0000	2.9438	8.6660	10.6994
6	0.0000	3.0848	9.5164	11.4664

Tab. 2: Numerical results for 2d central vortex states in BEC.

Example 5. The first excited state solution of BEC in 1d with a harmonic oscillator potential, i.e.

$$V(x) = \frac{x^2}{2}, \qquad \phi_0(x) = \frac{\sqrt{2}}{(\pi)^{1/4}}\ x\ e^{-x^2/2}, \quad x \in \mathbb{R}.$$

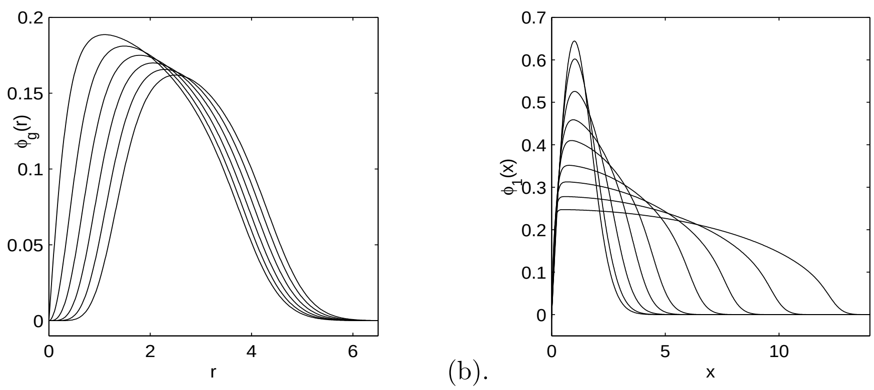

(a). (b).

Fig. 4: (a). 2d central vortex states $\phi_g(r)$ in Example 4. $\beta = 200$ for $m = 1$ to 6 (with decreasing peak). (b). First excited state solution $\phi_1(x)$ (an odd function) in Example 5. For $\beta = 0$, 3.1371, 12.5484, 31.371, 62.742, 156.855, 313.71, 627.42, 1254.8 (with decreasing peak).

The CNGF (10.15)-(10.16) with $d = 1$ is solved on $\Omega = [-16, 16]$ with mesh size $h = 1/64$ and time step $k = 0.1$ by using BEFD. Fig. 4b shows the first excited state solution $\phi_1(x)$ for different β. Tab. 3 displays the radius mean square $x_{\rm rms} = \|x\phi_1\|_{L^2(\Omega)}$, ground state and first excited state energies $E(\phi_g)$ and $E(\phi_1)$, ratio $E(\phi_1)/E(\phi_g)$, chemical potentials $\mu_g = \mu_\beta(\phi_g)$ and $\mu_1 = \mu_\beta(\phi_1)$, ratio μ_1/μ_g.

β	$x_{\rm rms}$	$E(\phi_g)$	$E(\phi_1)$	$\frac{E(\phi_1)}{E(\phi_g)}$	μ_g	μ_1	$\frac{\mu_1}{\mu_g}$
0	1.2247	0.500	1.500	3.000	0.500	1.500	3.000
3.1371	1.3165	1.044	1.941	1.859	1.527	2.357	1.544
12.5484	1.5441	2.233	3.037	1.360	3.598	4.344	1.207
31.371	1.8642	3.981	4.743	1.192	6.558	7.279	1.110
62.742	2.2259	6.257	6.999	1.119	10.38	11.089	1.068
156.855	2.8973	11.46	12.191	1.063	19.08	19.784	1.037
313.71	3.5847	18.17	18.889	1.040	30.28	30.969	1.023
627.42	4.4657	28.82	29.539	1.025	48.06	48.733	1.014
1254.8	5.5870	45.74	46.453	1.016	76.31	76.933	1.008

Tab. 3: Numerical results for the first excited state solution in 1d in Example 5.

From the results in Tab. 3 and Fig. 4b, we can see that the BEFD can be applied directly to compute the first excited states in BEC. Furthermore, we have

$$\lim_{\beta\to+\infty} \frac{E(\phi_1)}{E(\phi_g)} = 1, \qquad \lim_{\beta\to+\infty} \frac{\mu_1}{\mu_g} = 1.$$

These results are confirmed with the results in [5] where the ground and first excited states are computed by directly minimizing the energy functional through the finite element discretization.

11. Numerical methods for dynamics of NLSE

In this section we present time-splitting sine pseudospectral (TSSP) methods for the problem (4.1), (4.2) with/without external driven field with homogeneous Dirichlet boundary conditions. For the simplicity of notation we shall introduce the method for the case of one space dimension ($d = 1$). Generalizations to $d > 1$ are straightforward for tensor product grids and the results remain valid without modifications. For $d = 1$, the problem with an external driven field becomes

$$i\partial_t\psi = -\frac{1}{2}\partial_{xx}\psi + V(x)\psi + W(x,t)\psi + \beta|\psi|^2\psi, \ a < x < b, \ t > 0, \quad (11.1)$$

$$\psi(x, t = 0) = \psi_0(x), \quad a \le x \le b, \quad \psi(a, t) = \psi(b, t) = \mathbf{0}, \quad t \ge 0; \quad (11.2)$$

where $W(x, t)$ is an external driven field. Typical external driven fields used in physical literatures include a far-blued detuned Gaussian laser beam stirrer [27]

$$W(\mathbf{x}, t) = W_s(t) \exp\left[-\left(\frac{|\mathbf{x} - \mathbf{x}_s(t)|^2}{w_s/2}\right)\right], \quad (11.3)$$

with W_s the height, w_s the width, and $\mathbf{x}_s(t)$ the position of the stirrer; or a Delta-kicked potential [77]

$$W(x, t) = K \cos(kx) \sum_{n=-\infty}^{\infty} \delta(t - n\tau), \quad (11.4)$$

with K the kick strength, k the wavenumber, τ the time interval between kicks, and $\delta(\tau)$ is the Dirac delta function.

11.1. *General high-order split-step method*

As preparatory steps, we begin by introducing the general high-order split-step method [53] for a general evolution equation

$$i\ \partial_t u = f(u) = A\ u + B\ u, \quad (11.5)$$

where $f(u)$ is a nonlinear operator and the splitting $f(u) = Au + Bu$ can be quite arbitrary, in particular, A and B do not need to commute. For a given time step $k = \Delta t > 0$, let $t_n = n\ k$, $n = 0, 1, 2, \ldots$ and u^n be the approximation of $u(t_n)$. A second-order symplectic time integrator (cf. [111]) for (11.5) is as follows:

$$\begin{aligned} u^{(1)} &= e^{-ik\ A/2}\ u^n; \\ u^{(2)} &= e^{-ik\ B}\ u^{(1)}; \\ u^{n+1} &= e^{-ik\ A/2}\ u^{(2)}. \end{aligned} \tag{11.6}$$

A fourth-order symplectic time integrator (cf. [120]) for (11.5) is as follows:

$$\begin{aligned} u^{(1)} &= e^{-i2w_1k\ A}\ u^n; \\ u^{(2)} &= e^{-i2w_2k\ B}\ u^{(1)}; \\ u^{(3)} &= e^{-i2w_3k\ A}\ u^{(2)}; \\ u^{(4)} &= e^{-i2w_4k\ B}\ u^{(3)}; \\ u^{(5)} &= e^{-i2w_3k\ A}\ u^{(4)}; \\ u^{(6)} &= e^{-i2w_2k\ B}\ u^{(5)}; \\ u^{n+1} &= e^{-i2w_1k\ A}\ u^{(6)}; \end{aligned} \tag{11.7}$$

where

$$w_1 = 0.33780\ 17979\ 89914\ 40851,\ w_2 = 0.67560\ 35959\ 79828\ 81702,$$
$$w_3 = -0.08780\ 17979\ 89914\ 40851,\ w_4 = -0.85120\ 71979\ 59657\ 63405.$$

11.2. *Fourth-order TSSP for GPE without external driving field*

We choose the spatial mesh size $h = \triangle x > 0$ with $h = (b-a)/M$ for M an even positive integer, and let $x_j := a + j\ h$, $j = 0, 1, \cdots, M$. Let ψ_j^n be the approximation of $\psi(x_j, t_n)$ and ψ^n be the solution vector at time $t = t_n = nk$ with components ψ_j^n.

We now rewrite the GPE (11.1) without external driven field, i.e. $W(\mathbf{x}, t) \equiv 0$, in the form of (11.5) with

$$A\psi = V(x)\psi(x,t) + \beta|\psi(x,t)|^2\psi(x,t), \qquad B\psi = -\frac{1}{2}\partial_{xx}\psi(x,t). \tag{11.8}$$

Thus, the key for an efficient implementation of (11.7) is to solve efficiently the following two subproblems:

$$i\ \partial_t\psi(x,t) = B\psi = -\frac{1}{2}\partial_{xx}\psi, \tag{11.9}$$

and

$$i\,\partial_t\psi(x,t) = V(x)\psi(x,t) + \beta|\psi(x,t)|^2\psi(x,t). \tag{11.10}$$

Equation (11.9) will be discretized in space by the sine pseudospectral method and integrated in time *exactly*. For $t \in [t_n, t_{n+1}]$, the ODE (11.10) leaves $|\psi|$ invariant in t [11, 10] and therefore becomes

$$i\psi_t(x,t) = V(x)\psi(x,t) + \beta|\psi(x,t_n)|^2\psi(x,t) \tag{11.11}$$

and thus can be integrated *exactly*.

From time $t = t_n$ to $t = t_{n+1}$, we combine the splitting steps via the fourth-order split-step method and obtain a fourth-order time-splitting sine-spectral (**TSSP4**) method for the GPE (10.34). The detailed method is given by

$$\begin{aligned}
\psi_j^{(1)} &= e^{-i2w_1k(V(x_j)+\beta|\psi_j^n|^2)}\ \psi_j^n, \\
\psi_j^{(2)} &= \sum_{l=1}^{M-1} e^{-iw_2k\mu_l^2}\ \widehat{\psi}_l^{(1)}\ \sin(\mu_l(x_j-a)), \\
\psi_j^{(3)} &= e^{-i2w_3k(V(x_j)+\beta|\psi_j^{(2)}|^2)}\ \psi_j^{(2)}, \\
\psi_j^{(4)} &= \sum_{l=1}^{M-1} e^{-iw_4k\mu_l^2}\ \widehat{\psi}_l^{(3)}\ \sin(\mu_l(x_j-a)), \qquad j = 1,2,\cdots,M-1, \\
\psi_j^{(5)} &= e^{-i2w_3k(V(x_j)+\beta|\psi_j^{(4)}|^2)}\ \psi_j^{(4)}, \\
\psi_j^{(6)} &= \sum_{l=1}^{M-1} e^{-iw_2k\mu_l^2}\ \widehat{\psi}_l^{(5)}\ \sin(\mu_l(x_j-a)), \\
\psi_j^{n+1} &= e^{-i2w_1k(V(x_j)+\beta|\psi_j^{(6)}|^2)}\ \psi_j^{(6)},
\end{aligned} \tag{11.12}$$

where $\widehat{U}_l$, the sine-transform coefficients of a complex vector $U = (U_0, U_1, \cdots, U_M)$ with $U_0 = U_M = \mathbf{0}$, are defined as

$$\mu_l = \frac{\pi l}{b-a}, \quad \widehat{U}_l = \frac{2}{M}\sum_{j=1}^{M-1} U_j\ \sin(\mu_l(x_j-a)),\ l = 1,2,\cdots,M-1, \tag{11.13}$$

with

$$\psi_j^0 = \psi(x_j,0) = \psi_0(x_j), \qquad j = 0,1,2,\cdots,M. \tag{11.14}$$

Note that the only time discretization error of TSSP4 is the splitting error, which is fourth order in k for any fixed mesh size $h > 0$.

This scheme is explicit, time reversible, just as the IVP for the GPE. Also, a main advantage of the time-splitting method is its time-transverse invariance, just as it holds for the GPE itself. If a constant α is added to the potential V_1, then the discrete wave functions ψ_j^{n+1} obtained from TSSP4 get multiplied by the phase factor $e^{-i\alpha(n+1)k}$, which leaves the discrete quadratic observables unchanged. This property does not hold for finite difference schemes.

11.3. *Second-order TSSP for GPE with external driving field*

We now rewrite the GPE (11.1) with an external driven field

$$\begin{aligned} A\psi &= -\frac{1}{2}\partial_{xx}\psi(x,t), \\ B\psi &= V(x)\psi(x,t) + W(x,t)\psi(x,t) + \beta|\psi(x,t)|^2\psi(x,t). \end{aligned} \tag{11.15}$$

Due to the external driven field could be vary complicated, e.g. it may be a Delta-function [77], here we only use a second-order split-step scheme in time discretization. More precisely, from time $t = t_n$ to $t = t_{n+1}$, we proceed as follows:

$$\begin{aligned} \psi_j^* &= \sum_{l=1}^{M-1} e^{-ik\mu_l^2/4}\, \widehat{(\psi^n)}_l \, \sin(\mu_l(x_j - a)), \qquad j = 1, 2, \cdots, M-1, \\ \psi_j^{**} &= \exp\left[-ik(V(x_j) + \beta|\psi_j^n|^2) - i\int_{t_n}^{t_{n+1}} W(x_j,t)dt\right]\ \psi_j^*, \\ \psi_j^{n+1} &= \sum_{l=1}^{M-1} e^{-ik\mu_l^2/4}\, \widehat{(\psi^{**})}_l \, \sin(\mu_l(x_j - a)). \end{aligned} \tag{11.16}$$

Remark 11.1: If the integral in (11.16) could not be evaluated analytically, one can use numerical quadrature to evaluate, e.g.

$$\int_{t_n}^{t_{n+1}} W(x_j,t)dt \approx \frac{k}{6}\left[W(x_j,t_n) + 4W(x_j,t_n + k/2) + W(x_j,t_{n+1})\right].$$

11.4. *Stability*

Let $U = (U_0, U_1, \cdots, U_M)^T$ with $U_0 = U_M = \mathbf{0}$, $f(x)$ a homogeneous periodic function on the interval $[a,b]$, and let $\|\cdot\|_{l^2}$ be the usual discrete

l^2-norm on the interval (a,b), i.e.,

$$\|U\|_{l^2} = \sqrt{\frac{b-a}{M}\sum_{j=1}^{M-1}|U_j|^2}, \qquad \|f\|_{l^2} = \sqrt{\frac{b-a}{M}\sum_{j=1}^{M-1}|f(x_j)|^2}. \quad (11.17)$$

For the *stability* of the second-order time-splitting spectral approximations TSSP2 (11.16) and fourth-order scheme (11.12), we have the following lemma, which shows that the total charge is conserved.

Lemma 11.2: *The second-order time-splitting sine pseudospectral scheme (11.16) and fourth-order scheme (11.12) are unconditionally stable. In fact, for every mesh size $h > 0$ and time step $k > 0$,*

$$\|\psi^n\|_{l^2} = \|\psi^0\|_{l^2} = \|\psi_0\|_{l^2}, \qquad n = 1, 2, \cdots \quad (11.18)$$

Proof: For the scheme TSSP2 (11.16), noting (10.43) and (11.17), one has

$$\begin{aligned}
\frac{1}{b-a}\|\psi^{n+1}\|_{l^2}^2 &= \frac{1}{M}\sum_{j=1}^{M-1}\left|\psi_j^{n+1}\right|^2 \\
&= \frac{1}{M}\sum_{j=1}^{M-1}\left|\sum_{l=1}^{M-1} e^{-ik\mu_l^2/4}\,\widehat{(\psi^{**})}_l\,\sin(\mu_l(x_j-a))\right|^2 \\
&= \frac{1}{M}\sum_{j=1}^{M-1}\left|\sum_{l=1}^{M-1} e^{-ik\mu_l^2/4}\,\widehat{(\psi^{**})}_l\,\sin(jl\pi/M)\right|^2 \\
&= \frac{1}{2}\sum_{l=1}^{M-1}\left|e^{-ik\mu_l^2/4}\,\widehat{(\psi^{**})}_l\right|^2 = \frac{1}{2}\sum_{l=1}^{M-1}\left|\widehat{(\psi^{**})}_l\right|^2. \quad (11.19)
\end{aligned}$$

Plugging (10.43) into (11.19), we obtain

$$\begin{aligned}
&\frac{1}{b-a}\|\psi^{n+1}\|_{l^2}^2 = \frac{1}{2}\sum_{l=1}^{M-1}\left|\frac{2}{M}\sum_{j=1}^{M-1}\psi_j^{**}\,\sin(\mu_l(x_j-a))\right|^2 \\
&= \frac{1}{2}\sum_{l=1}^{M-1}\left|\frac{2}{M}\sum_{j=1}^{M-1}\psi_j^{**}\,\sin(lj\pi/M)\right|^2 = \frac{1}{M}\sum_{j=1}^{M-1}\left|\psi_j^{**}\right|^2 \\
&= \frac{1}{M}\sum_{j=1}^{M-1}\left|\exp\left[-ik(V(x_j)+\beta|\psi_j^n|^2) - i\int_{t_n}^{t_{n+1}} W(x_j,t)dt\right]\ \psi_j^*\right|^2 \\
&= \frac{1}{M}\sum_{j=1}^{M-1}\left|\psi_j^*\right|^2 = \frac{1}{M}\sum_{j=1}^{M-1}\left|\psi_j^n\right|^2 = \frac{1}{b-a}\|\psi^n\|_{l^2}^2. \quad (11.20)
\end{aligned}$$

Here we used the identities

$$\sum_{j=1}^{M-1} \sin(lj\pi/M)\sin(kj\pi/M) = \begin{cases} 0, & k = l, \\ M/2, & k \neq l. \end{cases} \tag{11.21}$$

For the scheme TSSP4 (11.12), using (10.43), (11.17) and (11.21), we get similarly

$$\begin{aligned}
\frac{1}{b-a}\|\psi^{n+1}\|_{l^2}^2 &= \frac{1}{M}\sum_{j=0}^{M-1}\left|\psi_j^{n+1}\right|^2 \\
&= \frac{1}{M}\sum_{j=0}^{M-1}\left|e^{-i2w_1k(V(x_j)+\beta|\psi_j^{(6)}|^2)}\ \psi_j^{(6)}\right|^2 \\
&= \frac{1}{M}\sum_{j=0}^{M-1}\left|\psi_j^{(6)}\right|^2 \\
&= \frac{1}{M}\sum_{j=0}^{M-1}\left|\sum_{l=1}^{M-1} e^{-iw_2k\mu_l^2}\ \widehat{\psi}_l^{(5)}\ \sin(\mu_l(x_j-a))\right|^2 \\
&= \frac{1}{M}\sum_{j=0}^{M-1}\left|\sum_{l=1}^{M-1} e^{-iw_2k\mu_l^2}\ \widehat{\psi}_l^{(5)}\ \sin(lj\pi/M)\right|^2 \\
&= \frac{1}{2}\sum_{l=1}^{M-1}\left|e^{-iw_2k\mu_l^2}\ \widehat{\psi}_l^{(5)}\right|^2 = \frac{1}{2}\sum_{l=1}^{M-1}\left|\widehat{\psi}_l^{(5)}\right|^2.
\end{aligned} \tag{11.22}$$

Plugging (10.43)) into (11.22), we have

$$\begin{aligned}
\frac{1}{b-a}\|\psi^{n+1}\|_{l^2}^2 &= \frac{1}{2}\sum_{l=1}^{M-1}\left|\frac{2}{M}\sum_{j=1}^{M-1}\psi_j^{(5)}\ \sin(\mu_l(x_j-a))\right|^2 \\
&= \frac{1}{2}\sum_{l=1}^{M-1}\left|\frac{2}{M}\sum_{j=1}^{M-1}\psi_j^{(5)}\ \sin(jl\pi/M)\right|^2 = \frac{1}{M}\sum_{j=1}^{M-1}\left|\psi_j^{(5)}\right|^2 \\
&= \frac{1}{M}\sum_{j=1}^{M-1}\left|\psi_j^{(4)}\right|^2 = \frac{1}{M}\sum_{j=1}^{M-1}\left|\psi_j^{(3)}\right|^2 = \frac{1}{M}\sum_{j=1}^{M-1}\left|\psi_j^{(2)}\right|^2 \\
&= \frac{1}{M}\sum_{j=1}^{M-1}\left|\psi_j^{(1)}\right|^2 = \frac{1}{M}\sum_{j=1}^{M-1}\left|\psi_j^{n}\right|^2 \\
&= \frac{1}{b-a}\|\psi^n\|_{l^2}^2.
\end{aligned} \tag{11.23}$$

Thus the equality (11.18) can be obtained from (11.19) for the scheme TSSP2 and (11.22) for the scheme TSSP4 by induction. □

11.5. *Crank-Nicolson finite difference method (CNFD)*

Another scheme used to disretize the NLSE (11.1) is the *Crank-Nicolson finite difference method (CNFD)*. In this method one uses the Crank-Nicolson scheme for time derivative and the second order central difference scheme for spatial derivative. The detailed method is:

$$\begin{aligned} i\frac{\psi_j^{n+1}-\psi_j^n}{k} &= -\frac{1}{4h^2}\left(\psi_{j+1}^{n+1}-2\psi_j^{n+1}+\psi_{j-1}^{n+1}+\psi_{j+1}^{n}-2\psi_j^{n}+\psi_{j-1}^{n}\right) \\ &\quad +\frac{V(x_j)}{2}\left(\psi_j^{n+1}+\psi_j^n\right)+\frac{\beta}{2}\left(|\psi_j^{n+1}|^2+|\psi_j^n|^2\right)\left(\psi_j^{n+1}+\psi_j^n\right), \\ &\quad j=1,2,\cdots,M-1, \qquad n=0,1,\cdots, \qquad (11.24) \\ \psi_0^{n+1} &= \psi_M^{n+1}=0, \qquad n=0,1,\cdots, \\ \psi_j^0 &= \psi_0(x_j), \qquad j=0,1,2,\cdots,M. \end{aligned}$$

11.6. *Numerical results*

In this subsection we present numerical results to confirm spectral accuracy in space and fourth order accuracy in time of the numerical method (11.12), and then apply it to study time-evolution of condensate width in 1D, 2D and 3D.

Example 6 1d Gross-Pitaevskii equation, i.e. in (4.1) we choose $d=1$ and $\gamma_x=1$. The initial condition is taken as

$$\psi_0(x)=\frac{1}{\pi^{1/4}}e^{-x^2/2}, \qquad x\in\mathbb{R}.$$

We solve on the interval $[-32,32]$, i.e. $a=-32$ and $b=32$ with homogeneous Dirichlet boundary condition (11.2). We compute a numerical solution by using TSSP4 with a very fine mesh, e.g. $h=\frac{1}{128}$, and a very small time step, e.g. $k=0.0001$, as the 'exact' solution ψ. Let $\psi^{h,k}$ denote the numerical solution under mesh size h and time step k.

First we test the spectral accuracy of TSSP4 in space. In order to do so, for each fixed β_1, we solve the problem with different mesh size h but a very small time step, e.g. $k=0.0001$, such that the truncation error from time discretization is negligible comparing to that from space discretization. Tab. 4 shows the errors $\|\psi(t)-\psi^{h,k}(t)\|_{l^2}$ at $t=2.0$ with $k=0.0001$ for different β_1 and h.

mesh	$h=1$	$h=\frac{1}{2}$	$h=\frac{1}{4}$	$h=\frac{1}{8}$	$h=\frac{1}{16}$
$\beta_1=10$	0.2745	1.081E-2	1.805E-6	3.461E-11	
$\beta_1=20\sqrt{2}$	1.495	0.1657	7.379E-4	7.588E-10	
$\beta_1=80$	1.603	1.637	6.836E-2	3.184E-5	3.47E-11

Tab. 4: Spatial error analysis: Error $\|\psi(t)-\psi^{h,k}(t)\|_{l^2}$ at $t=2.0$ with $k=0.0001$ in Example 6.

Then we test the fourth-order accuracy of TSSP4 in time. In order to do so, for each fixed β_1, we solve the problem with different time step k but a very fine mesh, e.g. $h=\frac{1}{64}$, such that the truncation error from space discretization is negligible comparing to that from time discretization. Tab. 5 shows the errors $\|\psi(t)-\psi^{h,k}(t)\|_{l^2}$ at $t=2.0$ with $h=\frac{1}{64}$ for different β_1 and k.

time step	$k=\frac{1}{20}$	$k=\frac{1}{40}$	$k=\frac{1}{80}$	$k=\frac{1}{160}$	$k=\frac{1}{320}$
$\delta=10.0$	1.261E-4	8.834E-6	5.712E-7	3.602E-8	2.254E-9
$\delta=20\sqrt{2}$	1.426E-3	9.715E-5	6.367E-6	4.034E-7	2.529E-8
$\delta=80$	4.375E-2	1.693E-3	8.982E-5	5.852E-6	3.706E-7

Tab. 5: Temporal error analysis: $\|\psi(t)-\psi^{h,k}(t)\|_{l^2}$ at $t=2.0$ with $h=\frac{1}{64}$ in Example 6.

As shown in Tabs. 4&5, spectral order accuracy for spatial derivatives and fourth-order accuracy for time derivative of TSSP4 are demonstrated numerically for 1d GPE, respectively. Another issue is how to choose mesh size h and time step k in the strong repulsive interaction regime or semiclassical regime, i.e. $\beta_d \gg 1$, in order to get "correct" physical observables. In fact, after a rescaling in (4.1) under the normalization (4.3): $\mathbf{x}\to\varepsilon^{-1/2}\mathbf{x}$ and $\psi\to\varepsilon^{d/4}\psi$ with $\varepsilon=\beta_d^{-2/(d+2)}$, then the GPE (4.1) can be rewritten as

$$i\varepsilon\,\partial_t\psi(\mathbf{x},t)=-\frac{\varepsilon^2}{2}\nabla^2\psi+V_d(\mathbf{x})\psi+|\psi|^2\psi,\quad \mathbf{x}\in\mathbb{R}^d. \tag{11.25}$$

As demonstrated in [10, 11], the meshing strategy to capture 'correct' phys-

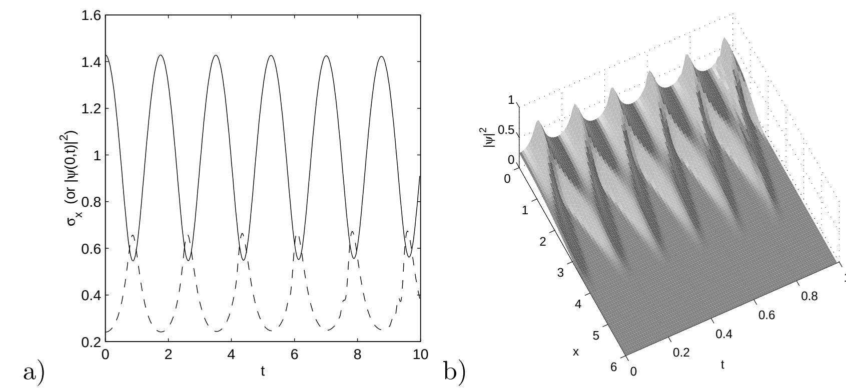

Fig. 5: Numerical results for Example 7: a) Condensate width σ_x ('—') and central density $|\psi(0,t)|^2$ ('- - - '). b) Evolution of the density function $|\psi|^2$.

ical observables for this this problem is

$$h = O(\varepsilon), \qquad k = O(\varepsilon).$$

Thus the admissible meshing strategy for the GPE with strong repulsive interaction is

$$h = O(\varepsilon) = O\left(1/\beta_d^{2/(d+2)}\right), \quad k = O(\varepsilon) = O\left(1/\beta_d^{2/(d+2)}\right), \qquad d = 1, 2, 3. \tag{11.26}$$

Example 7 1d Gross-Pitaevskii equation, i.e. in (4.1) we choose $d = 1$. The initial condition is taken as the ground-state solution of (4.1) under $d = 1$ with $\gamma_x = 1$ and $\beta_1 = 20.0$ [6, 5], i.e. initially the condensate is assumed to be in its ground state. When $t = 0$, we double the trap frequency by setting $\gamma_x = 2$.

We solve this problem on the interval $[-12, 12]$ under mesh size $h = \frac{3}{64}$ and time step $k = 0.005$ with homogeneous Dirichlet boundary condition. Fig. 5 plots the condensate width and central density $|\psi(0,t)|^2$ as functions of time, as well as evolution of the density $|\psi|^2$ in space-time. One can see from this figure that the sudden change in the trap potential leads to oscillations in the condensate width and the peak value of the wave function. Note that the condensate width contracts in an oscillatory way (cf. Fig. 5a), which agrees with the analytical results in (4.43).

Example 8 2d Gross-Pitaevskii equation, i.e. in (4.1) we choose $d = 2$. The initial condition is taken as the ground-state solution of (4.1) under

a) 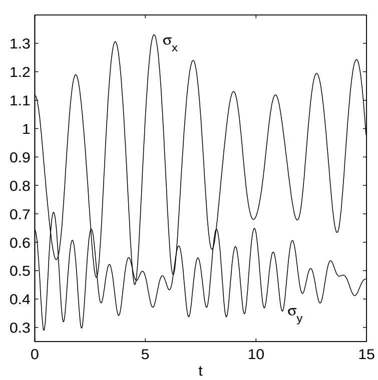

b) 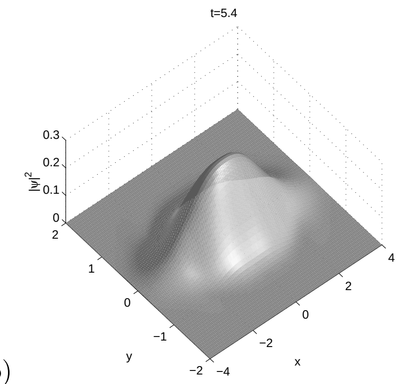

Fig. 6: Numerical results for Example 8: a) Condensate width. b) Surface plot of the density $|\psi|^2$ at $t = 5.4$.

$d = 2$ with $\gamma_x = 1$, $\gamma_y = 2$ and $\beta_2 = 20.0$ [6, 5], i.e. initially the condensate is assumed to be in its ground state. When at $t = 0$, we double the trap frequency by setting $\gamma_x = 2$ and $\gamma_y = 4$.

We solve this problem on $[-8, 8]^2$ under mesh size $h = \frac{1}{32}$ and time step $k = 0.005$ with homogeneous Dirichlet boundary condition. Fig. 6 shows the condensate widths σ_x and σ_y as functions of time and the surface of the density $|\psi|^2$ at time $t = 5.4$. Fig. 7 the contour plots of the density $|\psi|^2$ at different times. Again, the sudden change in the trap potential leads to oscillations in the condensate width. Due to $\gamma_y = 2\gamma_x$, the oscillation frequency of σ_y is roughly double that of σ_x and the amplitudes of σ_x are larger than those of σ_y in general (cf. Fig. 6a). Again this agrees with the analytical results in (4.43).

Example 9 3d Gross-Pitaevskii equation, i.e. in (4.1) we choose $d = 3$. We present computations for two cases:

Case I. Intermediate ratio between trap frequencies along different axis (data for ^{87}Rb used in JILA [3]). The initial condition is taken as the ground-state solution of (4.1) under $d = 3$ with $\gamma_x = \gamma_y = 1$, $\gamma_z = 4$ and $\beta_3 = 37.62$ [6, 5]. When at $t = 0$, we four times the trap frequency by setting $\gamma_x = \gamma_y = 4$ and $\gamma_z = 16$.

Case II. High ratio between trap frequencies along different axis (data for ^{23}Na used in MIT (group of Ketterle) [38]). The initial condition is taken as the ground-state solution of (4.1) under $d = 3$ with $\gamma_x = \gamma_y = \frac{360}{3.5}$,

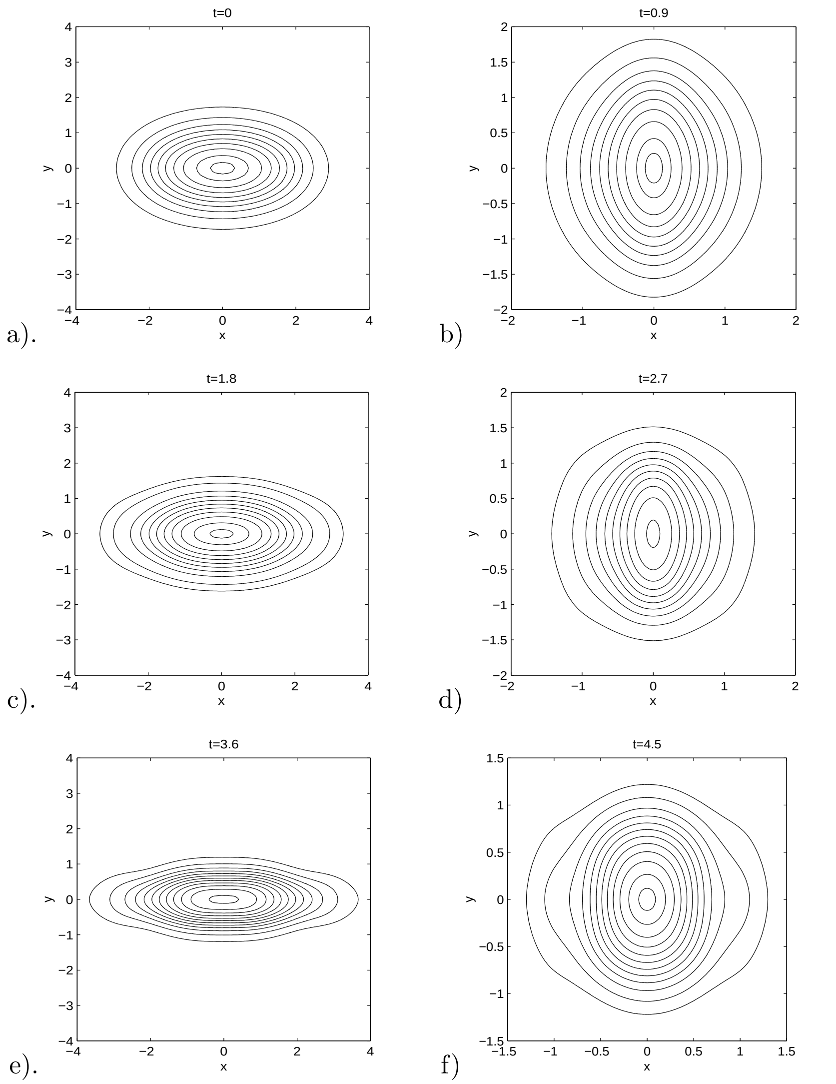

Fig. 7: Contour plots of the density $|\psi|^2$ at different times in Example 8. a). $t = 0$, b). $t = 0.9$, c). $t = 1.8$, d). $t = 2.7$, e). $t = 3.6$, f). $t = 4.5$.

$\gamma_z = 1$ and $\beta_3 = 3.083$ [6, 5]. When at $t = 0$, we double the trap frequency by setting $\gamma_x = \gamma_y = \frac{720}{3.5}$ and $\gamma_z = 2$.

For case I, we solve the problem on $[-6, 6] \times [-6, 6] \times [-3, 3]$ under mesh size $h_x = h_y = \frac{3}{32}$ and $h_z = \frac{3}{64}$, and time step $k = 0.0025$ with homoge-

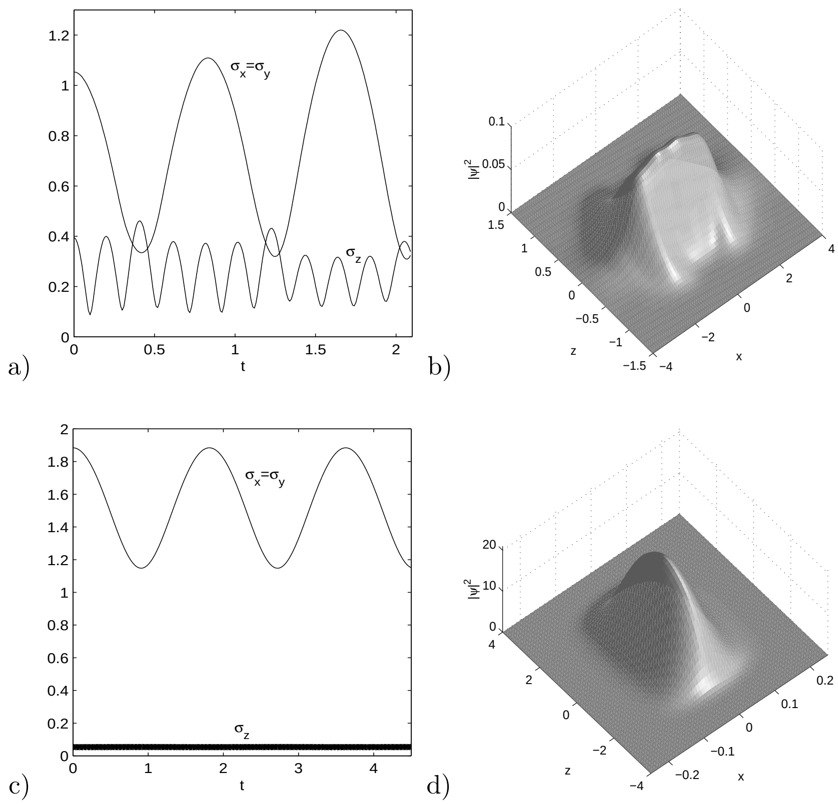

Fig. 8: Numerical results for Example 9: Left column: Condensate width; right column: Surface plot of the density in xz-plane, $|\psi(x,0,z,t)|^2$. Case I: a) and b) at $t = 1.64$. Case II: c) and d) at $t = 4.5$.

neous Dirichlet boundary condition. For case II, we solve the problem on $[-0.5, 0.5] \times [-0.5, 0.5] \times [-8, 8]$ under mesh size $h_x = h_y = \frac{1}{128}$ and $h_z = \frac{1}{8}$, and time step $k = 0.0005$ with homogeneous Dirichlet boundary condition along their boundaries.

Fig. 8 shows the condensate widths $\sigma_x = \sigma_y$ and σ_z as functions of time, as well as the surface of the density in xz-plane $|\psi(x,0,z,t)|^2$. Similar phenomena in case I in 3d is observed as those in Example 8 which is in 2d (cf. Fig. 6a). The ratio between the condensate widths increases with increasing the ratio between trap frequencies along different axis, i.e. it becomes more difficult to excite oscillations for large trap frequencies. In case II, the curves of the condensate widths are very well separated. This behavior is one of the basic assumptions allowing the reduction of GPE to 2d and 1d in the cases one or two of the trap frequencies are much larger than the others [85, 5, 8].

12. Derivation of the vector Zakharov system

In this section, we derive VZS from the two-fluid model [113] for ion-electron dynamics in plasma physics. Here we will use a more formal approach based on the multiple-scale modulation analysis. Following from [113], we will consider a plasma as two interpenetrating fluids, an electron fluid and an ion fluid, and denote the mass, number density (number of particles per unit volume) and velocity of the electrons (respectively of the ions), by m_e, $N_e(\mathbf{x}, t)$ and $\mathbf{v}_e(\mathbf{x}, t)$ (respectively m_i, $N_i(\mathbf{x}, t)$ and $\mathbf{v}_i(\mathbf{x}, t)$). The continuity equations for these fluids read

$$\partial_t N_e + \nabla \cdot (N_e \mathbf{v}_e) = 0, \tag{12.1}$$

$$\partial_t N_i + \nabla \cdot (N_i \mathbf{v}_i) = 0, \qquad \mathbf{x} \in \mathbb{R}^3, \quad t > 0 \tag{12.2}$$

and the momentum equations read

$$m_e\, N_e(\partial_t \mathbf{v}_e + \mathbf{v}_e \cdot \nabla \mathbf{v}_e) = -\nabla p_e - e\, N_e \left(\mathcal{E} + \frac{1}{c}\, \mathbf{v}_e \times \mathcal{B}\right), \tag{12.3}$$

$$m_i\, N_i(\partial_t \mathbf{v}_i + \mathbf{v}_i \cdot \nabla \mathbf{v}_i) = -\nabla p_i + e\, N_i \left(\mathcal{E} + \frac{1}{c}\, \mathbf{v}_i \times \mathcal{B}\right), \tag{12.4}$$

where $-e$ and e represent the charge of the electron and the ions assumed to reduce to protons, respectively; p_e and p_i are the pressure. For small fluctuations, we write $\nabla p_e = \gamma_e\, T_e\, \nabla N_e$ and $\nabla p_i = \gamma_i\, T_i\, \nabla N_i$, where γ_e and γ_i denote the specific heat ratios of the electrons and the ions and T_e and T_i their respective temperatures in energy units. The electric field $\mathcal{E}$ and magnetic field $\mathcal{B}$ are provided by the Maxwell equations

$$-\frac{1}{c}\, \partial_t \mathcal{E} + \nabla \times \mathcal{B} = \frac{4\pi}{c}\, \mathbf{j}, \qquad \nabla \cdot \mathcal{E} = 4\pi\rho, \tag{12.5}$$

$$\frac{1}{c}\, \partial_t \mathcal{B} + \nabla \times \mathcal{E} = 0, \qquad \nabla \cdot \mathcal{B} = 0, \tag{12.6}$$

where $\rho = -e(N_e - N_i)$ and $\mathbf{j} = -e(N_e \mathbf{v}_e - N_i \mathbf{v}_i)$ are the densities of total charge and total current, respectively.

Equations (12.5) and (12.6) yield

$$\frac{1}{c^2} \partial_{tt} \mathcal{E} + \nabla \times (\nabla \times \mathcal{E}) + \frac{4\pi}{c^2} \partial_t \mathbf{j} = 0, \tag{12.7}$$

and using equations (12.1)-(12.4), we have

$$\begin{aligned}\partial_t \mathbf{j} = e(\nabla\cdot(N_e\mathbf{v}_e)\mathbf{v}_e + N_e\mathbf{v}_e\cdot\nabla\mathbf{v}_e + \frac{1}{m_e}\nabla p_e + \frac{eN_e}{m_e}(\mathcal{E} + \frac{1}{c}\mathbf{v}_e\times\mathcal{B}))\\ -e(\nabla\cdot(N_i\mathbf{v}_i)\mathbf{v}_i + N_i\mathbf{v}_i\cdot\nabla\mathbf{v}_i + \frac{1}{m_i}\nabla p_i + \frac{eN_i}{m_i}(\mathcal{E} + \frac{1}{c}\mathbf{v}_i\times\mathcal{B})). \quad (12.8)\end{aligned}$$

In order to get VZS from the two-fluid model just mentioned, as in [113], we consider a long-wavelength small-amplitude Langmuir oscillation of the form

$$\mathcal{E} = \frac{\varepsilon}{2}(\mathbf{E}(\mathbf{X},T)e^{-i\omega_e t} + c.c.) + \varepsilon^2\hat{\mathbf{E}}(\mathbf{X},T) + \cdots, \qquad (12.9)$$

where the complex amplitude $\mathbf{E}$ depends on the slow variables $\mathbf{X} = \varepsilon\mathbf{x}$ and $T = \varepsilon^2 t$, the notation *c.c.* stands for the complex conjugate and $\hat{\mathbf{E}}(\mathbf{X},T)$ denotes the mean complex amplitude. It induces fluctuations for the density and velocity of the electrons and of the ions whose dynamical time will be seen to be $\tau = \varepsilon t$, thus shorter than T. We write

$$N_e = N_0 + \frac{\varepsilon^2}{2}(\tilde{N}_e(\mathbf{X},\tau)e^{-i\omega_e t} + c.c.) + \varepsilon^2\hat{N}_e(\mathbf{X},\tau) + \cdots, \qquad (12.10)$$

$$N_i = N_0 + \frac{\varepsilon^2}{2}(\tilde{N}_i(\mathbf{X},\tau)e^{-i\omega_e t} + c.c.) + \varepsilon^2\hat{N}_i(\mathbf{X},\tau) + \cdots, \qquad (12.11)$$

$$\mathbf{v}_e = \frac{\varepsilon}{2}(\tilde{\mathbf{v}}_e(\mathbf{X},\tau)e^{-i\omega_e t} + c.c.) + \varepsilon^2\hat{\mathbf{v}}_e(\mathbf{X},\tau) + \cdots, \qquad (12.12)$$

$$\mathbf{v}_i = \frac{\varepsilon}{2}(\tilde{\mathbf{v}}_i(\mathbf{X},\tau)e^{-i\omega_e t} + c.c.) + \varepsilon^2\hat{\mathbf{v}}_i(\mathbf{X},\tau) + \cdots, \qquad (12.13)$$

where N_0 is the unperturbed plasma density.

From the momentum equation (12.3), considering the leading order and noting that the magnetic field $\mathcal{B}$ is of order ε^2, we can easily get

$$m_e\, N_e\left(i\omega_e\tilde{\mathbf{v}}_e\frac{\varepsilon}{2}e^{-i\omega_e t}\right) = e\, N_e\left(\mathbf{E}\frac{\varepsilon}{2}e^{-i\omega_e t}\right),$$

thus the amplitude of the electron velocity oscillations is given by

$$\tilde{\mathbf{v}}_e = -\frac{ie}{m_e\omega_e}\mathbf{E}. \qquad (12.14)$$

Neglecting the velocity oscillations of the ions due to their large mass, we take

$$\tilde{\mathbf{v}}_i = 0. \qquad (12.15)$$

Applying (12.14) and (12.15) into the continuity equations (12.1) and (12.2), at the order of ε^2, we have

$$-i\omega_e\tilde{N}_e\frac{\varepsilon^2}{2}e^{-i\omega_e t}+N_0\nabla\cdot\tilde{\mathbf{v}}_e\frac{\varepsilon^2}{2}e^{-i\omega_e t}=0,$$

thus the density fluctuations are obtained as

$$\tilde{N}_e=-i\frac{N_0}{\omega_e}\nabla\cdot\tilde{\mathbf{v}}_e=-\frac{eN_0}{m_e\omega_e^2}\nabla\cdot\mathbf{E}, \tag{12.16}$$

$$\tilde{N}_i=0. \tag{12.17}$$

At leading order, the equation for the electric field (12.7) with $\mathbf{j}=-e(N_e\mathbf{v}_e-N_i\mathbf{v}_i)$ becomes

$$-\frac{1}{c^2}\omega_e^2\mathbf{E}\frac{\varepsilon}{2}e^{-i\omega_e t}+\frac{4\pi}{c^2}i\omega_e eN_0\tilde{\mathbf{v}}_e\frac{\varepsilon}{2}e^{-i\omega_e t}=0,$$

from which, with (12.14), we finally get the electron plasma frequency

$$\omega_e=\sqrt{\frac{4\pi e^2N_0}{m_e}}. \tag{12.18}$$

At the order of ε^3, if no large-scale magnetic field is generated, then the equation (12.7) with (12.8) implies that

$$\begin{aligned}&-2i\frac{\omega_e}{c^2}\partial_T\mathbf{E}\frac{\varepsilon^3}{2}e^{-i\omega_e t}+\nabla\times(\nabla\times\mathbf{E})\frac{\varepsilon^3}{2}e^{-i\omega_e t}\\&-\frac{4\pi e^2N_0\gamma_eT_e}{c^2m_e^2\omega_e^2}\nabla(\nabla\cdot\mathbf{E})\frac{\varepsilon^3}{2}e^{-i\omega_e t}+\frac{4\pi e^2\hat{N}_e\mathbf{E}}{c^2m_e}\frac{\varepsilon^3}{2}e^{-i\omega_e t}=0,\end{aligned}$$

and thus

$$-2i\frac{\omega_e}{c^2}\partial_T\mathbf{E}+\nabla\times(\nabla\times\mathbf{E})-\frac{\gamma_eT_e}{m_ec^2}\nabla(\nabla\cdot\mathbf{E})+\frac{4\pi e^2}{c^2m_e}\hat{N}_e\mathbf{E}=0, \tag{12.19}$$

where, resulting from (12.15) and (12.17), the contribution of the ions is negligible.

We rewrite the amplitude equation (12.19) as

$$i\partial_T\mathbf{E}-\frac{c^2}{2\omega_e}\nabla\times(\nabla\times\mathbf{E})+\frac{3v_e^2}{2\omega_e}\nabla(\nabla\cdot\mathbf{E})=\frac{\omega_e}{2}\frac{\hat{N}_e}{N_0}\mathbf{E}, \tag{12.20}$$

where the electron thermal velocity v_e is defined by

$$v_e=\sqrt{\frac{T_e}{m_e}} \tag{12.21}$$

and γ_e is taken to be 3 [113].

It is seen from (12.3), (12.4) and (12.15) that the mean electron velocity $\hat{\mathbf{v}}_e$ and the mean ion velocity $\hat{\mathbf{v}}_i$ satisfy

$$m_e\left(\partial_\tau \hat{\mathbf{v}}_e + \frac{1}{4}(\tilde{\mathbf{v}}_e \cdot \nabla \tilde{\mathbf{v}}_e^* + \tilde{\mathbf{v}}_e^* \cdot \nabla \tilde{\mathbf{v}}_e)\right) = -\frac{\gamma_e T_e}{N_0}\nabla \hat{N}_e - e\hat{\mathcal{E}}, \quad (12.22)$$

$$m_i \partial_\tau \hat{\mathbf{v}}_i = -\frac{\gamma_i T_i}{N_0}\nabla \hat{N}_i + e\hat{\mathcal{E}}, \quad (12.23)$$

where

$$\frac{1}{4}(\tilde{\mathbf{v}}_e \cdot \nabla \tilde{\mathbf{v}}_e^* + \tilde{\mathbf{v}}_e^* \cdot \nabla \tilde{\mathbf{v}}_e) = \frac{e^2}{4m_e^2\omega_e^2}\nabla |\mathbf{E}|^2, \quad (12.24)$$

and $\overline{\tilde{\mathbf{v}}_e}$ denotes the conjugate of $\tilde{\mathbf{v}}_e$ and $m_e \partial_\tau \hat{\mathbf{v}}_e$ is negligible because of the small mass of the electron. Furthermore, $\hat{\mathcal{E}}$ denotes the leading contribution (of order ε^3) of the mean electron field. We thus replace (12.22) by

$$\frac{e^2}{4m_e\omega_e^2}\nabla |\mathbf{E}|^2 = -\frac{\gamma_e T_e}{N_0}\nabla \hat{N}_e - e\hat{\mathcal{E}}. \quad (12.25)$$

The system is closed by using the quasi-neutrality of the plasma in the form

$$\hat{N}_e = \hat{N}_i, \quad (12.26)$$

$$\hat{\mathbf{v}}_e = \hat{\mathbf{v}}_i, \quad (12.27)$$

which we denote by N and $\mathbf{v}$, respectively. Then from the continuity equations, one gets

$$\partial_\tau N + N_0 \nabla \cdot \mathbf{v} = 0. \quad (12.28)$$

Adding (12.25) to (12.23) and noting (12.28), we have

$$\partial_\tau \mathbf{v} = -\frac{c_s^2}{N_0}\nabla N - \frac{1}{16\pi m_i N_0}\nabla |\mathbf{E}|^2, \quad (12.29)$$

with the speed of sound c_s,

$$c_s^2 = \eta \frac{T_e}{m_i}, \qquad \eta = \frac{\gamma_e T_e + \gamma_i T_i}{T_e}. \quad (12.30)$$

Finally, we obtain the VZS [113] from equations (12.20), (12.28) and (12.29) as

$$i\partial_T \mathbf{E} - \frac{c^2}{2\omega_e}\nabla \times (\nabla \times \mathbf{E}) + \frac{3v_e^2}{2\omega_e}\nabla(\nabla \cdot \mathbf{E}) = \frac{\omega_e}{2}\frac{N}{N_0}\mathbf{E}, \quad (12.31)$$

$$\varepsilon^2 \partial_{TT} N - c_s^2 \triangle N = \frac{1}{16\pi m_i} \triangle |\mathbf{E}|^2. \quad (12.32)$$

This VZS governs the coupled dynamics of the electric-field amplitude and of the low-frequency density fluctuations of the ions and describes the dynamics of the complex envelope of the electric field oscillations near the electron plasma frequency and the slow variations of the density perturbations.

In order to obtain a dimensionless form of the system (12.31)-(12.32), we define the normalized variables

$$t' = \frac{2\eta}{3}\mu_m\,\omega_e\,T, \qquad \mathbf{x}' = \frac{2}{3}\,(\eta\mu_m)^{1/2}\,\frac{\mathbf{X}}{\zeta_d}, \tag{12.33}$$

$$N' = \frac{3}{4\eta}\frac{1}{\mu_m}\frac{N}{N_0}, \qquad \mathbf{E}' = \frac{1}{\eta}\frac{1}{\mu_m^{1/2}}\left(\frac{3}{64\pi N_0 T_e}\right)^{1/2}\mathbf{E}. \tag{12.34}$$

with

$$\zeta_d = \sqrt{\frac{T_e}{4\pi e^2 N_0}}, \qquad \mu_m = \frac{m_e}{m_i}, \tag{12.35}$$

where ζ_d is the Debye length and μ_m is the ratio of the electron to the ion masses. Then defining

$$a = \frac{c^2}{3v_e^2} = \frac{c^2}{3\omega_e^2\zeta_d^2} \tag{12.36}$$

and plugging (12.33)-(12.34) into (12.31)-(12.32), and then removing all primes, we get the following dimensionless vector Zakharov system in three dimension

$$i\partial_t\mathbf{E} - a\nabla\times(\nabla\times\mathbf{E}) + \nabla(\nabla\cdot\mathbf{E}) = N\,\mathbf{E}, \tag{12.37}$$

$$\varepsilon^2\partial_{tt}N - \triangle N = \triangle|\mathbf{E}|^2, \qquad \mathbf{x}\in\mathbb{R}^3, \quad t>0. \tag{12.38}$$

In fact, the equation (12.37) is equalivent to

$$i\partial_t\mathbf{E} + a\,\triangle\,\mathbf{E} + (1-a)\nabla(\nabla\cdot\mathbf{E}) = N\,\mathbf{E}. \tag{12.39}$$

13. Generalization and simplification of ZS

The VZS (12.37), (12.38) can be easily generalized to a physical situation when the dispersive waves interact with $\mathcal{M}$ different acoustic modes, e.g. in a multi-component plasma, which may be described by the following VZSM [113, 72, 73]:

$$i\,\partial_t\mathbf{E} + a\ \triangle\,\mathbf{E} + (1-a)\ \nabla(\nabla\cdot\mathbf{E}) - \mathbf{E}\ \sum_{J=1}^{\mathcal{M}} N_J = 0,\ \mathbf{x}\in\mathbb{R}^d,\ t>0, \tag{13.1}$$

$$\varepsilon_J^2\ \partial_{tt}N_J - \triangle N_J + \nu_J\ \triangle\,|\mathbf{E}|^2 = 0, \quad J = 1,\cdots,\mathcal{M}; \tag{13.2}$$

where the real unknown function N_J is the Jth-component deviation of the ion density from its equilibrium value, $\varepsilon_J > 0$ is a parameter inversely proportional to the acoustic speed of the Jth-component, and ν_J are real constants.

The VZSM (13.1), (13.2) is time reversible and time transverse invariant, and preserves the following three conserved quantities. They are the wave energy

$$D^{VZSM} = \int_{\mathbb{R}^d} |\mathbf{E}(\mathbf{x},t)|^2 \, d\mathbf{x}, \tag{13.3}$$

the momentum

$$\mathbf{P}^{VZSM} = \int_{\mathbb{R}^d} \left[\frac{i}{2} \sum_{j=1}^{d} \left(E_j \, \nabla E_j^* - E_j^* \, \nabla E_j \right) - \sum_{J=1}^{\mathcal{M}} \frac{\varepsilon_J^2}{\nu_J} N_J \mathbf{V_J} \right] \, d\mathbf{x} \tag{13.4}$$

and the Hamiltonian

$$\begin{aligned} H^{VZSM} = \int_{\mathbb{R}^d} \Big[a \, \|\nabla \mathbf{E}\|_{l^2}^2 + (1-a)|\nabla \cdot \mathbf{E}|^2 + \sum_{J=1}^{\mathcal{M}} N_J |\mathbf{E}|^2 \\ -\frac{1}{2} \sum_{J=1}^{\mathcal{M}} \left(\frac{\varepsilon_J^2}{\nu_J} |\mathbf{V}_J|^2 + \frac{1}{\nu_J} N_J^2 \right) \Big] \, d\mathbf{x}; \end{aligned} \tag{13.5}$$

where the flux vector $\mathbf{V_J} = ((v_J)_1, \cdots, (v_J)_d)^T$ for the Jth-component is introduced through the equations

$$\partial_t N_J = -\nabla \cdot \mathbf{V}_J, \quad \partial_t \mathbf{V}_J = -\frac{1}{\varepsilon_J^2} \nabla (N_J - \nu_J |\mathbf{E}|^2), \qquad J = 1, \cdots, \mathcal{M}. \tag{13.6}$$

13.1. *Reduction from VZSM to GVZS*

In the VZSM (13.1)-(13.2), if we choose $\mathcal{M} = 2$, and assume that $1/\varepsilon_2^2 \gg 1/\varepsilon_1^2$, i.e. the acoustic speed of the second component is much faster than the first component, then formally the fast nondispersive component N_2 can be excluded by means of the relation

$$N_2 = \nu_2 \, |\mathbf{E}|^2 + \varepsilon_2^2 \, \triangle^{-1} \, \partial_{tt} N_2 \approx \nu_2 \, |\mathbf{E}|^2 + O(\varepsilon_2^2), \qquad \text{when } \varepsilon_2 \to 0. \tag{13.7}$$

Plugging (13.7) into (13.1), then the VZSM (13.1), (13.2) is reduced to GVZS with $N = N_1$, $\nu = \nu_1$, $\varepsilon = \varepsilon_1$, $\lambda = -\nu_2$ and $\alpha = 1$:

$$i \, \partial_t \mathbf{E} + a \, \triangle \mathbf{E} + (1-a) \, \nabla(\nabla \cdot \mathbf{E}) - \alpha \, N \, \mathbf{E} + \lambda \, |\mathbf{E}|^2 \mathbf{E} = 0, \tag{13.8}$$

$$\varepsilon^2 \partial_{tt} N - \triangle N + \nu \, \triangle \, |\mathbf{E}|^2 = 0, \qquad \mathbf{x} \in \mathbb{R}^d, \quad t > 0. \tag{13.9}$$

The GVZS (13.8), (13.9) is time reversible, time transverse invariant and preserves the following three conserved quantities, i.e. the wave energy, momentum and Hamiltonian:

$$D^{GVZS} = \int_{\mathbb{R}^d} |\mathbf{E}(\mathbf{x},t)|^2 \, d\mathbf{x}, \tag{13.10}$$

$$\mathbf{P}^{GVZS} = \int_{\mathbb{R}^d} \left[\frac{i}{2} \sum_{j=1}^{d} \left(E_j \, \nabla E_j^* - E_j^* \, \nabla E_j \right) - \frac{\alpha \varepsilon^2}{\nu} N \mathbf{V} \right] \, d\mathbf{x}, \tag{13.11}$$

$$\begin{aligned} H^{GVZS} &= \int_{\mathbb{R}^d} \Big[a \, \|\nabla \mathbf{E}\|_{l^2}^2 + (1-a)|\nabla \cdot \mathbf{E}|^2 + \alpha N |\mathbf{E}|^2 - \frac{\lambda}{2}|\mathbf{E}|^4 \\ &\qquad - \frac{\alpha}{2\nu} N^2 - \frac{\alpha \varepsilon^2}{2\nu} |\mathbf{V}|^2 \Big] \, d\mathbf{x}; \end{aligned} \tag{13.12}$$

where the flux vector $\mathbf{V} = (v_1, \cdots, v_d)^T$ is introduced through the equations

$$\partial_t N = -\nabla \cdot \mathbf{V}, \qquad \partial_t \mathbf{V} = -\frac{1}{\varepsilon^2} \nabla (N - \nu |\mathbf{E}|^2). \tag{13.13}$$

In the case of $\mathcal{M} = 2$, $\nu = \nu_1$ and $\varepsilon = \varepsilon_1$, $N = N_1$ and $\mathbf{V} = \mathbf{V}_1$ in (13.4) and (13.5), and $\lambda = -\nu_2$, $\alpha = 1$ in (13.11), (13.12), letting $\varepsilon_2 \to 0$ and noting (13.7), we get formally quadratic convergence rate of the momentum and Hamiltonian from VZSM to GVZS in the 'subsonic limit' regime of the second component, i.e., $0 < \varepsilon_2 \ll 1$:

$$\begin{aligned} \mathbf{P}^{VZSM} &= \int_{\mathbb{R}^d} \left[\frac{i}{2} \sum_{j=1}^{d} \left(E_j \, \nabla E_j^* - E_j^* \, \nabla E_j \right) - \frac{\varepsilon_1^2}{\nu_1} N_1 \mathbf{V} \right] \, d\mathbf{x} \\ &\qquad - \frac{\varepsilon_2^2}{\nu_2} \int_{\mathbb{R}^d} N_2 \mathbf{V_2} \, d\mathbf{x} \\ &\approx \mathbf{P}^{GVZS} + O(\varepsilon_2^2), \end{aligned} \tag{13.14}$$

$$\begin{aligned} H^{VZSM} &= \int_{\mathbb{R}^d} \Big[a \, \|\nabla \mathbf{E}\|_{l^2}^2 + (1-a)|\nabla \cdot \mathbf{E}|^2 + N_1 |\mathbf{E}|^2 - \frac{1}{2\nu_1} N_1^2 \\ &\qquad - \frac{\varepsilon_1^2}{2\nu_1} |\mathbf{V_1}|^2 \Big] \, d\mathbf{x} + \int_{\mathbb{R}^d} \left[N_2 |\mathbf{E}|^2 - \frac{1}{2\nu_2} N_2^2 - \frac{\varepsilon_2^2}{2\nu_2} |\mathbf{V_2}|^2 \right] \, d\mathbf{x} \\ &\approx H^{GVZS} + O(\varepsilon_2^2). \end{aligned} \tag{13.15}$$

Choosing $a = 1$, $\alpha = 1$, $\nu = -1$ and $\lambda = 0$ in the GVZS (13.8)-(13.9), it collapses to the standard VZS [113]

$$i \, \partial_t \mathbf{E} + \triangle \mathbf{E} - N \mathbf{E} = 0, \qquad \mathbf{x} \in \mathbb{R}^d, \quad t > 0, \tag{13.16}$$

$$\varepsilon^2 \, \partial_{tt} N - \triangle N - \triangle |\mathbf{E}|^2 = 0. \tag{13.17}$$

13.2. *Reduction from GVZS to GZS*

In the case when $E_2 = \cdots = E_d = 0$ and $a = 1$ in the GVZS (13.8), (13.9), it reduces to the scalar GZS [113, 15],

$$i\,\partial_t E + \triangle E - \alpha\; N\; E + \lambda\,|E|^2 E = 0, \qquad \mathbf{x} \in \mathbb{R}^d, \quad t > 0, \tag{13.18}$$

$$\varepsilon^2\;\partial_{tt} N - \triangle N + \nu\;\;\triangle\,|E|^2 = 0. \tag{13.19}$$

The GZS (13.18), (13.19) is time reversible, time transverse invariant and conserved the following wave energy, momentum and Hamiltonian:

$$D^{GZS} = \int_{\mathbb{R}^d} |E(\mathbf{x},t)|^2\;d\mathbf{x}, \tag{13.20}$$

$$\mathbf{P}^{GZS} = \int_{\mathbb{R}^d} \left[\frac{i}{2}\,(E\nabla E^* - E^*\nabla E) - \frac{\varepsilon^2\alpha}{\nu} N\mathbf{V}\right]\;d\mathbf{x}, \tag{13.21}$$

$$H^{GZS} = \int_{\mathbb{R}^d} \left[|\nabla E|^2 + \alpha N|E|^2 - \frac{\lambda}{2}|E|^4 - \frac{\alpha}{2\nu}N^2 - \frac{\alpha\varepsilon^2}{2\nu}|\mathbf{V}|^2\right]\;d\mathbf{x}; \tag{13.22}$$

where the flux vector $\mathbf{V} = (v_1, \cdots, v_d)^T$ is introduced through the equations

$$N_t = -\nabla\cdot\mathbf{V}, \qquad \mathbf{V}_t = -\frac{1}{\varepsilon^2}\nabla(N - \nu|E|^2). \tag{13.23}$$

Choosing $\alpha = 1$, $\nu = -1$, $\varepsilon = 1$ and $\lambda = 0$ in the GZS (13.18)-(13.19), it collapses to the standard ZS [113, 15, 121]. When $\lambda \neq 0$, a cubic nonlinear term is added to the standard ZS.

Proof of the conservation laws in GZS: Multiplying (13.18) by $\overline{E}$, the conjugate of E, we get

$$iE_t\,E^* + E^*\;\triangle\,E - \alpha\,N\,|E|^2 + \lambda\,|E|^4 = 0. \tag{13.24}$$

Then calculating the conjugate of (13.24) and multiplying it by E, one finds

$$-iE_t^*\,E + E\;\triangle\,E^* - \alpha\,N\,|E|^2 + \lambda\,|E|^4 = 0. \tag{13.25}$$

Subtracting (13.25) from (13.24) and then multiplying both sides by $-i$, one gets

$$E_t\,E^* + E_t^* E + i(E\triangle E^* - E^*\triangle E) = 0. \tag{13.26}$$

Integrating over $\mathbb{R}^d$, integration by parts, (13.26) leads to the conservation of the wave energy

$$\frac{d}{dt}D^{GZS} = \frac{d}{dt}\int_{\mathbb{R}^d} |E(\mathbf{x},t)|^2\;d\mathbf{x} = 0.$$

From (13.21), noting (13.23), (13.18), one has the conservation of the momentum

$$\begin{aligned}\frac{d}{dt}\mathbf{P}^{GZS} &= \frac{i}{2}\int_{\mathbb{R}^d}(E_t\nabla E^* + E\nabla E_t^* - E^*\nabla E_t - E_t^*\nabla E)\,d\mathbf{x}\\ &\quad -\frac{\varepsilon^2\alpha}{\nu}\int_{\mathbb{R}^d}(N_t\mathbf{V} + N\mathbf{V}_t)\,d\mathbf{x}\\ &= i\int_{\mathbb{R}^d}(E_t\nabla E^* - E_t^*\nabla E)\,d\mathbf{x} - \frac{\varepsilon^2\alpha}{\nu}\int_{\mathbb{R}^d}(N_t\mathbf{V} + N\mathbf{V}_t)\,d\mathbf{x}\\ &= i\int_{\mathbb{R}^d}\nabla E^*(i\triangle E - i\alpha NE + i\lambda|E|^2E)d\mathbf{x}\\ &\quad -\frac{\varepsilon^2\alpha}{\nu}\int_{\mathbb{R}^d}(N_t\mathbf{V} + N\mathbf{V}_t)\,d\mathbf{x}\\ &\quad -i\int_{\mathbb{R}^d}\nabla E(-i\triangle E^* + i\alpha NE^* - i\lambda|E|^2E^*)\,d\mathbf{x}\\ &= \alpha\int_{\mathbb{R}^d}N\nabla|E|^2\,d\mathbf{x} + \frac{\varepsilon^2\alpha}{\nu}\int_{\mathbb{R}^d}\mathbf{V}\nabla\cdot\mathbf{V}\,d\mathbf{x}\\ &\quad +\frac{\alpha}{\nu}\int_{\mathbb{R}^d}\nabla(N - \nu|E|^2)N\,d\mathbf{x} = 0.\end{aligned}$$

Noting (13.23), (13.19) and multiplying (13.18) by E_t^*, the conjugate of E_t, we write it

$$\mathcal{T} = \int_{\mathbb{R}^d}\left[i|E_t|^2 + E_t^*\triangle E - \alpha NEE_t^* + \lambda|E|^2EE_t^*\right]\,d\mathbf{x} = 0. \quad (13.27)$$

Then the real part of $\mathcal{T}$ is

$$\begin{aligned}0 = Re(\mathcal{T}) &= Re\int_{\mathbb{R}^d}\left[E_t^*\triangle E - \alpha NEE_t^* + \lambda|E|^2EE_t^*\right]\,d\mathbf{x}\\ &= Re\int_{\mathbb{R}^d}\left[-\nabla E\nabla E_t^* - \frac{\alpha}{2}(N|E|^2)_t + \frac{\alpha}{2}N_t|E|^2 + \frac{\lambda}{4}(|E|^4)_t\right]\,d\mathbf{x}\\ &= -\frac{1}{2}\int_{\mathbb{R}^d}\left[\left(|\nabla E|^2 + \alpha N|E|^2 - \frac{\lambda}{2}|E|^4\right)_t + \frac{\alpha}{2}N_t|E|^2\right]\,d\mathbf{x}\\ &= -\frac{1}{2}\int_{\mathbb{R}^d}\left[\left(|\nabla E|^2 + \alpha N|E|^2 - \frac{\lambda}{2}|E|^4\right)_t - \frac{\alpha}{2}|E|^2\nabla\cdot\mathbf{V}\right]\,d\mathbf{x}\\ &= -\frac{1}{2}\int_{\mathbb{R}^d}\left[\left(|\nabla E|^2 + \alpha N|E|^2 - \frac{\lambda}{2}|E|^4\right)_t + \frac{\alpha}{2}\nabla|E|^2\cdot\mathbf{V}\right]\,d\mathbf{x}\\ &= -\frac{1}{2}\int_{\mathbb{R}^d}\left[\left(|\nabla E|^2 + \alpha N|E|^2 - \frac{\lambda}{2}|E|^4\right)_t + \frac{\alpha}{2}(\frac{\varepsilon^2}{\nu}\mathbf{V}_t + \frac{1}{\nu}\nabla N)\cdot\mathbf{V}\right]\,d\mathbf{x}.\end{aligned}$$

Thus we have,

$$\begin{aligned}
0 &= -\frac{1}{2}\int_{\mathbb{R}^d}\left(|\nabla E|^2 + \alpha N|E|^2 - \frac{\lambda}{2}|E|^4\right)\,d\mathbf{x} \\
&\quad + \frac{\alpha\varepsilon^2}{2\nu}\int_{\mathbb{R}^d}\frac{1}{2}(|\mathbf{V}|^2)_t\,d\mathbf{x} - \frac{\alpha}{2\nu}\int_{\mathbb{R}^d} N\nabla\cdot\mathbf{V}\,d\mathbf{x} \\
&= -\frac{1}{2}\int_{\mathbb{R}^d}\partial_t\left(|\nabla E|^2 + \alpha N|E|^2 - \frac{\lambda}{2}|E|^4\right)\,d\mathbf{x} \\
&\quad + \frac{\alpha\varepsilon^2}{2\nu}\int_{\mathbb{R}^d}\frac{1}{2}(|\mathbf{V}|^2)_t\,d\mathbf{x} + \frac{\alpha}{2\nu}\int_{\mathbb{R}^d} N\partial_t N\,d\mathbf{x} \\
&= -\frac{1}{2}\int_{\mathbb{R}^d}\partial_t\left(|\nabla E|^2 + \alpha N|E|^2 - \frac{\lambda}{2}|E|^4 - \frac{\alpha}{2\nu}N^2 - \frac{\alpha\varepsilon^2}{2\nu}|\mathbf{V}|^2)\right)\,d\mathbf{x},
\end{aligned}$$

which implies the conservation of Hamiltonian

$$\frac{d}{dt}H^{GZS} = 0.$$

13.3. *Reduction from GVZS to VNLS*

In the "subsonic limit", i.e. $\varepsilon \to 0$ in GVZS (13.8), (13.9), which corresponds to that the density fluctuations are assumed to follow adiabatically the modulation of the Langmuir wave, it collapses to the VNLS equation. In fact, letting $\varepsilon \to 0$ in (13.9), we get formally

$$N = \nu\,|\mathbf{E}|^2 + \varepsilon^2\ \triangle^{-1}\,\partial_{tt}N = \nu\,|\mathbf{E}|^2 + O(\varepsilon^2), \qquad \text{when } \varepsilon \to 0. \quad (13.28)$$

Plugging (13.28) into (13.8), we obtain formally the VNLS:

$$i\,\partial_t\mathbf{E} + a\ \triangle\mathbf{E} + (1-a)\ \nabla(\nabla\cdot\mathbf{E}) + (\lambda - \alpha\nu)|\mathbf{E}|^2\mathbf{E} = 0, \quad \mathbf{x}\in\mathbb{R}^d,\ t>0. \quad (13.29)$$

The VNLS (13.29) is time reversible, time transverse invariant and preserves the following wave energy, momentum and Hamiltonian:

$$D^{VNLS} = \int_{\mathbb{R}^d}|\mathbf{E}(\mathbf{x},t)|^2\,d\mathbf{x}, \quad (13.30)$$

$$\mathbf{P}^{VNLS} = \int_{\mathbb{R}^d}\frac{i}{2}\sum_{j=1}^{d}\left(E_j\ \nabla E_j^* - E_j^*\ \nabla E_j\right)\,d\mathbf{x}, \quad (13.31)$$

$$H^{VNLS} = \int_{\mathbb{R}^d}\left[a\ \|\nabla\mathbf{E}\|_{l^2}^2 + (1-a)|\nabla\cdot\mathbf{E}|^2 + \frac{\alpha\nu-\lambda}{2}|\mathbf{E}|^4\right]\,d\mathbf{x}. \quad (13.32)$$

Letting $\varepsilon \to 0$ in (13.11), (13.12), noting (13.28), we get formally quadratic convergence rate of the momentum and Hamiltonian from GVZS to VNLS in the 'subsonic limit' regime, i.e., $0 < \varepsilon \ll 1$:

$$\begin{aligned}
\mathbf{P}^{GVZS} &= \int_{\mathbb{R}^d} \frac{i}{2} \sum_{j=1}^{d} \left(E_j \, \nabla E_j^* - E_j^* \, \nabla E_j \right) \, d\mathbf{x} - \frac{\alpha\varepsilon^2}{\nu} \int_{\mathbb{R}^d} N\mathbf{V} \, d\mathbf{x} \\
&\approx \mathbf{P}^{VNLS} + O(\varepsilon^2), \\
H^{GVZS} &= \int_{\mathbb{R}^d} \left[a \, \|\nabla \mathbf{E}\|_{l^2}^2 + (1-a)|\nabla \cdot \mathbf{E}|^2 + \frac{\alpha\nu - \lambda}{2} |\mathbf{E}|^4 \right] \, d\mathbf{x} \\
&\quad - \frac{\alpha\varepsilon^2}{2\nu} \int_{\mathbb{R}^d} |\mathbf{V}|^2 \, d\mathbf{x} \\
&\approx H^{VNLS} + O(\varepsilon^2).
\end{aligned}$$

13.4. *Reduction from GZS to NLSE*

Similarly, in the "subsonic limit", i.e. $\varepsilon \to 0$ in GZS (13.18), (13.19), it collpases to the well-known NLSE with a cubic nonlinearity. In fact, letting $\varepsilon \to 0$ in (13.19), we get formally

$$N = \nu \, |E|^2 + \varepsilon^2 \; \triangle^{-1} \, \partial_{tt} N = \nu \, |E|^2 + O(\varepsilon^2), \qquad \text{when } \varepsilon \to 0. \quad (13.33)$$

Plugging (13.33) into (13.18), we obtain formally the NLS equation:

$$i \;\; E_t + \triangle \, E + (\lambda - \alpha\nu)|E|^2 \; E = 0, \qquad \mathbf{x} \in \mathbb{R}^d, \quad t > 0. \qquad (13.34)$$

The NLSE (13.34) is time reversible, time transverse invariant, and preserves the following wave energy, momentum and Hamiltonian:

$$D^{NLS} = \int_{\mathbb{R}^d} |E(\mathbf{x},t)|^2 \, d\mathbf{x}, \qquad (13.35)$$

$$\mathbf{P}^{NLS} = \int_{\mathbb{R}^d} \left[\frac{i}{2} \left(E \nabla E^* - E^* \nabla E \right) \right] \, d\mathbf{x}, \qquad (13.36)$$

$$H^{NLS} = \int_{\mathbb{R}^d} \left[|\nabla E|^2 + \frac{\alpha\nu - \lambda}{2} |E|^4 \right] \, d\mathbf{x}. \qquad (13.37)$$

Similarly, letting $\varepsilon \to 0$ in (13.21), (13.22), noting (13.33), we get formally the quadratic convergence rate of the momentum and Hamiltonian from GZS to NLSE in the 'subsonic limit' regime, i.e., $0 < \varepsilon \ll 1$:

$$\begin{aligned}
\mathbf{P}^{GZS} &= \int_{\mathbb{R}^d} \frac{i}{2} \left(E \nabla E^* - E^* \nabla E \right) \, d\mathbf{x} - \frac{\varepsilon^2 \alpha}{\nu} \int_{\mathbb{R}^d} N\mathbf{V} \, d\mathbf{x} \\
&\approx \mathbf{P}^{NLS} + O(\varepsilon^2), \qquad (13.38) \\
H^{GZS} &= \int_{\mathbb{R}^d} \left[|\nabla E|^2 + \frac{\alpha\nu - \lambda}{2} |E|^4 \right] \, d\mathbf{x} - \frac{\alpha\varepsilon^2}{2\nu} \int_{\mathbb{R}^d} |\mathbf{V}|^2 \, d\mathbf{x} \\
&\approx H^{NLS} + O(\varepsilon^2). \qquad (13.39)
\end{aligned}$$

13.5. *Add a linear damping term to arrest blowup*

When $d \geq 2$ and initial Hamiltonian $H^{GZS} < 0$ in the GZS (13.18), (13.19), mathematically, it will blowup in finite time [113]. However, the physical quantities modeled by E and N do not become infinite which implies the validity of (13.18), (13.19) breaks down near singularity. Additional physical mechanisms, which were initially small, become important near the singular point and prevent the formation of singularity. In order to arrest blowup, in physical literatures, a small linear damping (absorption) term is introduced into the GZS [64]:

$$i\,\partial_t E + \triangle E - \alpha\, N\, E + \lambda\,|E|^2 E + i\,\gamma\, E = 0, \tag{13.40}$$

$$\varepsilon^2\,\partial_{tt} N - \triangle N + \nu\,\triangle\,|E|^2 = 0, \qquad \mathbf{x} \in \mathbb{R}^d, \quad t > 0; \tag{13.41}$$

where $\gamma > 0$ is a damping parameter. The decay rate of the wave energy D^{GZS} of the damped GZS (13.40), (13.41) is

$$\begin{aligned} D^{GZS}(t) &= \int_{\mathbb{R}^d} |E(\mathbf{x},t)|^2\, d\mathbf{x} = e^{-2\gamma t}\int_{\mathbb{R}^d} |E(\mathbf{x},0)|^2\, d\mathbf{x} \\ &= e^{-2\gamma t} D^{GZS}(0), \qquad t \geq 0. \end{aligned} \tag{13.42}$$

Similarly, when $d \geq 2$ and initial Hamiltonian $H^{GVZS} < 0$ in the GVZS (13.8), (13.9) (or $H^{VZSM} < 0$ in the VZSM (13.1), (13.2)), mathematically, it will blowup in finite time too. In order to arrest blowup, in physical literatures, a small linear damping (absorption) term is introduced into the GVZS (or VZSM):

$$i\,\partial_t \mathbf{E} + a\ \triangle\,\mathbf{E} + (1-a)\ \nabla(\nabla\cdot\mathbf{E}) - \alpha\, N\,\mathbf{E} + \lambda\,|\mathbf{E}|^2\mathbf{E} + i\,\gamma\,\mathbf{E} = 0, \tag{13.43}$$

$$\varepsilon^2\partial_{tt} N - \triangle N + \nu\,\triangle\,|\mathbf{E}|^2 = 0, \qquad \mathbf{x} \in \mathbb{R}^d, \quad t > 0; \tag{13.44}$$

where $\gamma > 0$ is a damping parameter. The decay rate of the wave energy D^{GVZS} of the damped GVZS (13.43), (13.44) is

$$\begin{aligned} D^{GVZS}(t) &= \int_{\mathbb{R}^d} |\mathbf{E}(\mathbf{x},t)|^2\ d\mathbf{x} = e^{-2\gamma t}\int_{\mathbb{R}^d} |\mathbf{E}(\mathbf{x},0)|^2\ d\mathbf{x} \\ &= e^{-2\gamma t} D^{GVZS}(0), \quad t \geq 0. \end{aligned} \tag{13.45}$$

14. Well-posedness of ZS

Based on the conservation laws, the wellposedness for the standard ZS (13.16)-(13.17) were proven [113, 112, 23, 24]

Theorem 14.1: *In one dimension, for initial conditions, $E^0 \in H^p(\mathbb{R})$, $N^0 \in H^{p-1}(\mathbb{R})$, and $N^{(1)} \in H^{p-2}(\mathbb{R})$ with $p \leq 3$, there exists a unique solution $E \in L^\infty(\mathbb{R}^+, H^p(\mathbb{R}))$, $N \in L^\infty(\mathbb{R}^+, H^{p-1}(\mathbb{R}))$ for (13.16)-(13.17).*

Theorem 14.2: *In dimensions 2 and 3, for initial conditions $E^0 \in H^p(\mathbb{R}^d)$, $N^0 \in H^{p-1}(\mathbb{R}^d)$, and $N^{(1)} \in H^{p-2}(\mathbb{R}^d)$ with $p \leq 3$, there exists a unique solution $E \in L^\infty([0,T^*), H^p(\mathbb{R}^d))$, $N \in L^\infty([0,T^*), H^{p-1}(\mathbb{R}^d))$ for (13.16)-(13.17), where time T^* depends on the initial conditions.*

15. Plane wave and soliton wave solutions of ZS

In one spatial dimension (1D), the GZS (13.40)- (13.41) collapses to

$$i\, E_t + E_{xx} - \alpha N\, E + \lambda |E|^2\, E + i\gamma\, E = 0,\ a < x < b,\ t > 0, \qquad (15.1)$$

$$\varepsilon^2 N_{tt} - N_{xx} + \nu(|E|^2)_{xx} = 0, \qquad a < x < b, \quad t > 0, \qquad (15.2)$$

which admits plane wave and soliton wave solutions.

Firstly, it is instructive to examine some explicit solutions to (15.1) and (15.2). The well-known plane wave solutions [97] can be given in the following form:

$$N(x,t) = d, \qquad a < x < b, \quad t \geq 0, \qquad (15.3)$$

$$E(x,t) = \begin{cases} c\, e^{i\left(\frac{2\pi r x}{b-a} - \omega_1 t\right)}, & \gamma = 0, \\ c\, e^{-\gamma t} e^{i\left(\frac{2\pi r x}{b-a} - \omega_2 t - \frac{\lambda c^2}{2\gamma}(e^{-2\gamma t}-1)\right)}, & \gamma \neq 0, \end{cases} \qquad (15.4)$$

where r is an integer, c, d are constants and

$$\omega_1 = \alpha d + \frac{4\pi^2 r^2}{(b-a)^2} - \lambda c^2, \qquad \omega_2 = \alpha d + \frac{4\pi^2 r^2}{(b-a)^2}.$$

Secondly, as is well known, the standard ZS is not exactly integrable. Therefore the generalized ZS cannot be exactly integrable, either. However, it has exact one-soliton solutions to (15.1) and (15.2) for $\gamma = 0$ [72] for $x \in \mathbb{R}$ and $t \geq 0$:

$$E_s(x,t;\eta,V,\varepsilon,\nu) = \left[\frac{\lambda}{2} - \frac{\alpha\nu}{2\varepsilon^2}(1/\varepsilon^2 - V^2)^{-1}\right]^{-1/2} U_s, \qquad (15.5)$$

$$U_s \equiv 2i\eta\, \mathrm{sech}[2\eta(x-Vt)]\, \exp\left[iVx/2 + i(4\eta^2 - V^2/4)t + i\Phi_0\right], \qquad (15.6)$$

$$N_s(x,t;\eta,V,\varepsilon,\nu) = \frac{\nu}{\varepsilon^2}(1/\varepsilon^2 - V^2)^{-1}|E_s|^2, \qquad (15.7)$$

where η and V are the soliton's amplitude and velocity, respectively, and Φ_0 is a trivial phase constant.

Finally, we will consider the periodic soliton solution with a period L in 1d of the standard ZS, that is, $d = 1$, $\varepsilon = 1$, $\alpha = 1$, $\lambda = 0$, $\gamma = 0$ and

$\nu = -1$ in (13.40)-(13.41). The analytic solution of the ZS (15.1)-(15.2) was derived [100] and used to test different numerical methods for the ZS in [100, 28]. The solution can be written as

$$E_s(x,t;v,E_{\max}) = F(x-vt)\exp[i\phi(x-ut)], \tag{15.8}$$
$$N_s(x,t;v,E_{\max}) = G(x-vt), \tag{15.9}$$

where

$$F(x-vt) = E_{\max}\cdot dn(w,q), \quad G(x-vt) = \frac{|F(x-vt)|^2}{v^2-1} + N_0,$$
$$w = \frac{E_{\max}}{\sqrt{(2(1-v^2))}}\cdot(x-vt), \quad q = \frac{\sqrt{(E_{\max}^2 - E_{\min}^2)}}{E_{\max}},$$
$$\phi = v/2,\ \frac{v}{2}L = 2\pi m,\ m = 1,2,3\cdots,\ u = \frac{v}{2} + \frac{2N_0}{v} - \frac{E_{\max}^2 + E_{\min}^2}{v(1-v^2)},$$
$$L = \frac{2\sqrt{2(1-v^2)}}{E_{\max}}K(q) = \frac{2\sqrt{2(1-v^2)}}{E_{\max}}K'\left(\frac{E_{\min}}{E_{\max}}\right),$$

with $dn(w,q)$ a Jacobian elliptic function, L the period of the Jacobian elliptic functions, K and K' the complete elliptic integrals of the first kind satisfying $K(q) = K'\left(\sqrt{1-q^2}\right)$, and N_0 chosen such that $\langle N_s\rangle = \frac{1}{L}\int_0^L N_s(x,t)\,dx = 0$.

16. Time-splitting spectral method for GZS

In this section we present new numerical methods for the GZS (13.40), (13.41). For simplicity of notations, we shall introduce the method in one space dimension ($d = 1$) of the GZS with periodic boundary conditions. Generalizations to $d > 1$ are straightforward for tensor product grids and the results remain valid without modifications. For $d = 1$, the problem becomes

$$i\,\partial_t E + \partial_{xx}E - \alpha N\,E + \lambda|E|^2\,E + i\gamma\,E = 0,\ a < x < b,\ t > 0, \tag{16.1}$$
$$\varepsilon^2\partial_{tt}N - \partial_{xx}(N - \nu\,|E|^2) = 0, \qquad a < x < b, \quad t > 0, \tag{16.2}$$
$$E(x,0) = E^{(0)}(x),\ N(x,0) = N^{(0)}(x),\ \partial_t N(x,0) = N^{(1)}(x), \tag{16.3}$$
$$E(a,t) = E(b,t), \qquad \partial_x E(a,t) = \partial_x E(b,t), \qquad t \ge 0, \tag{16.4}$$
$$N(a,t) = N(b,t), \qquad \partial_x N(a,t) = \partial_x N(b,t), \qquad t \ge 0. \tag{16.5}$$

Moreover, we supplement (16.1)-(16.5) by imposing the compatibility condition

$$E^{(0)}(a) = E^{(0)}(b), \qquad N^{(0)}(a) = N^{(0)}(b),$$
$$N^{(1)}(a) = N^{(1)}(b), \qquad \int_a^b N^{(1)}(x)\,dx = 0. \tag{16.6}$$

As is well known, the GZS has the following property

$$D^{GZS}(t) = \int_a^b |E(x,t)|^2\,dx = e^{-2\gamma t}\int_a^b |E^{(0)}(x)|^2\,dx$$
$$= e^{-2\gamma t} D^{GZS}(0), \quad t \geq 0. \tag{16.7}$$

When $\gamma = 0$, $D^{GZS}(t) \equiv D^{GZS}(0)$, i.e., it is an invariant of the GZS [28]. When $\gamma > 0$, it decays to 0 exponentially. Furthermore, the GZS also has the following properties for $t \geq 0$

$$\int_a^b \partial_t N(x,t)\,dx = 0, \quad \int_a^b N(x,t)\,dx = \int_a^b N^{(0)}(x)\,dx = \text{const}. \tag{16.8}$$

In some cases, the boundary conditions (16.4) and (16.5) may be replaced by

$$E(a,t) = E(b,t) = 0, \qquad N(a,t) = N(b,t) = 0, \qquad t \geq 0. \tag{16.9}$$

We choose the spatial mesh size $h = \triangle x > 0$ with $h = (b-a)/M$ for M being an even positive integer, the time step $k = \triangle t > 0$ and let the grid points and the time step be

$$x_j := a + j\,h, \qquad j = 0, 1, \cdots, M; \qquad\qquad t_m := m\,k, \qquad m = 0, 1, 2, \cdots.$$

Let E_j^m and N_j^m be the approximations of $E(x_j, t_m)$ and $N(x_j, t_m)$, respectively. Furthermore, let E^m and N^m be the solution vector at time $t = t_m = mk$ with components E_j^m and N_j^m, respectively.

From time $t = t_m$ to $t = t_{m+1}$, the first NLS-type equation (16.1) is solved in two splitting steps. One solves first

$$i\,\partial_t E + \partial_{xx} E = 0, \tag{16.10}$$

for the time step of length k, followed by solving

$$i\,\partial_t E = \alpha N\,E - \lambda |E|^2\,E - i\gamma\,E, \tag{16.11}$$

for the same time step. Equation (16.10) will be discretized in space by the Fourier spectral method and integrated in time *exactly*. For $t \in [t_m, t_{m+1}]$, multiplying (16.11) by $\overline{E}$, we get

$$i\,\partial_t E\,E^* = \alpha N |E|^2 - \lambda |E|^4 - i\gamma |E|^2. \tag{16.12}$$

Then calculating the conjugate of the ODE (16.11) and multiplying it by E, one finds

$$-i\,\partial_t E^*\,E = \alpha N|E|^2 - \lambda|E|^4 + i\gamma|E|^2. \tag{16.13}$$

Subtracting (16.13) from (16.12) and then multiplying both sides by $-i$, one gets

$$\begin{aligned}\partial_t(|E(x,t)|^2) &= \partial_t E(x,t)E(x,t)^* + \partial_t E(x,t)^* E(x,t)\\ &= -2\gamma|E(x,t)|^2\end{aligned} \tag{16.14}$$

and therefore

$$|E(x,t)|^2 = e^{-2\gamma(t-t_m)}|E(x,t_m)|^2, \quad t_m \le t \le t_{m+1}. \tag{16.15}$$

Substituting (16.15) into (16.11), we obtain

$$\begin{aligned}i\partial_t E(x,t) &= \alpha N(x,t)E(x,t) - \lambda e^{-2\gamma(t-t_m)}|E(x,t_m)|^2 E(x,t)\\ &\quad -i\gamma E(x,t).\end{aligned} \tag{16.16}$$

Integrating (16.16) from t_m to t_{m+1}, and then approximating the integral of N on $[t_m, t_{m+1}]$ via the trapezoidal rule, one obtains

$$\begin{aligned}E(x,t_{m+1}) &= e^{-i\int_{t_m}^{t_{m+1}}[\alpha N(x,\tau)-\lambda e^{-2\gamma(\tau-t_m)}|E(x,t_m)|^2-i\gamma]\,d\tau}\;E(x,t_m)\\ &\approx \begin{cases} e^{-ik[\alpha(N(x,t_m)+N(x,t_{m+1}))/2-\lambda|E(x,t_m)|^2]}\;E(x,t_m), & \gamma=0,\\ e^{-\gamma k-i[k\alpha(N(x,t_m)+N(x,t_{m+1}))/2+\lambda|E(x,t_m)|^2(e^{-2\gamma k}-1)/2\gamma]}\;E(x,t_m), & \gamma\ne 0.\end{cases}\end{aligned}$$

16.1. *Crank-Nicolson leap-frog time-splitting spectral discretizations (CN-LF-TSSP) for GZS*

The second wave-type equation (16.2) in the GZS is discretized by pseudo-spectral method for spatial derivatives, and then applying Crank-Nicolson /leap-frog for linear/nonlinear terms for time derivatives:

$$\begin{aligned}&\varepsilon^2\frac{N_j^{m+1}-2N_j^m+N_j^{m-1}}{k^2} - D_{xx}^f\Big[\big(\beta N^{m+1}+(1-2\beta)N^m+\beta N^{m-1}\big)\\ &\quad -\nu|E^m|^2\Big]_{x=x_j} = 0, \qquad j=0,\cdots,M, \qquad m=1,2,\cdots,\end{aligned} \tag{16.17}$$

where $0\le\beta\le 1$ is a constant, D_{xx}^f, a spectral differential operator approximation of ∂_{xx}, is defined as

$$D_{xx}^f U\big|_{x=x_j} = -\sum_{l=-M/2}^{M/2-1}\mu_l^2\,\widetilde{U}_l\,e^{i\mu_l(x_j-a)} \tag{16.18}$$

and $\widetilde{U}_l$, the Fourier coefficients of a vector $U = (U_0, U_1, U_2, \cdots, U_M)^T$ with $U_0 = U_M$, are defined as

$$\mu_l = \frac{2\pi l}{b-a}, \ \widetilde{U}_l = \frac{1}{M}\sum_{j=0}^{M-1} U_j \ e^{-i\mu_l(x_j-a)}, \ l = -\frac{M}{2}, \cdots, \frac{M}{2}-1. \tag{16.19}$$

When $\beta = 0$ in (16.17), the discretization (16.17) to the wave-type equation (16.2) is *explicit* and was used in [15, 114]. When $0 < \beta \leq 1$, the discretization is *implicit*, but can be solved *explicitly*. In fact, suppose

$$N_j^m = \sum_{l=-M/2}^{M/2-1} (\widetilde{N^m})_l \ e^{i\mu_l(x_j-a)}, \qquad j = 0, \cdots, M; \quad m = 0, 1, \cdots, \tag{16.20}$$

Plugging (16.20) into (16.17), using the orthogonality of the Fourier basis, we obtain for $m \geq 1$

$$\begin{aligned} &\varepsilon^2 \frac{(\widetilde{N^{m+1}})_l - 2(\widetilde{N^m})_l + (\widetilde{N^{m-1}})_l}{k^2} + \mu_l^2 \Big[\beta(\widetilde{N^{m+1}})_l + (1-2\beta)(\widetilde{N^m})_l \\ &+\beta(\widetilde{N^{m-1}})_l - \nu(\widetilde{|E^m|^2})_l\Big] = 0, \ l = -\frac{M}{2}, \cdots, \frac{M}{2}-1. \end{aligned} \tag{16.21}$$

Solving the above equation, we get

$$\begin{aligned} (\widetilde{N^{m+1}})_l = \left(2 - \frac{k^2\mu_l^2}{\varepsilon^2 + \beta k^2 \mu_l^2}\right) (\widetilde{N^m})_l - (\widetilde{N^{m-1}})_l + \frac{\nu k^2 \mu_l^2}{\varepsilon^2 + \beta k^2 \mu_l^2} (\widetilde{|E^m|^2})_l, \\ l = -M/2, \cdots, M/2-1; \qquad m = 1, 2, \cdots. \end{aligned} \tag{16.22}$$

From time $t = t_m$ to $t = t_{m+1}$, we combine the splitting steps via the standard Strang splitting for $m \geq 0$:

$$N_j^{m+1} = \sum_{l=-M/2}^{M/2-1} (\widetilde{N^{m+1}})_l \ e^{i\mu_l(x_j-a)}, \tag{16.23}$$

$$\begin{aligned} E_j^* &= \sum_{l=-M/2}^{M/2-1} e^{-ik\mu_l^2/2} (\widetilde{E^m})_l \ e^{i\mu_l(x_j-a)}, \\ E_j^{**} &= \begin{cases} e^{-ik[\alpha(N_j^m + N_j^{m+1})/2 - \lambda |E_j^*|^2]} \ E_j^*, & \gamma = 0, \\ e^{-\gamma k - i[k\alpha(N_j^m + N_j^{m+1})/2 + \lambda |E_j^*|^2 (e^{-2\gamma k} - 1)/2\gamma]} \ E_j^*, & \gamma \neq 0, \end{cases} \\ E_j^{m+1} &= \sum_{l=-M/2}^{M/2-1} e^{-ik\mu_l^2/2} (\widetilde{E^{**}})_l \ e^{i\mu_l(x_j-a)}, \ 0 \leq j \leq M-1; \end{aligned} \tag{16.24}$$

where $(\widetilde{N^{m+1}})_l$ is given in (16.22) for $m > 0$ and (16.27) for $m = 0$. The initial conditions (16.3) are discretized as

$$E_j^0 = E^{(0)}(x_j),\ N_j^0 = N^{(0)}(x_j),\ \frac{N_j^1 - N_j^{-1}}{2k} = N_j^{(1)}, \quad j = 0, 1, 2, \cdots, M-1, \tag{16.25}$$

where

$$N_j^{(1)} = \begin{cases} N^{(1)}(x_j), & 0 \le j \le M-2, \\ -\displaystyle\sum_{l=0}^{M-2} N^{(1)}(x_l), & j = M-1. \end{cases} \tag{16.26}$$

This implies that

$$\begin{aligned}(\widetilde{N^1})_l = &\left(1 - \frac{k^2\mu_l^2}{2(\varepsilon^2 + \beta k^2 \mu_l^2)}\right) (\widetilde{N^{(0)}})_l + k\, (\widetilde{N^{(1)}})_l \\ &+ \frac{\nu k^2 \mu_l^2}{2(\varepsilon^2 + \beta k^2\mu_l^2)}\, (\widetilde{|E^{(0)}|^2})_l,\ l = -\frac{M}{2}, \cdots, \frac{M}{2} - 1. \end{aligned} \tag{16.27}$$

This type of discretization for the initial condition (16.3) is equivalent to use the trapezoidal rule for the periodic function $N^{(1)}$ and such that (16.8) is satisfied in discretized level. The discretization error converges to 0 exponentially fast as the mesh size h goes to 0.

Note that the spatial discretization error of the method is of spectral-order accuracy in h and time discretization error is demonstrated to be second-order accuracy in k from our numerical results.

16.2. *Phase space analytical solver + time-splitting spectral discretizations (PSAS-TSSP)*

Another way to discretize the second wave-type equation (16.2) in GZS is by pseudo-spectral method for spatial derivatives, and then solving the ODEs in phase space analytically under appropriate chosen transmission conditions between different time intervals. From time $t = t_m$ to $t = t_{m+1}$, assume

$$N(x,t) = \sum_{l=-M/2}^{M/2-1} \widetilde{N}_l^m(t)\, e^{i\mu_l(x-a)}, \qquad a \le x \le b, \quad t_m \le t \le t_{m+1}. \tag{16.28}$$

Plugging (16.28) into (16.2) and noticing the orthogonality of the Fourier series, we get the following ODEs for $m \ge 0$:

$$\varepsilon^2 \,\frac{d^2 \widetilde{N}_l^m(t)}{d\,t^2} + \mu_l^2 \left[\widetilde{N}_l^m(t) - \nu\,(|\widetilde{E(t_m)}|^2)_l\right] = 0, \quad t_m \le t \le t_{m+1}, \quad (16.29)$$

$$\widetilde{N}_l^m(t_m) = \begin{cases} (\widetilde{N^{(0)}})_l, & m = 0, \\ \widetilde{N}_l^{m-1}(t_m), & m > 0, \end{cases} \qquad l = -M/2, \cdots, M/2-1. \quad (16.30)$$

For each fixed l $(-M/2 \le l \le M/2-1)$, Eq. (16.29) is a second-order ODE. It needs two initial conditions such that the solution is unique. When $m = 0$ in (16.29), (16.30), we have the initial condition (16.30) and we can pose the other initial condition for (16.29) due to the initial condition (16.3) for the GZS (16.1)-(16.5):

$$\frac{d}{dt}\widetilde{N}_l^0(t_0) = \frac{d}{dt}\widetilde{N}_l^0(0) = (\widetilde{N^{(1)}})_l, \qquad l = -M/2, \cdots, M/2-1. \quad (16.31)$$

Then the solution of (16.29), (16.30) with $m = 0$ and (16.31) is:

$$\widetilde{N}_l^0(t) = \begin{cases} (\widetilde{N^{(0)}})_0 + t\,(\widetilde{N^{(1)}})_0, & l = 0, \\[2ex] \left[(\widetilde{N^{(0)}})_l - \nu(|\widetilde{E^{(0)}}|^2)_l\right]\cos(\mu_l\, t/\varepsilon) + \nu\,(|\widetilde{E^{(0)}}|^2)_l & \\ + \frac{\varepsilon}{\mu_l}(\widetilde{N^{(1)}})_l \sin(\mu_l\, t/\varepsilon), & l \ne 0, \end{cases} \quad (16.32)$$
$$0 \le t \le t_1, \quad l = -M/2, \cdots, M/2-1.$$

But when $m > 0$, we only have one initial condition (16.30). One **can't** simply pose the continuity between $\frac{d}{dt}\widetilde{N}_l^m(t)$ and $\frac{d}{dt}\widetilde{N}_l^{m-1}(t)$ across the time $t = t_m$ due to the last term in (16.29) is usually different in two adjacent time intervals $[t_{m-1}, t_m]$ and $[t_m, t_{m+1}]$, i.e. $(|\widetilde{E(t_{m-1})}|^2)_l \ne (|\widetilde{E(t_m)}|^2)_l$. Since our goal is to develop explicit scheme and we need linearize the nonlinear term in (16.2) in our discretization (16.29), in general,

$$\frac{d}{dt}\widetilde{N}_l^{m-1}(t_m^-) = \lim_{t\to t_m^-} \frac{d}{dt}\widetilde{N}_l^{m-1}(t) \ne \lim_{t\to t_m^+}\frac{d}{dt}\widetilde{N}_l^m(t) = \frac{d}{dt}\widetilde{N}_l^m(t_m^+), \quad (16.33)$$
$$m = 1, \cdots, \qquad l = -M/2, \cdots, M/2-1.$$

Unfortunely, we don't know the jump $\frac{d}{dt}\widetilde{N}_l^m(t_m^+) - \frac{d}{dt}\widetilde{N}_l^{m-1}(t_m^-)$ across the time $t = t_m$. In order to get a unique solution of (16.29), (16.30) for $m > 0$, here we pose an additional condition:

$$\widetilde{N}_l^m(t_{m-1}) = \widetilde{N}_l^{m-1}(t_{m-1}), \qquad l = -M/2, \cdots, M/2-1. \quad (16.34)$$

The condition (16.34) is equivalent to pose the solution $\widetilde{N}_l^m(t)$ on the time interval $[t_m, t_{m+1}]$ of (16.29), (16.30) is also continuity at the time $t = t_{m-1}$. After a simple computation, we get the solution of (16.29), (16.30) and (16.34) for $m > 0$:

$$\widetilde{N}_l^m(t) = \begin{cases} \widetilde{N}_0^{m-1}(t_m) + \frac{t-t_m}{k}\left[\widetilde{N}_0^{m-1}(t_m) - \widetilde{N}_0^{m-1}(t_{m-1})\right], & l = 0, \\ \left[\widetilde{N}_l^{m-1}(t_m) - \nu\,(\widetilde{|E^m|^2})_l\right]\cos(\mu_l(t-t_m)/\varepsilon) & \\ +\nu\,(\widetilde{|E^m|^2})_l + \frac{\sin(\mu_l(t-t_m)/\varepsilon)}{\sin(k\mu_l/\varepsilon)}\left[\widetilde{N}_l^{m-1}(t_m)\cos(k\mu_l/\varepsilon)\right. & \\ \left. -\widetilde{N}_l^{m-1}(t_{m-1}) + \nu\,[1-\cos(k\mu_l/\varepsilon)]\,(\widetilde{|E^m|^2})_l\right], & l \neq 0, \end{cases} \tag{16.35}$$

$$t_m \le t \le t_{m+1}, \quad l = -M/2, \cdots, M/2-1.$$

From time $t = t_m$ to $t = t_{m+1}$, we combine the splitting steps via the standard Strang splitting for $m \ge 0$:

$$N_j^{m+1} = \sum_{l=-M/2}^{M/2-1} \widetilde{N}_l^m(t_{m+1})\, e^{i\mu_l(x_j-a)}, \tag{16.36}$$

$$E_j^* = \sum_{l=-M/2}^{M/2-1} e^{-ik\mu_l^2/2}(\widetilde{E^m})_l\, e^{i\mu_l(x_j-a)},$$

$$E_j^{**} = \begin{cases} e^{-ik[\alpha(N_j^m+N_j^{m+1})/2-\lambda|E_j^*|^2]}\, E_j^*, & \gamma = 0, \\ e^{-\gamma k - i[k\alpha(N_j^m+N_j^{m+1})/2+\lambda|E_j^*|^2(e^{-2\gamma k}-1)/2\gamma]}\, E_j^*, & \gamma \neq 0, \end{cases}$$

$$E_j^{m+1} = \sum_{l=-M/2}^{M/2-1} e^{-ik\mu_l^2/2}(\widetilde{E^{**}})_l\, e^{i\mu_l(x_j-a)}, \; 0 \le j \le M-1; \tag{16.37}$$

where

$$\widetilde{N}_l^m(t_{m+1}) = \begin{cases} (\widetilde{N^{(0)}})_0 + k\,(\widetilde{N^{(1)}})_0, & l = 0, \; m = 0, \\ (\widetilde{N^{(0)}})_l\cos(k\mu_l/\varepsilon) + \frac{\varepsilon}{\mu_l}(\widetilde{N^{(1)}})_l\sin(k\mu_l/\varepsilon) & l \neq 0, \; m = 0, \\ +\nu\,[1-\cos(k\mu_l/\varepsilon)]\,(\widetilde{|E^{(0)}|^2})_l, & \\ 2\widetilde{N}_l^{m-1}(t_m)\cos(k\mu_l/\varepsilon) - \widetilde{N}_l^{m-1}(t_{m-1}) & m \ge 1, \\ +2\nu\,[1-\cos(k\mu_l/\varepsilon)]\,(\widetilde{|E^m|^2})_l, & \end{cases} \tag{16.38}$$

The initial conditions (16.3) are discretized as

$$E_j^0 = E^{(0)}(x_j), \; N_j^0 = N^{(0)}(x_j), \; (\partial_t N)_j^0 = N_j^{(1)}, \quad j = 0, 1, 2, \cdots, M-1. \tag{16.39}$$

Note that the spatial discretization error of the above method is again of spectral-order accuracy in h and time discretization error is demonstrated to be second-order accuracy in k from our numerical results.

16.3. *Properties of the numerical methods*

(1). Plane wave solution: If the initial data in (16.3) is chosen as

$$E^{(0)}(x) = c\, e^{i2\pi l x/(b-a)}, \quad N^{(0)}(x) = d, \quad N^{(1)}(x) = 0, \quad a \le x \le b, \tag{16.40}$$

where l is an integer and c, d are constants, then the GZS (16.1)-(16.5) admits the plane wave solution [97]

$$N(x,t) = d, \qquad a < x < b, \quad t \ge 0, \tag{16.41}$$

$$E(x,t) = \begin{cases} c\, e^{i\left(\frac{2\pi l x}{b-a} - \omega_1 t\right)}, & \gamma = 0, \\ c\, e^{-\gamma t} e^{i\left(\frac{2\pi l x}{b-a} - \omega_2 t - \frac{\lambda c^2}{2\gamma}(e^{-2\gamma t}-1)\right)}, & \gamma \ne 0. \end{cases} \tag{16.42}$$

where

$$\omega_1 = \alpha d + \frac{4\pi^2 l^2}{(b-a)^2} - \lambda c^2, \qquad \omega_2 = \alpha d + \frac{4\pi^2 l^2}{(b-a)^2}.$$

It is easy to see that in this case our numerical methods CN-LF-TSSP (16.23), (16.24) and PAAS-TSSP (16.36), (16.37) give exact results provided that $M \ge 2(|l|+1)$.

(2). Time transverse invariant: A main advantage of CN-LF-TSSP and PAAS-TSSP is that if a constant r is added to the initial data $N^0(x)$ in (16.3) when $\gamma = 0$ in (16.1), then the discrete functions N_j^{m+1} obtained from (16.23) or (16.36) get added by r and E_j^{m+1} obtained from (16.24) or (16.37) get multiplied by the phase factor $e^{-ir(m+1)k}$, which leaves the discrete function $|E_j^{m+1}|^2$ unchanged. This property also holds for the exact solution of GZS, but does not hold for the finite difference schemes proposed in [62, 28] and the spectral method proposed in [100].

(3). Conservation: Let $U = (U_0, U_1, \cdots, U_M)^T$ with $U_0 = U_M$, $f(x)$ a periodic function on the interval $[a,b]$, and let $\|\cdot\|_{l^2}$ be the usual discrete l^2-norm on the interval (a,b), i.e.,

$$\|U\|_{l^2} = \sqrt{\frac{b-a}{M}\sum_{j=0}^{M-1}|U_j|^2}, \qquad \|f\|_{l^2} = \sqrt{\frac{b-a}{M}\sum_{j=0}^{M-1}|f(x_j)|^2}. \tag{16.43}$$

Then we have

Theorem 16.1: *The CN-LF-TSSP (16.23), (16.24) and PSAS-TSSP (16.36), (16.37) for GZS possesses the following properties (in fact, they are the discretized version of (16.7) and (16.8)):*

$$\|E^m\|_{l^2}^2 = e^{-2\gamma t_m}\|E^0\|_{l^2}^2 = e^{-2\gamma t_m}\|E^{(0)}\|_{l^2}^2, \quad m = 0, 1, 2, \cdots, \tag{16.44}$$

$$\frac{b-a}{M}\sum_{j=0}^{M-1}\frac{N_j^{m+1} - N_j^m}{k} = 0, \qquad m = 0, 1, 2, \cdots \tag{16.45}$$

and

$$\frac{b-a}{M}\sum_{j=0}^{M-1} N_j^m = \frac{b-a}{M}\sum_{j=0}^{M-1} N_j^0 = \frac{b-a}{M}\sum_{j=0}^{M-1} N^{(0)}(x_j), \quad m \geq 0. \tag{16.46}$$

Proof: From (16.43), (16.37) and (16.19), using the orthogonality of the discrete Fourier series and noticing the Pasavel equality, we have

$$\begin{aligned}
\frac{M}{b-a}\|E^{m+1}\|_{l^2}^2 &= \sum_{j=0}^{M-1}|E_j^{m+1}|^2 = M\sum_{l=-M/2}^{M/2-1}\left|e^{-ik\mu_l^2/2}(\widetilde{E^{**}})_l\right|^2 \\
&= M\sum_{l=-M/2}^{M/2-1}|(\widetilde{E^{**}})_l|^2 = \sum_{j=0}^{M-1}|E_j^{**}|^2 \\
&= e^{-2\gamma k}\sum_{j=0}^{M-1}|E_j^*|^2 = e^{-2\gamma k}\sum_{j=0}^{M-1}|E_j^m|^2 \\
&= e^{-2\gamma k}\frac{M}{b-a}\|E^m\|_{l^2}^2, \quad m \geq 0.
\end{aligned} \tag{16.47}$$

Thus (16.44) is obtained from (16.47) by induction. The equalities (16.45) and (16.46) can be obtained in a similar way.

(4). Unconditional stability: By the standard Von Neumann analysis for (16.23) and (16.36), noting (16.44), we get PSAS-TSSP and CN-LF-TSSP with $1/4 \leq \beta \leq 1$ are unconditionally stable, and CN-LF-TSSP with $0 \leq \beta < 1/4$ is conditionally stable with stability constraint $k \leq \frac{2h\varepsilon}{\pi\sqrt{d(1-4\beta)}}$ in d-dimensions ($d = 1, 2, 3$). In fact, for PSAS-TSSP (16.36), (16.37), setting $(\widetilde{|E^m|^2})_l = 0$ and plugging $\widetilde{N}_l^m(t_{m+1}) = \mu\widetilde{N}_l^{m-1}(t_m) = \mu^2\widetilde{N}_l^{m-1}(t_{m-1})$ into (16.38) with $|\mu|$ the amplification factor, we obtain the characteristic equation:

$$\mu^2 - 2\cos(k\mu_l/\varepsilon)\mu + 1 = 0. \tag{16.48}$$

This implies

$$\mu = \cos(k\mu_l/\varepsilon) \pm i\ \sin(k\mu_l/\varepsilon). \tag{16.49}$$

Thus the amplification factor

$$G_l = |\mu| = \sqrt{\cos^2(k\mu_l/\varepsilon) + \sin^2(k\mu_l/\varepsilon)} = 1, \qquad l = -M/2, \cdots M/2-1.$$

This together with (16.44) imply that PSAS-TSSP is unconditionally stable. Similarly for CN-LF-TSSP (16.23), (16.24), noting (16.22), we have the characteristic equation:

$$\mu^2 - \left(2 - \frac{k^2\mu_l^2}{\varepsilon^2 + \beta k^2\mu_l^2}\right)\mu + 1 = 0. \tag{16.50}$$

This implies

$$\mu = 1 - \frac{k^2\mu_l^2}{2(\varepsilon^2 + \beta k^2\mu_l^2)} \pm \sqrt{\left(1 - \frac{k^2\mu_l^2}{2(\varepsilon^2 + \beta k^2\mu_l^2)}\right)^2 - 1}. \tag{16.51}$$

When $1/4 \le \beta \le 1$, we have

$$\left|1 - \frac{k^2\mu_l^2}{2(\varepsilon^2 + \beta k^2\mu_l^2)}\right| \le 1, \qquad k > 0, \quad l = -M/2, \cdots M/2-1.$$

Thus

$$\mu = 1 - \frac{k^2\mu_l^2}{2(\varepsilon^2 + \beta k^2\mu_l^2)} \pm i\sqrt{1 - \left(1 - \frac{k^2\mu_l^2}{2(\varepsilon^2 + \beta k^2\mu_l^2)}\right)^2}. \tag{16.52}$$

This implies the amplification factor

$$\begin{aligned} G_l = |\mu| &= \sqrt{\left(1 - \frac{k^2\mu_l^2}{2(\varepsilon^2 + \beta k^2\mu_l^2)}\right)^2 + 1 - \left(1 - \frac{k^2\mu_l^2}{2(\varepsilon^2 + \beta k^2\mu_l^2)}\right)^2} \\ &= 1, \qquad l = -M/2, \cdots M/2-1. \end{aligned}$$

This together with (16.44) imply that CN-LF-TSSP with $1/4 \le \beta \le 1/2$ is unconditionally stable. On the other hand, when $0 \le \beta < 1/4$, we need the stability condition

$$\left|1 - \frac{k^2\mu_l^2}{2(\varepsilon^2 + \beta k^2\mu_l^2)}\right| \le 1 \Longrightarrow k \le \min_{-M/2 \le l \le M/2-1} \frac{2\varepsilon}{\sqrt{(1-4\beta)\mu_l^2}} = \frac{2h\varepsilon}{\pi\sqrt{1-4\beta}}.$$

This together with (16.44) imply that CN-LF-TSSP with $0 \le \beta < 1/4$ is conditionally stable in one dimension with stability condition

$$k \le \frac{2h\varepsilon}{\pi\sqrt{1-4\beta}}. \tag{16.53}$$

All above stability results are confirmed by our numerical experiments.
(5). ε-resolution in the 'subsonic limit' regime ($0 < \varepsilon \ll 1$): As our numerical results suggest: The meshing strategy (or ε-resolution) which guarantees good numerical approximations of our new numerical methods PSAS-TSSP and CN-LF-TSSP with $1/4 \le \beta \le 1/2$ in the 'subsonic limit' regime, i.e. $0 < \varepsilon \ll 1$, is: i). for initial data with $O(\varepsilon)$-wavelength: $h = O(\varepsilon)$ and $k = O(\varepsilon)$; ii). for initial data with $O(1)$-wavelength: $h = O(1)$ and $k = O(1)$. Where the meshing strategy for CN-LF-TSSP with $0 \le \beta < 1/4$ is: $h = O(\varepsilon)$ & $k = O(h\varepsilon) = O(\varepsilon^2)$; $h = O(1)$ & $k = O(\varepsilon)$, respectively.

Remark 16.2: If the periodic boundary conditions (16.4) and (16.5) are replaced by the homogeneous Dirichlet boundary condition (16.9), then the Fourier basis used in the above algorithm can be replaced by the sine basis [15] or the algorithm in section 4 for VZSM. Similarly, if homogeneous Neumann conditions are used, then cosine series can be applied in designing the algorithm.

16.4. *Extension TSSP to GVZS*

The idea to construct the numerical methods CN-LF-TSSP and PSAS-TSSP for GZS (16.1)-(16.5) can be easily extended to the VZSM [114] in three dimensions for $\mathcal{M}$ different acoustic modes in a box $\Omega = [a_1, b_1] \times [a_2, b_2] \times [a_3, b_3]$ with homogeneous Dirichlet boundary conditions:

$$i\partial_t \mathbf{E} + a \, \triangle \mathbf{E} + (1-a)\, \nabla(\nabla \cdot \mathbf{E}) - \alpha \mathbf{E} \sum_{J=1}^{\mathcal{M}} N_J + \lambda |\mathbf{E}|^2 \mathbf{E} + i\gamma \mathbf{E} = 0, \quad (16.54)$$

$$\varepsilon_J^2 \partial_{tt} N_J - \triangle N_J + \nu_J \triangle |\mathbf{E}|^2 = 0, \quad J = 1, \cdots, \mathcal{M}, \qquad \mathbf{x} \in \Omega,\ t > 0, \quad (16.55)$$

$$\mathbf{E}(\mathbf{x}, 0) = \mathbf{E}^{(0)}(\mathbf{x}),\ N_J(\mathbf{x}, 0) = N_J^{(0)}(\mathbf{x}),\ \partial_t N_J(\mathbf{x}, 0) = N_J^{(1)}(\mathbf{x}),\ \mathbf{x} \in \Omega, \quad (16.56)$$

$$\mathbf{E}(\mathbf{x}, t) = \mathbf{0},\ N_J(\mathbf{x}, t) = 0 \qquad (J = 1, \cdots, \mathcal{M}), \qquad \mathbf{x} \in \partial\Omega; \quad (16.57)$$

where $\mathbf{x} = (x, y, z)^T$ and $\mathbf{E}(\mathbf{x}, t) = (E_1(\mathbf{x}, t), E_2(\mathbf{x}, t), E_3(\mathbf{x}, t))^T$. Moreover, we supplement (16.54)-(16.57) by imposing the compatibility condition

$$\mathbf{E}^{(0)}(\mathbf{x}) = \mathbf{0}, \quad N_J^{(0)}(\mathbf{x}) = N_J^{(1)}(\mathbf{x}) = 0, \quad \mathbf{x} \in \partial\Omega,\ J = 1, \cdots, \mathcal{M}. \quad (16.58)$$

In some cases, the homogeneous Dirichlet boundary condition (16.57) may be replaced by periodic boundary conditions:

$$\text{With periodic boundary conditions for } \mathbf{E}, N_J (J = 1, \cdots, \mathcal{M}) \text{ on } \partial\Omega. \quad (16.59)$$

We choose the spatial mesh sizes $h_1 = \frac{b_1 - a_1}{M_1}$, $h_2 = \frac{b_2 - a_2}{M_2}$ and $h_3 = \frac{b_3 - a_3}{M_3}$ in x-, y- and z-direction respectively, with M_1, M_2 and M_3 given positive integers; the time step $k = \triangle t > 0$. Denote grid points and time steps as

$$x_j := a_1 + jh_1,\ j = 0, 1, \cdots, M_1; \quad y_p := a_2 + ph_2,\ p = 0, 1, \cdots, M_2;$$
$$z_s := a_3 + sh_3,\ s = 0, 1, \cdots, M_3; \quad t_m := mk,\ m = 0, 1, 2, \cdots .$$

Let $\mathbf{E}^m_{j,p,s}$ and $(N_J)^m_{j,p,s}$ be the approximations of $\mathbf{E}(x_j, y_p, z_s, t_m)$ and $N_J(x_j, y_p, z_s, t_m)$, respectively.

For simplicity, here we only extend PSAS-TSSP from GZS (16.1)-(16.5) to VZSM (16.54)-(16.57) with homogeneous Dirichlet conditions. For periodic boundary conditions (16.59) or extension of CN-LF-TSSP can be done in a similar way. Following the idea of constructing PSAS-TSSP for GZS and the TSSP for VZSM in [114] here we only present the numerical algorithm. From time $t = t_m$ to $t = t_{m+1}$, the PSAS-TSSP method for VZSM (16.54)-(16.57) reads:

$$(N_J)^{m+1}_{j,p,s} = \sum_{(l,g,r)\in\mathcal{N}} \widetilde{(N_J)}^{\,m}_{l,g,r}(t_{m+1})\ \sin\left(\frac{lj\pi}{M_1}\right)\sin\left(\frac{pg\pi}{M_2}\right)\sin\left(\frac{sr\pi}{M_3}\right),$$
$$\mathbf{E}^*_{j,p,s} = \sum_{(l,g,r)\in\mathcal{N}} B_{l,g,r}(k/2)\ (\widetilde{\mathbf{E}^m})_{l,g,r}\ \sin\left(\frac{lj\pi}{M_1}\right)\sin\left(\frac{pg\pi}{M_2}\right)\sin\left(\frac{sr\pi}{M_3}\right),$$
$$\mathbf{E}^{**}_{j,p,s} = \begin{cases} e^{-ik[\alpha\sum_{J=1}^{\mathcal{M}}((N_J)^m_{j,p,s}+(N_J)^{m+1}_{j,p,s})/2-\lambda|\mathbf{E}^*_{j,p,s}|^2]}\ \mathbf{E}^*_{j,p,s}, & \gamma = 0,\\[2ex] e^{-\gamma k-i[k\alpha\sum_{J=1}^{\mathcal{M}}((N_J)^m_{j,p,s}+(N_J)^{m+1}_{j,p,s})/2+\lambda|\mathbf{E}^*_{j,p,s}|^2(e^{-2\gamma k}-1)/2\gamma]}\ \mathbf{E}^*_{j,p,s}, & \gamma \neq 0,\end{cases}$$
$$\mathbf{E}^{m+1}_{j,p,s} = \sum_{(l,g,r)\in\mathcal{N}} B_{l,g,r}(k/2)\ (\widetilde{\mathbf{E}^{**}})_{l,g,r}\ \sin\left(\frac{lj\pi}{M_1}\right)\sin\left(\frac{pg\pi}{M_2}\right)\sin\left(\frac{sr\pi}{M_3}\right),$$

where

$$\mathcal{N} = \{(l, g, r) \mid 1 \le l \le M_1 - 1,\ 1 \le g \le M_2 - 1,\ 1 \le r \le M_3 - 1\}.$$

$$\widetilde{(N_J)}^{\,m}_{l,g,r}(t_{m+1}) = \begin{cases} \widetilde{(N_J^{(0)})}_{0,0,0} + k\ \widetilde{(N_J^{(1)})}_{0,0,0}, & R_{l,g,r} = 0, m = 0,\\[2ex] \widetilde{(N_J^{(0)})}_{l,g,r}\cos(kR_{l,g,r}/\varepsilon_J) & R_{l,g,r} \neq 0, m = 0,\\ +\frac{\varepsilon_J}{R_{l,g,r}}\widetilde{(N_J^{(1)})}_{l,g,r}\sin(kR_{l,g,r}/\varepsilon_J) & \\ +\nu_J\left[1-\cos(kR_{l,g,r}/\varepsilon_J)\right](\widetilde{|\mathbf{E}^{(0)}|^2})_{l,g,r}, & \\[2ex] 2\widetilde{(N_J)}^{\,m-1}_{l,g,r}(t_m)\cos(kR_{l,g,r}/\varepsilon_J) & m \ge 1,\\ +2\nu_J\left[1-\cos(kR_{l,g,r}/\varepsilon_J)\right](\widetilde{|\mathbf{E}^m|^2})_{l,g,r} & \\ -\widetilde{(N_J)}^{\,m-1}_{l,g,r}(t_{m-1}), & \end{cases}$$

and

$$B_{l,g,r}(\tau) = \begin{cases} I_3, & l=g=r=0, \\ e^{-ia\tau R_{l,g,r}^2}\left[I_3 + \dfrac{e^{-i(1-a)\tau R_{l,g,r}^2}-1}{R_{l,g,r}^2} A_{l,g,r}\right], & \text{otherwise}, \end{cases}$$

with

$$R_{l,g,r}^2 = \kappa_l^2 + \zeta_g^2 + \eta_r^2, \ A_{l,g,r} = \begin{pmatrix} \kappa_l^2 & \kappa_l\zeta_g & \kappa_l\eta_r \\ \kappa_l\zeta_g & \zeta_g^2 & \zeta_g\eta_r \\ \kappa_l\eta_r & \zeta_g\eta_r & \eta_r^2 \end{pmatrix} = \begin{pmatrix} \kappa_l \\ \zeta_g \\ \eta_r \end{pmatrix} \left(\kappa_l \ \zeta_g \ \eta_r \right);$$

where I_3 is the 3×3 identity matrix, and $\widetilde{\mathbf{U}}_{l,g,r}$, the sine-transform coefficients, are defined as

$$\widetilde{\mathbf{U}}_{l,g,r} = \frac{8}{M_1M_2M_3}\sum_{j=1}^{M_1-1}\sum_{p=1}^{M_2-1}\sum_{s=1}^{M_3-1} \mathbf{U}_{j,p,s}\ \sin\left(\frac{lj\pi}{M_1}\right)\sin\left(\frac{pg\pi}{M_2}\right)\sin\left(\frac{sr\pi}{M_3}\right), \tag{16.60}$$

with

$$\kappa_l = \frac{\pi l}{b_1-a_1}, \quad l=1,\ldots,M_1-1, \qquad \zeta_g = \frac{\pi g}{b_2-a_2}, \quad g=1,\ldots,M_2-1,$$
$$\eta_r = \frac{\pi r}{b_3-a_3}, \qquad r=1,\ldots,M_3-1.$$

The initial conditions (16.56) are discretized as

$$\begin{aligned} &\mathbf{E}^0_{j,p,s} = \mathbf{E}^{(0)}(x_j,y_p,z_s), \\ &(N_J)^0_{j,p,s} = N_J^{(0)}(x_j,y_p,z_s), \ j=0,\cdots,M_1, \ p=0,\cdots,M_2, \ s=0,\cdots,M_3, \\ &(\partial_t N_J)^0_{j,p,s} = N_J^{(1)}(x_j,y_p,z_s), \qquad J=1,\cdots,\mathcal{M}. \end{aligned}$$

The properties of the numerical method for GZS in section 3 are still valid here.

17. Crank-Nicolson finite difference (CNFD) method for GZS

Another method for the GZS (13.40)-(13.41) is to use centered finite difference for spatial derivatives and Crank-Nicolson for time derivative. For simplicity of notations , here we only present the CNFD method for the standard ZS [28] with homogeneous Dirichlet boundary condition (16.9), i.e., in (16.1)-(16.2) with $\varepsilon = 1$, $\nu = -1$, $\alpha = 1$, $\lambda = 0$ and $\gamma = 0$:

$$
\begin{aligned}
& i\frac{E_j^{m+1} - E_j^m}{k} + \frac{1}{2}\left(\frac{E_{j+1}^{m+1} - 2E_j^{m+1} + E_{j-1}^{m+1}}{h^2} + \frac{E_{j+1}^m - 2E_j^m + E_{j-1}^m}{h^2}\right) \\
& = \frac{1}{4}(N_j^m + N_j^{m+1})(E_j^{m+1} + E_j^m), \qquad j = 1, 2, \cdots, M-1, \\
& \frac{N_j^{m+1} - 2N_j^m + N_j^{m-1}}{k^2} - \theta\frac{N_{j+1}^{m+1} - 2N_j^{m+1} + N_{j-1}^{m+1}}{h^2} \\
& \quad -\theta\frac{N_{j+1}^{m-1} - 2N_j^{m-1} + N_{j-1}^{m-1}}{h^2} - (1-2\theta)\frac{N_{j+1}^m - 2N_j^m + N_{j-1}^m}{h^2} \\
& \quad = \frac{|E_{j+1}^m|^2 - 2|E_j^m|^2 + |E_{j-1}^m|^2}{h^2}, \\
& \quad E_0^{m+1} = E_M^{m+1} = 0, \qquad N_0^{m+1} = N_0^{m+1} = 0, \qquad m = 0, 1 \cdots .
\end{aligned}
$$

where $0 \le \theta \le 1$ is a parameter. The initial conditions are discretized as:

$$
\begin{aligned}
E_j^0 &= E^0(x_j), \qquad N_j^0 = N^0(x_j), \qquad j = 0, 1, \cdots, M, && (17.1)\\
N_j^1 &= N_j^0 + kN^1(x_j) + \frac{k^2}{2}\Big[\frac{N_{j+1}^0 - 2N_j^0 + N_{j-1}^0}{h^2} \\
&\qquad + \frac{|E_{j+1}^0|^2 - 2|E_j^0|^2 + |E_{j-1}^0|^2}{h^2}\Big]. && (17.2)
\end{aligned}
$$

When $\theta = 0$, the discretization (17.1) for wave-type equation is explicit; when $\theta > 0$, it is implicit but can be solved explicitly when periodic boundary conditions are applied. Generalization of the method to GZS are straightforward. In our computations in next subsection, we choose $\theta = 0.5$.

Remark 17.1: In [62, 63], convergence and error estimate of the CNFD discretization (17.1), (17.1) are proved.

18. Numerical results of GZS

In this section, we present numerical results of GZS with a solitary wave solution in one dimension to compare the accuracy, stability and ε-resolution of different methods. We also present numerical examples solitary-wave collisions in one dimension GZS.

In our computation, the initial conditions for (16.3) are always chosen such that $|E^0|$, N^0 and $N^{(1)}$ decay to zero sufficiently fast as $|\mathbf{x}| \to \infty$. We always compute on a domain, which is large enough such that the periodic boundary conditions do not introduce a significant aliasing error relative to the problem in the whole space.

Example 10 The standard ZS with a solitary-wave solution, i.e., we choose $d = 1$, $\alpha = 1$, $\lambda = 0$, $\gamma = 0$ and $\nu = -1$ in (13.40)-(13.41). The well-known solitary-wave solution (15.5)-(15.7) of the ZS in this case is given in [97, 73]

$$E(x,t) = \sqrt{2B^2(1-\varepsilon^2 C^2)}\,\mathrm{sech}(B(x-Ct))\; e^{i[(C/2)x-((C/2)^2-B^2)t]}, \quad (18.1)$$

$$N(x,t) = -2B^2\,\mathrm{sech}^2(B(x-Ct)), \quad -\infty < x < \infty, \quad t \geq 0, \quad (18.2)$$

where B, C are constants. The initial condition is taken as

$$E^{(0)}(x) = E(x,0),\ N^{(0)}(x) = N(x,0),\ N^{(1)}(x,0) = \partial_t N(x,0), \quad (18.3)$$

where $E(x,0)$, $N(x,0)$ and $\partial_t N(x,0)$ are obtained from (18.1), (18.2) by setting $t = 0$.

We present computations for two different regimes of the acoustic speed, i.e. $1/\varepsilon$:

Case I. $O(1)$-acoustic speed, i.e. we choose $\varepsilon = 1$, $B = 1$, $C = 0.5$ in (18.1), (18.2). Here we test the spatial and temporal discretization errors, conservation of the conserved quantities as well as the stability constraint of different numerical methods. We solve the problem on the interval [-32, 32], i.e., $a = -32$ and $b = 32$ with periodic boundary conditions. Let $E_{h,k}$ and $N_{h,k}$ be the numerical solution of (16.1), (16.5) in one dimension with the initial condition (18.3) by using a numerical method with mesh size h and time step k. To quantify the numerical methods, we define the error functions as

$$\begin{aligned} e_1 &= \|E(\cdot,t) - E_{h,k}(t)\|_{l^2}, \qquad e_2 = \|N(\cdot,t) - N_{h,k}(t)\|_{l^2}, \\ e &= \frac{\|E(\cdot,t) - E_{h,k}(t)\|_{l^2}}{\|E(\cdot,t)\|_{l^2}} + \frac{\|N(\cdot,t) - N_{h,k}(t)\|_{l^2}}{\|N(\cdot,t)\|_{l^2}} \\ &= \frac{e_1}{\|E(\cdot,t)\|_{l^2}} + \frac{e_2}{\|N(\cdot,t)\|_{l^2}} \end{aligned}$$

and evaluate the conserved quantities D^{GZS}, P^{GZS} and H^{GZS} by using the numerical solution, i.e. replacing E and N by their numerical counterparts $E_{h,k}$ and $N_{h,k}$ respectively, in (13.20)-(13.22).

First, we test the discretization error in space. In order to do this, we choose a very small time step, e.g., $k = 0.0001$ such that the error from time discretization is negligible comparing to the spatial discretization error, and solve the ZS with different methods under different mesh sizes h. Tab. 6

lists the numerical errors of e_1 and e_2 at $t = 2.0$ with different mesh sizes h for different numerical methods.

	Mesh	$h = 1.0$	$h = \frac{1}{2}$	$h = \frac{1}{4}$
PSAS-TSSP	e_1	9.810E-2	1.500E-4	8.958E-9
	e_2	0.143	1.168E-3	6.500E-8
CN-LF-TSSP	e_1	9.810E-2	1.500E-4	7.409E-9
$(\beta = 0)$	e_2	0.143	1.168E-3	3.904E-8
CN-LF-TSSP	e_1	9.810E-2	1.500E-4	8.628E-9
$(\beta = 1/4)$	e_2	0.143	1.168E-3	6.521E-8
CN-LF-TSSP	e_1	9.810E-2	1.500E-4	1.098E-8
$(\beta = 1/2)$	e_2	0.143	1.168E-3	6.326E-8
CNFD	e_1	0.491	0.120	2.818E-2
	e_2	0.889	0.209	4.726E-2

Tab. 6: Spatial discretization error analysis: e_1, e_2 at time t=2 under $k = 0.0001$.

Secondly, we test the discretization error in time. Tab. 7 shows the numerical errors of e_1 and e_2 at $t = 2.0$ under different time steps k and mesh sizes h for different numerical methods.

Thirdly, we test the conservation of conserved quantities. Tab. 8 presents the quantities and numerical errors at different times with mesh size $h = \frac{1}{8}$ and time step $k = 0.0001$ for different numerical methods.

Case II: 'Subsonic limit' regime, i.e. $0 < \varepsilon \ll 1$, we choose $B = 1$ and $C = 1/2\varepsilon$ in (18.1), (18.2). Here we test the ε-resolution of different numerical methods. We solve the problem on the interval [-8, 120], i.e., $a = -8$ and $b = 120$ with periodic boundary conditions. Fig. 9 shows the numerical results of PSAS-TSSP at $t = 1$ when we choose the meshing strategy $h = O(\varepsilon)$ and $k = O(\varepsilon)$: $\mathcal{T}_0 = (\varepsilon_0, h_0, k_0) = (0.125, 0.5, 0.04)$, $\mathcal{T}_0/4$, $\mathcal{T}_0/16$; and $h = O(\varepsilon)$ and $k = 0.04$-independent of ε: $\mathcal{T}_0 = (\varepsilon_0, h_0) = (0.125, 0.5)$, $\mathcal{T}_0/4$, $\mathcal{T}_0/16$. CN-LF-TSSP with $\beta = 1/4$ or $\beta = 1/2$ gives similar numerical results at the same meshing strategies, where CN-LF-TSSP with $\beta = 0$ gives correct numerical results at meshing strategy $h = O(\varepsilon)$ and $k = O(\varepsilon^2)$ and incorrect results at $h = O(\varepsilon)$ and $k = O(\varepsilon)$ [15]. Furthermore, our additional numerical experiments confirm that PSAS-TSSP and CN-LF-TSSP with $1/4 \le \beta \le 1/2$ are unconditionally stable and CN-LF-TSSP with $\beta = 0$ is stable under the stability constraint (16.53).

From Tabs. 6-8 and Fig. 9, we can draw the following observations:

	h	Error	$k=\frac{1}{100}$	$k=\frac{1}{400}$	$k=\frac{1}{1600}$	$k=\frac{1}{6400}$
PSAS-TSSP	$\frac{1}{4}$	e_1	4.968E-5	3.109E-6	1.944E-7	1.226E-8
		e_2	1.225E-4	7.664E-6	4.797E-7	3.871E-8
	$\frac{1}{8}$	e_1	4.968E-5	3.109E-6	1.944E-7	1.172E-8
		e_2	1.225E-4	7.664E-6	4.797E-7	3.157E-8
CN-LF-TSSP	$\frac{1}{4}$	e_1	4.829E-5	3.022E-6	1.888E-7	1.156E-8
$(\beta=0)$		e_2	1.032E-4	6.456E-6	4.041E-7	3.673E-8
	$\frac{1}{8}$	e_1	4.829E-5	3.022E-6	1.888E-7	1.100E-8
		e_2	1.032E-4	6.456E-6	4.043E-7	2.946E-8
CN-LF-TSSP	$\frac{1}{4}$	e_1	5.679E-5	3.556E-6	2.224E-7	1.425E-8
$(\beta=1/4)$		e_2	1.623E-4	1.015E-5	6.351E-7	4.970E-8
	$\frac{1}{8}$	e_1	5.679E-5	3.556E-6	2.224E-7	1.377E-8
		e_2	1.623E-4	1.015E-5	6.351E-7	4.356E-8
CN-LF-TSSP	$\frac{1}{4}$	e_1	7.468E-5	4.678E-6	2.924E-7	1.868E-8
$(\beta=1/2)$		e_2	2.232E-4	1.396E-5	8.732E-7	6.360E-8
	$\frac{1}{8}$	e_1	7.468E-5	4.678E-6	2.924E-7	1.841E-8
		e_2	2.232E-4	1.396E-5	8.732E-7	5.942E-8
CNFD	$\frac{1}{4}$	e_1	0.802	3.480E-2	2.855E-2	2.820E-2
		e_2	0.674	9.012-2	5.005E-2	4.743E-2
	$\frac{1}{8}$	e_1	0.809	1.753E-2	7.363E-3	6.961E-3
		e_2	0.656	5.491E-2	1.427E-2	1.167E-2

Tab. 7: Time discretization error analysis: e_1, e_2 at time t=2.

In $O(1)$-acoustic speed regime, our new methods PSAS-TSSP and CN-LF-TSSP with $\beta = 1/2$ or $1/4$ give similar results as the old method, i.e. CN-LF-TSSP with $\beta = 0$, proposed in [15]: they are of spectral order accuracy in space discretization and second-order accuracy in time, conserve D^{GZS} exactly and P^{GZS}, H^{GZS} very well (up to 8 digits). However, they are improved in two aspects: (i) They are unconditionally stable where the old method is conditionally stable under the stability condition $k \le \frac{2h\varepsilon}{\pi\sqrt{d(1-4\beta)}}$ in d-dimensions ($d = 1, 2$ or 3); (ii) In the 'subsonic limit' regime for initial data with $O(\varepsilon)$-wavelength, i.e. $0 < \varepsilon \ll 1$, the ε-resolution of our new methods is improved to $h = O(\varepsilon)$ and $k = O(\varepsilon)$, where the old

	Time	D^{GZS}	P^{GZS}	H^{GZS}
PSAS-TSSP	1.0	3.0000000000	3.41181556	0.510202736
	2.0	3.0000000000	3.41181562	0.510202765
$\beta = 0$	1.0	3.0000000000	3.41181557	0.510202736
	2.0	3.0000000000	3.41181562	0.510202766
$\beta = 1/4$	1.0	3.0000000000	3.41181556	0.510202740
	2.0	3.0000000000	3.41181564	0.510202779
$\beta = 1/2$	1.0	3.0000000000	3.41181556	0.510202737
	2.0	3.0000000000	3.41181562	0.510202768
CNFD	1.0	3.0000000000	3.394829741	0.510115589
	2.0	3.0000000000	3.394791238	0.510076710

Tab. 8: Conserved quantities analysis: $k = 0.0001$ and $h = \frac{1}{8}$.

method required $h = O(\varepsilon)$ and $k = O(\varepsilon h) = O(\varepsilon^2)$. Thus in the following, we only present numerical results by PSAS-TSSP. In fact, CN-LF-TSSP with $1/4 \leq \beta \leq 1$ gives similar numerical results at the same mesh size and time step for all the following numerical examples.

Example 11 Soliton-soliton collisions in one dimension GZS, i.e., we choose $d = 1$, $\varepsilon = 1$, $\alpha = -2$ and $\gamma = 0$ in (13.40)-(13.41). We use the family of one-soliton solutions (15.5)-(15.7) in [72] to test our new numerical method PSAS-TSSP.

The initial data is chosen as

$$\begin{aligned}
E(x,0) &= E_s(x+p,0,\eta_1,V_1,\varepsilon,\nu) + E_s(x-p,0,\eta_2,V_2,\varepsilon,\nu),\\
N(x,0) &= N_s(x+p,0,\eta_1,V_1,\varepsilon,\nu) + N_s(x-p,0,\eta_2,V_2,\varepsilon,\nu),\\
\partial_t N(x,0) &= \partial_t N_s(x+p,0,\eta_1,V_1,\varepsilon,\nu) + \partial_t N_s(x-p,0,\eta_2,V_2,\varepsilon,\nu),
\end{aligned}$$

where $x = \mp p$ are initial locations of the two solitons.

In all the numerical simulations reported in this example, we set $\lambda = 2$, and $\Phi_0 = 0$. We only simulated the symmetric collisions, i.e., the collisions of solitons with equal amplitudes $\eta_1 = \eta_2 = \eta$ and opposite velocities $V_1 = -V_2 \equiv V$. Here, we present computations for two cases:

I. Collision between solitons moving with the subsonic velocities, $V < 1/\varepsilon = 1$, i.e. we take $\nu = 0.2$, $\eta = 0.3$ and $V = 0.5$;

II. Collision between solitons in the transonic regime, $V > 1/\varepsilon = 1$, i.e. we take $\nu = 2.0$, $\eta = 0.3$ and $V = 3.0$.

We solve the problem on the interval [-128,128], i.e., a = -128 and b = 128 with mesh size $h = \frac{1}{4}$ and time step $k = 0.005$. We take p = 10. Fig.

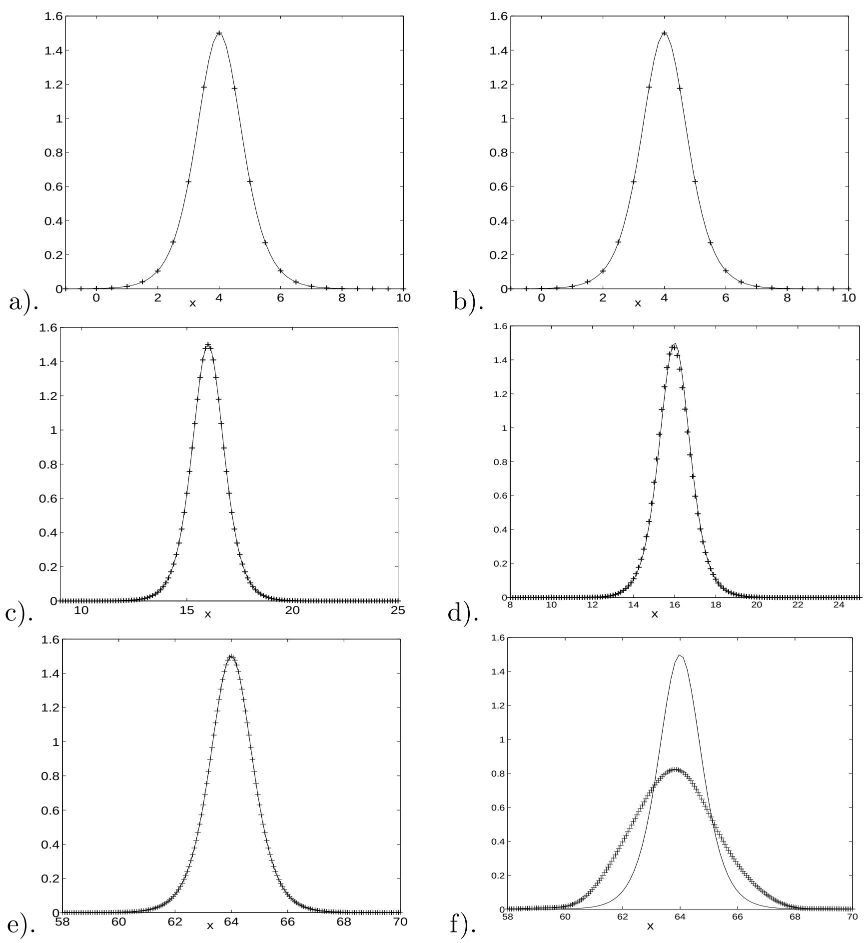

Fig. 9: Numerical solutions of the electric field $|E(x,t)|^2$ at $t = 1$ for Example 10 in the 'subsonic limit' regime by PSAS-TSSP. '—': exact solution, '+ + +': numerical solution. Left column corresponds to $h = O(\varepsilon)$ and $k = O(\varepsilon)$: a). $\mathcal{T}_0 = (\varepsilon_0, h_0, k_0) = (0.125, 0.5, 0.04)$; c). $\mathcal{T}_0/4$; e). $\mathcal{T}_0/16$. Right column corresponds to $h = O(\varepsilon)$ and $k = 0.04$-independent ε: b). $\mathcal{T}_0 = (\varepsilon_0, h_0) = (0.125, 0.5)$; d). $\mathcal{T}_0/4$; f). $\mathcal{T}_0/16$.

10 shows the evolution of the dispersive wave field $|E|^2$ and the acoustic (nondispersive) field N.

Case I corresponds to a soliton-soliton collision when the ratio ν/λ is small, i.e., the GZS (16.1), (16.2) is close to the NLSE. As is seen, the a).

b).

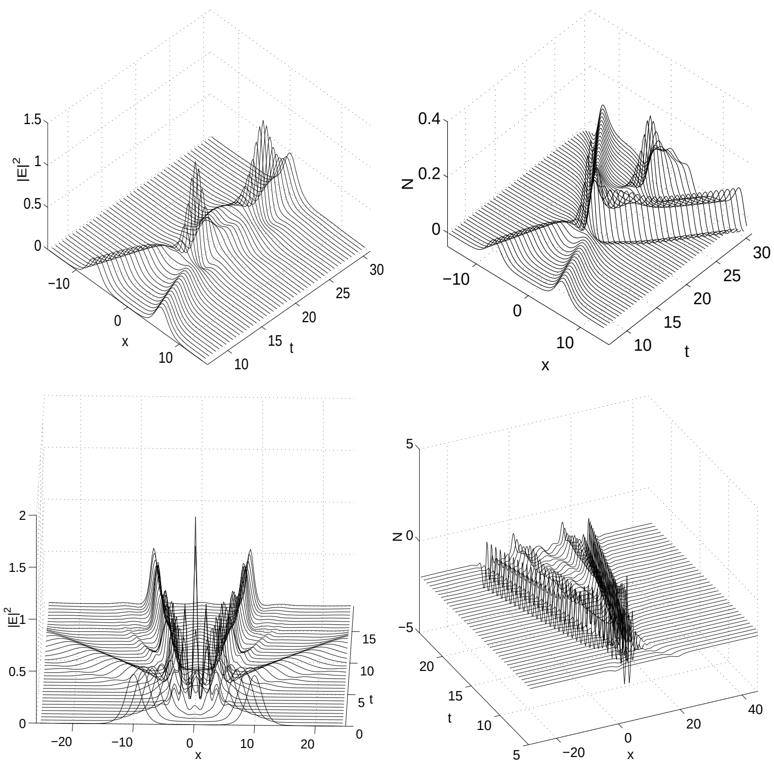

Fig. 10: Evolution of the wave field $|E|^2$ (left column) and acoustic field N (right column) in Example 11. a). For case I; b). For case II.

collision seems quite elastic (cf. Fig. 10a). This also validates the formal reduction from GZS to NLSE in section 2.5. Case II corresponds to the collision of two transonic solitons. Note that the emission of the sound waves is inconspicuous at this value of V (cf. Fig. 10b).

From Figs. 9&10, we can see that the unconditionally stable numerical method PSAS-TSSP can really be applied to solve solitary-wave collisions of GZS.

References

1. S. Abenda, Solitary waves for Maxwell-Dirac and Coulomb-Dirac models, Ann. Inst. H. Poincare Phys. Theor., 68 (1998), pp. 229–244.
2. A. Aftalion and Q. Du, Vortices in a rotating Bose-Einstein condensate: Critical angular velocities and energy diagrams in the Thomas-Fermi regime,

Phys. Rev. A, 64 (2001), pp. 063603.
3. M. H. Anderson, J. R. Ensher, M. R. Matthews, C. E. Wieman and E A. Cornell, Science, 269 (1995), 198.
4. W. Bao, Ground states and dynamics of multi-component Bose-Einstein condensates, Multiscale Modeling and Simulation, 2 (2004), pp. 210-236.
5. W. Bao, Numerical methods for nonlinear Schrödinger equation under nonzero far-field conditions, Methods Appl. Anal., 11 (2004), pp. 367-388.
6. W. Bao and Q. Du, Computing the ground state solution of Bose-Einstein condensates by a normalized gradient flow, SIAM J. Sci. Comp., 25 (2004), pp. 1674-1697.
7. W. Bao and D. Jaksch, An explicit unconditionally stable numerical methods for solving damped nonlinear Schrodinger equations with a focusing nonlinearity, SIAM J. Numer. Anal., 41(2003), pp. 1406-1426.
8. W. Bao, D. Jaksch and P.A. Markowich, Numerical solution of the Gross-Pitaevskii equation for Bose-Einstein condensation, J. Comput. Phys., 187 (2003), pp. 318-342.
9. W. Bao, D. Jaksch and P.A. Markowich, Three dimensional simulation of jet formation in collapsing condensates, J. Phys. B: At. Mol. Opt. Phys., 37 (2004), pp. 329-343.
10. W. Bao, S. Jin and P.A. Markowich, On time-splitting spectral approximations for the Schrödinger equation in the semiclassical regime, J. Comput. Phys., 175 (2002), pp. 487-524.
11. W. Bao, S. Jin and P.A. Markowich, Numerical study of time-splitting spectral discretizations of nonlinear Schrödinger equations in the semi-clasical regimes, SIAM J. Sci. Comp., 25 (2003), pp. 27-64.
12. W. Bao and X.-G. Li, An efficient and stable numerical method for the Maxwell-Dirac system, J. Comput. Phys., 199 (2004), pp. 663-687.
13. W. Bao and J. Shen, A fourth-order time-splitting Laguerre-Hermite pseudo-spectral method for Bose-Einstein condensates, SIAM J. Sci. Comput., 26 (2005), pp. 2010-2028.
14. W. Bao, F. Sun, Efficient and stable numerical methods for the generalized and vector Zakharov system, SIAM J. Sci. Comput., 26 (2005), pp. 1057-1088.
15. W. Bao, F.F. Sun and G.W. Wei, Numerical methods for the generalized Zakharov system, J. Comput. Phys. 190 (2003), pp. 201 - 228.
16. W. Bao and W. Tang, Ground state solution of trapped interacting Bose-Einstein condensate by directly minimizing the energy functional, J. Comput. Phys., 187(2003), pp. 230-254.
17. W. Bao and Y. Zhang, Dynamics of the ground state and central vortex states in Bose-Einstein condensation, Math. Mod. Meth. Appl. Sci., 66 (2006), pp. 758-786.
18. W. Bao, H.Q. Wang and P.A. Markowich, Ground, symmetric and central vortex states in rotating Bose-Einstein condensates, Commun. Math. Sci., 3 (2005), pp. 57-88.
19. G. Baym and C. J. Pethick, Phys. Rev. Lett., 76 (1996), 6.
20. P. Bechouche, N. J. Mauser and F. Poupaud, (Semi)-nonrelativistic limits

of the Dirac equation with external time-dependent electromagnetic field, Commun. Math. Phys., 197 (1998), pp. 405-425.
21. J. Bolte and S. Keppeler, A semiclassical approach to the Dirac equation, Ann. Phys., 274 (1999), pp. 125-162.
22. H. S. Booth, G. Legg and P. D. Jarvis, Algebraic solution for the vector potential in the Dirac equation, J. Phys. A: Math. Gen., 34 (2001), pp. 5667-5677.
23. J. Bourgain, On the Cauchy and invariant measure problem for the periodic Zakharov system, Duke Math. J. 76 (1994), pp. 175-202.
24. J. Bourgain and J. Colliander, On wellposedness of the Zakharov system, Internat. Math. Res. Notices, 11 (1996), pp. 515-546.
25. N. Bournaveas, Local existence for the Maxwell-Dirac equations in three space dimensions, Comm. Partial Differential Equations, 21 (1996), pp. 693–720.
26. C.C. Bradley, C.A. Sackett, R.G. Hulet, Bose-Einstein condensation of lithium: Observation of limited condensate number, Phys. Rev. Lett. 78 (1997), pp. 985-989.
27. B. M. Caradoc-Davis, R. J. Ballagh, K. Burnett, Coherent dynamics of vortex formation in trapped Bose-Einstein condensates, Phys. Rev. Lett., 83 (1999), 895.
28. Q. Chang and H. Jiang, A conservative difference scheme for the Zakharov equations, J. Comput. Phys., 113 (1994), pp. 309-319.
29. J. M. Chadam, Global solutions of the Cauchy problem for the (classical) coupled Maxwell-Dirac equations in one space dimension, J. Funct. Anal., 13 (1973), pp. 173-184.
30. T. F. Chan, D. Lee and L. Shen, Stable explicit schemes for equations of the Schrödinger type, SIAM J. Numer. Anal., 23 (1986), pp. 274-281.
31. T. F. Chan and L. Shen, Stability analysis of difference scheme for variable coefficient Schrödinger type equations, SIAM J. Numer. Anal., 24 (1987), pp. 336-349.
32. Q. Chang, B. Guo and H. Jiang, Finite difference method for generalized Zakharov equations, Math. Comp., 64 (1995), pp. 537-553.
33. J. Colliander, Wellposedness for Zakharov systems with generalized nonlinearity, J. Diff. Eqs., 148 (1998), pp. 351-363.
34. F. Dalfovo S. Giorgini, L.P. Pitaevskii, and S. Stringari, Rev. Mod. Phys., 71 (1999), 463.
35. A. Das, General solutions of Maxwell-Dirac equations in 1+1-dimensional space-time and a spatially confined solution, J. Math. Phys, 34 (1993), pp. 3986-3985.
36. A. Das, An ongoing big bang model in the special relativistic Maxwell-Dirac equations, J. Math. Phys., 37 (1996), pp. 2253-2259.
37. A. Das and D. Kay, A class of exact plane wave solutions of the Maxwell-Dirac equations, J. Math. Phys., 30 (1989), pp. 2280-2284.
38. K.B. Davis, M.O. Mewes, M.R. Andrews, N.J. van Druten, D.S. Durfee, D.M. Kurn, and W. Ketterle, Phys. Rev. Lett, 75 (1995), 3969.
39. A.S. Davydov, Phys. Scr., 20 (1979), pp. 387.

40. L.M. Degtyarev, V.G. Nakhan'kov and L.I. Rudakov, Dynamics of the formation and interaction of Langmuir solitons and strong turbulence, Sov. Phys. JETP, 40 (1974), pp. 264-268.
41. B. Desjardins, C. K. Lin and T. C. Tso, Semiclassical limit of the derivative nonlinear Schrödinger equation, M^3AS, 10 (2000), pp. 261-285.
42. P. A. M. Dirac, Principles of Quantum Mechanics, Oxford University Press, London (1958).
43. M. Edwards, P.A. Ruprecht, K. Burnett, R.J. Dodd, and C.W. Clark, Phys. Rev. Lett., 77 (1996), 1671; D.A.W. Hutchinson, E. Zaremba, and A. Griffin, Phys. Rev. Lett., 78 (1997), 1842.
44. M. Edwards and K. Burnett, Numerical solution of the nonlinear Schrödinger equation for small samples of trapped neutral atoms, Phys. Rev. A, 51 (1995), 1382.
45. M. Esteban, E. Sere, An overview on linear and nonlinear Dirac equations, Discrete Contin. Dyn. Syst., 8 (2002), pp. 381-397.
46. C. Fermanian-Kammerer, Semi-classical analysis of a Dirac equaiton without adiabatic decoupling, Monatsh. Math., to appear.
47. A. L. Fetter and A. A. Svidzinsky, Vortices in a trapped dilute Bose-Einstein condensate, J. Phys.: Condens. Matter, 13 (2001), pp. 135-194.
48. G. Fibich, An adiabatic law for self-focusing of optical beams, Opt. Lett., 21 (1996), pp. 1735-1737.
49. G. Fibich, Small beam nonparaxiality arrests self-focusing of optical beams, Phys. Rev. Lett., 76 (1996), 4356-4359.
50. G. Fibich, V. Malkin and G. Papanicolaou, Beam self-focusing in the presence of small normal time dispersion, Phys. Rev. A, 52 (1995), 4218-4228.
51. M. Flato, J. C. H. Simon and E. Taflin, Asymptotic completeness, global existence and the infrared problem for the Maxwell-Dirac equations, Mem. Amer. Math. Soc., 127 (1997), pp. 311.
52. E. Forest and R.D. Ruth, Fourth order symplectic integration, Phys. D, 43 (1990), pp. 105.
53. B. Fornberg and T. A. Driscoll, A fast spectral algorithm for nonlinear wave equations with linear dispersion, J. Comput. Phys., 155 (1999), pp. 456.
54. J. J. Garcia-Ripoll, V. M. Perez-Garcia and V. Vekslerchik, Construction of exact solutions by spatial translations in inhomogeneous nonlinear Schrödinger equaitons, Phys. Rev. E, 64 (2001), 056602.
55. I. Gasser and P.A. Markowich, Quantum hydrodynamics, Wigner transforms and the classical limit, Asymptotic Analysis, 14 (1997), pp. 97-116.
56. P. Gérard, Microlocal defect measures, Comm. PDE., 16 (1991), pp. 1761-1794.
57. V. Georgiev, Small amplitude solutions of the Maxwell-Dirac equations, Indiana Univ. Math. J., 40 (1991), pp. 845-883.
58. P. Gérard, P. A. Markowich, N. J. Mauser and F. Poupaud, Homogenization limits and Wigner transforms, Comm. Pure Appl. Math., 50 (1997), pp. 321-377.
59. J. Ginibre, Y. Tsutsumi and G. Velo, The Cauchy problem for the Zakharov system, J. Funt. Anal., 151 (1997), pp. 384-436.

60. R. Glassey, On the asymptotic behavior of nonlinear Schrödinger equations, Trans. Amer. Math. Soc., 182 (1973), pp. 187-200.
61. R. Glassey, On the blowing-up of solutions to the Cauchy problem for nonlinear Schrödinger equations, J. Math. Phys., 18 (1977), pp. 1794-1797.
62. R. Glassey, Approximate solutions to the Zakharov equations via finite differences, J. Comput. Phys., 100 (1992), pp. 377-383.
63. R. Glassey, Convergence of an energy-preserving scheme for the Zakharov equations in one space dimension, Math. Comp., 58 (1992), pp. 83-102.
64. O. Goubet and I. Moise, Attractor for dissipative Zakharov system, Nonlinear Anal., Theory, Methods & Applications, 31 (1998), pp. 823-847.
65. D. Gottlieb and S.A. Orszag, Numerical analysis of spectral methods, Soc. for Industr. & Appl. Math., Philadelphia, 1977.
66. E. Grenier, Semiclassical limit of the nonlinear Schrödinger equation in small time, Proc. Amer. Math. Soc., 126 (1998), pp. 523-530.
67. M. Greiner, O. Mandel, T. Esslinger, T.W. Hänsch, and I. Bloch, Quantum phase transition from a superfluid to a mott insulator in a gas of ultracold atoms, Nature, 415 (2002), pp. 39-45.
68. A. Griffin, D. Snoke, S. Stringaro (Eds.), Bose-Einstein condensation, Cambridge University Press, New York, 1995.
69. E.P. Gross, Nuovo. Cimento., 20 (1961), pp. 454.
70. L. Gross, The Cauchy problem for coupled Maxwell and Dirac equaitons, Comm. Pure Appl. Math., 19 (1966), pp. 1-15.
71. D.S. Hall, M.R. Mattthews, J.R. Ensher, C.E. Wieman and E.A. Cornell, Dynamics of component separation in a binary mixture of Bose-Einstein condensates, Phys. Rev. Lett., 81 (1998), pp. 1539-1542.
72. H. Hadouaj, B. A. Malomed and G.A. Maugin, Soliton-soliton collisions in a generalized Zakharov system, Phys. Rev. A, 44 (1991), pp. 3932-3940.
73. H. Hadouaj, B. A. Malomed and G.A. Maugin, Dynamics of a soliton in a generalized Zakharov system with dissipation, Phys. Rev. A, 44 (1991), pp. 3925-3931.
74. R.H. Hardin and F.D. Tappert, Applications of the split-step Fourier method to the numerical solution of nonlinear and variable coefficient wave equations, SIAM Rev. Chronicle, 15 (1973), pp. 423.
75. Z.Y. Huang, S. Jin, P.A. Markowich, C. Sparber and C.X. Zheng, A time-splitting spectral scheme for the Maxwell-Dirac system, preprint.
76. W. Hunziker, On the nonrelativistic limit of the Dirac theory, Commun. Math. Phys., 40 (1975), pp. 215-222.
77. D. Jaksch, C. Bruder, J. I. Cirac, C. W. Gardiner, and P. Zoller, Cold bosonic atoms in optical lattices, Phys. Rev. Lett., 81 (1998), pp. 3108-3111.
78. S. Jin, P.A. Markowich and C.X. Zheng, Numerical simulation of a generalized Zakharov system, J. Comput. Phys., to appear.
79. A. Jüngel, Nonlinear problems in quantum semiconductor modeling, Nonlin. Anal., Proceedings of WCNA2000, to appear.
80. A. Jüngel, Quasi-hydrodynamic semiconductor equations, Progress in Nonlinear Differential Equations and Its Applications, Birkhäuser, Basel, 2001.
81. T. Kato, On nonlinear Schrödinger equations, Ann. Inst. H. Poincaré. Phus.

Théor, 46 (1987), pp. 113-129.
82. M. Landman, G. Papanicolaou, C. Sulem and P. Sulem, Rate of blowup for solutions of the nonlinear Schrödinger equation at critical dimension, Phys. Rev. A, 38 (1988), pp. 3837-3843.
83. M. Landman, G. Papanicolaou, C. Sulem, P. Sulem and X. Wang, Stability of isotropic singularities for the nonlinear Schrödinger equation, Physica D, 47 (1991), pp. 393-415.
84. L. Laudau and E. Lifschitz, Quantum Mechanics: non-relativistic theory, Pergamon Press, New York, 1977.
85. P. Leboeuf and N. Pavloff, Phys. Rev. A **64**, 033602 (2001); V. Dunjko, V. Lorent, and M. Olshanii, Phys. Rev. Lett., 86 (2001), pp. 5413.
86. A. J. Leggett, Bose-Einstein condensation in the alkali gases: some fundamental concepts, Rev. Mod. Phys., 73 (2001), pp. 307-356.
87. E. H. Lieb, R. Seiringer, J. Yugvason, Bosons in a trap: a rigorous derivation of the Gross-Pitaevskii energy functional, Phys. Rev. A, 61 (2000), pp. 3602.
88. F. Lin and T. C. Lin, Vortices in two-dimensional Bose-Einstein condensates, Geometry and nonlinear partial differential equations (Hangzhou, 2001), pp. 87–114, AMS/IP Stud. Adv. Math., 29, Amer. Math. Soc., Providence, RI, 2002.
89. M.J. Landman, G.C. Papanicolaou, C. Sulem, P.L. Sulem, X.P. Wang, Stability of isotropic singularities for the nonlinear Schrödinger equation, Phys. D, 47 (1991), pp. 393–415.
90. A. G. Lisi, A solitary wave solution of the Maxwell-Dirac equations, J. Phys. A: Math. Gen., 28 (1995), pp. 5385-5392.
91. P.A. Markowich, N.J. Mauser and F. Poupaud, A Wigner function approach to semiclassical limits: electrons in a periodic potential, J. Math. Phys., 35 (1994), pp. 1066-1094.
92. P.A. Markowich, P. Pietra and C. Pohl, Numerical approximation of quadratic observables of Schrödinger-type equations in the semi-classical limit, Numer. Math., 81 (1999), pp. 595-630.
93. N. Masmoudi and N. J. Mauser, The selfconsistent Pauli equaiton, Monatsh. Math., 132 (2001), pp. 19-24.
94. R. McLachlan, Symplectic integration of Hamiltonian wave equations, Numer. Math., 66 (1994), pp. 465.
95. V. Masselin, A result of the blow-up rate for the Zakharov system in dimension 3, SIAM J. Math. Anal., 33 (2001), pp. 440-447.
96. B. Najman, The nonrelativstic limit of the nonlinear Dirac equaiton, Ann. Inst. Henri Poincare Non Lineaire, 9 (1992), pp. 3-12.
97. P.K. Newton, Wave interactions in the singular Zakharov system, J. Math. Phys., 32 (1991), pp. 431-440.
98. G.C. Papanicolaou, C. Sulem, P.L. Sulem, X.P. Wang, Singular solutions of the Zakharov equations for Langmuir turbulence, Phys. Fluids B, 3 (1991), pp. 969-980.
99. A.S. Parkins and D.F. Walls, Physics Reports, 303 (1998), pp. 1.
100. G.L. Payne, D.R. Nicholson, and R.M. Downie, Numerical solution of the Zakharov equations, J. Comput. Phys., 50 (1983), pp. 482-498.

101. N.R. Pereira, Collisions between Langmuir solitons, The Physics of Fluids, 20 (1977), pp. 750-755.
102. C.J. Pethick and H. Smith, Bose-Einstein Condensation in Dilute Gases, Cambridge University Press, 2002.
103. L.P. Pitaevskii, Zh. Eksp. Teor. Fiz., 40 (1961), pp. 646. (Sov. Phys. JETP, 13 (1961), pp. 451).
104. L. Pitaevskii and S. Stringari, Bose-Einstein condensation, Oxford University Press, Oxford, 2002.
105. D. S. Rokhsar, Phys. Rev. Lett., 79 (1997), pp. 2164; R. Dum, J.I. Cirac, M. Lewenstein, and P. Zoller, Phys. Rev. Lett., 80 (1998), pp. 2972; P. O. Fedichev, and G. V. Shlyapnikov, Phys. Rev. A, 60 (1999), pp. 1779.
106. L. Simon, Asymptotics for a class of nonlinear evolution equations, with applications to geometric problems, Annals of Math., 118 (1983), pp. 525-571.
107. E.I. Schulman, Dokl. Akad. Nauk. SSSR, 259 (1981), pp.579 [Sov. Phys. Dokl., 26 (1981), pp. 691].
108. C. Sparber and P. Markowich, Semiclassical asymptotics for the Maxwell-Dirac system, J. Math. Phys., 44 (2003), pp. 4555–4572.
109. H. Spohn, Semiclassical limit of the Dirac equaiton and spin precession, Ann. Phys., 282 (2000), pp. 420-431.
110. L. Stenflo, Phys. Scr., 33 (1986), pp. 156.
111. G. Strang, On the construction and comparison of differential schemes, SIAM J. Numer. Anal., 5 (1968), pp. 506.
112. C. Sulem and P.L. Sulem, Regularity properties for the equations of Langmuir turbulence, C. R. Acad. Sci. Paris Sér. A Math., 289 (1979), pp. 173-176.
113. C. Sulem and P.L. Sulem, The nonlinear Schrödinger equation, Springer, 1999.
114. F.F. Sun, Numerical studies on the Zakharov system, Master thesis, National University of Singapore, 2003.
115. T.R. Taha and M.J. Ablowitz, Analytical and numerical aspects of certain nonlinear evolution equations, II. Numerical, nonlinear Schrödinger equation, J. Comput. Phys., 55 (1984), pp. 203.
116. B. Thaller, The Dirac equation, New York, Springer, 1992.
117. M. Weinstein, Nonlinear Schrödinger equations and sharp interpolation estimates, Comm. Math. Phys., 87 (1983), pp. 567-576.
118. M. Weinstein, Modulational stability of ground states of nonlinear Schrödinger equations, SIAM J. Math. Anal., 16 (1985), pp. 472-490.
119. M. Weinstein, The nonlinear Schrödinger equations-singularity formation, stability and dispersion, Contemporary mathematics, 99 (1989), pp. 213-232.
120. H. Yoshida, Construction of higher order symplectic integrators, Phys. Lett. A., 150 (1990), pp. 262-268.
121. V.E. Zakharov, Zh. Eksp. Teor. Fiz., 62 (1972), pp. 1745 [Sov. Phys. JETP, 35 (1972), pp. 908].